X-RAY PHOTOELECTRON SPECTROSCOPY

A STUDY OF PLASMONS, ALLOYS AND GOLD COMPOUNDS

P. M. Th. M. VAN ATTEKUM

X–RAY PHOTOELECTRON SPECTROSCOPY

A STUDY OF PLASMONS, ALLOYS AND GOLD COMPOUNDS

PROMOTOR DR J M TROOSTI R

X-RAY PHOTOELECTRON SPECTROSCOPY

A STUDY OF PLASMONS, ALLOYS AND GOLD COMPOUNDS

P R O E F S C H R I F T

TER VERKRIJGING VAN DE GRAAD VAN DOCTOR
IN DE WISKUNDE EN NATUURWETENSCHAPPEN
AAN DE KATHOLIEKE UNIVERSITEIT TE NIJMEGEN, OP GEZAG VAN
DE RECTOR MAGNIFICUS, PROF DR P G A B WIJDEVELD,
VOLGENS BESLUIT VAN HET COLLEGE VAN DECANEN
IN HET OPENBAAR TE VERDEDIGEN
OP VRIJDAG 18 MEI 1979
DES NAMIDDAGS TE 2 UUR PRECIES

door

PAULUS MARIA THEODORUS MATTHEUS VAN ATTEKUM
geboren te Wateringen

Druk Krips Repro Meppel

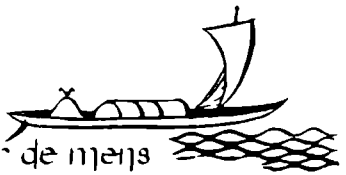

Voor de mens
staan drie wegen open
om verstandig te handelen:
de edelste weg:
— nadenken
de gemakkelijkste weg:
— navolgen —
de bitterste weg:
— ervaring —

CONFUCIUS

Aan mijn ouders

Aan elleke

Lay out: *Elly van Kuijck*

Illustrations: *Depts. of Illustration and Photography, Faculty of Science*

The contents of this thesis is not the result of the efforts of the author alone. Many people contributed in the underlying research and I am indebted to many of my colleagues for their stimulating discussions and kind cooperation. In particular, I want to mention Jan van der Velden, who as a student did most of the measurements and calculations discussed in chapter 7; Ad Swolfs performed technical assistance in all measurements.

I am grateful to Elly van Kuijck, who on her characteristic and energetic way typed and prepared the manuscript from my early drafts. Finally, I am indebted to my wife for her patience and support during the many evenings and weekends, which might have been spent more pleasant.

CONTENTS

CHAPTER 1

INTRODUCTION

In the photoelectric effect, electromagnetic radiation is absorbed by an atom, molecule or solid and the energy is used to eject an electron from a bound state. Conservation of energy yields the equation

$$h\nu + E_i = E_e + E_f \tag{1}$$

where $h\nu$ is the energy of the incident photons, E_i and E_f are, respectively, the energy of the atom, molecule or solid before and after the ejection of the electron and E_e is the kinetic energy of the ejected electron. If we define the binding energy of the electron, E_B, as

$$E_B = E_f - E_i \tag{2}$$

equation (1) reduces to

$$E_e = h\nu - E_B \tag{3}$$

Note from Eq.(3) that only electrons with a binding energy smaller than the photon energy can be ejected. For a long time photoelectron processes were mainly studied by changing $h\nu$ and measuring the total intensity of the electrons ejected. The last decade has seen a tremendous growth of what is commonly called photoelectron spectroscopy: in this technique the photon energy is kept constant and the electron intensity is measured as a function of E_e. This technique was pioneered and perfected by two groups. Siegbahn and coworkers concentrated on X-ray photoelectron spectroscopy (XPS) with $h\nu > 1$ keV [1]. Turner et al. developped a high resolution electron energy analyser for UV photoelectron spectroscopy and applied this technique to the study of molecules in the gaseous phase[2].

From Eq.(3) it follows that for a given photon energy, $h\nu$, measurement of the photoelectron intensity as a function of E_e will result in a replica of the various electron orbital energies. This is illustrated in Figure 1.1 where part of the X-ray photoelectron spectrum of the three coinage metals is

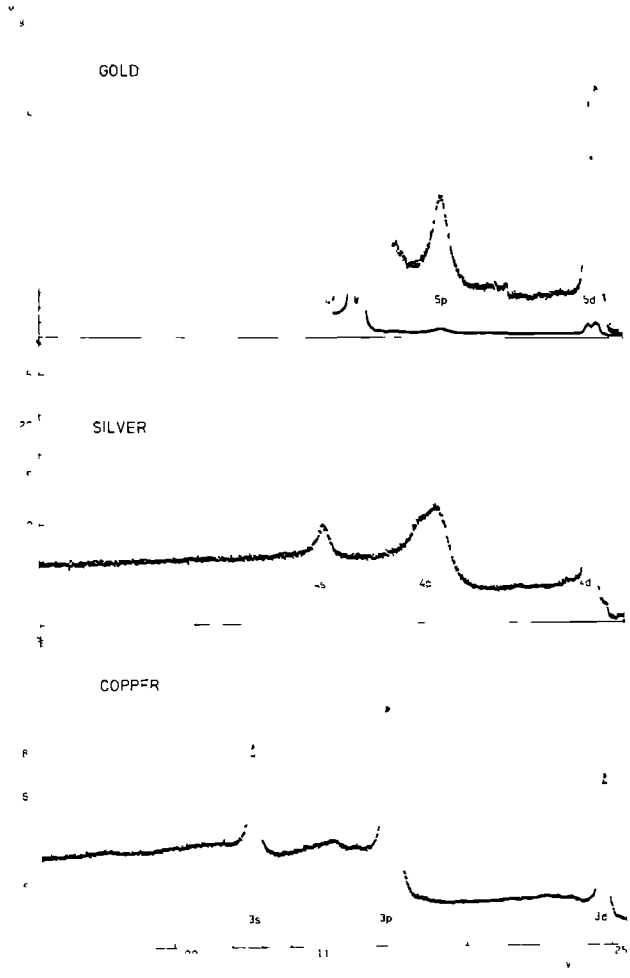

Figure 1.1 X-ray photoemission spectra of the outer electron shells of Cu, Ag and Au in the metallic state. The position of each peak is a measure of the binding energy (E_B is zero at 1949.3 eV). The intensity is a function of the number of electrons in each shell and, more important, is given by the cross section for photoionization. The outermost d and s electrons in these metals are delocalized and the levels are consequently broadened, which is clearly reflected in the spectra. The valence s electrons are visible as shoulders on the high energy side of the d band. A more detailed spectrum of the Au valence band is shown in Fig. 1.3. The large linewidth of Au(5p), Ag(4p) and Au(4f) is caused by the short lifetime of a hole in these levels. Spin orbit splitting is discernable in the Au($4f$), Ag(4p) and Cu(3p) lines. The separation which is visible between the Au(4f) and (4s) lines is mainly due to coulomb interaction between the photoelectrons.

given. Generally, the photoelectrons are divided into core and valence electrons. The former are ejected from a core level i.e. a level that does not participate in the bonding and which has an almost unperturbed atomic character. The binding energy of the core electrons is generally larger than about 20 eV. The valence electrons originate from the higher energy levels ($E_B < 20$ eV), which are perturbed by the bonding Once the XPS spectrum of a given element is known, it can be used to identify the constituent elements in compounds. This is illustrated in Fig. 1.2 for $P(C_6H_5)_3AuI$ and KSCN. The acronym ESCA (Electron Spectroscopy for Chemical Analysis) introduced by Siegbahn emphasizes this application of photoelectron spectroscopy In spite of the fact that XPS has only a limited energy resolution (0 4 - 1.0 eV) many details of orbital energies can be observed Fig. 1.3 gives a close-up of the highest orbitals of KSCN together with those of several other potassium (pseudo)-halides

Eq (3) is of a deceptive simplicity; closer inspection of XPS spectra soon reveals a sometimes bewildering complexity which reduces the use of XPS as an analytical tool, but on the other hand provides a way to study many interesting effects. For instance the Cu spectrum in Fig. 1.1 shows distinctive features between the 3s and 3p peaks, which cannot be associated with atomic energy levels. The Au(4f) lines are split and there are large differences in linewidth and intensity throughout the spectra. In Fig. 1.2 the background intensity is seen to increase stepwise with decreasing kinetic energy. Also, in these spectra peaks appear due to Auger processes, which invariably accompany the photoelectric process. In the following paragraphs the experimental and theoretical aspects that make XPS a complex but interesting tool are briefly discussed. The remaining chapters will discuss some of these subjects in more detail. Since these chapters deal solely with XPS studies on solids, this field will be emphasized in the following paragraphs.

1 1 Intensity and linewidth

From Figures 1.1-3 it is clear that the area intensity of the different photoelectron lines is not the same. The intensity is a function of the number of electrons in a given level and the transition probability per unit time, $P_{k\to1}$, for photoemission from the initial state ψ_1 to the final state ψ_k Quite generally, $P_{k\to1}$ follows from Fermi's "Golden Rule"

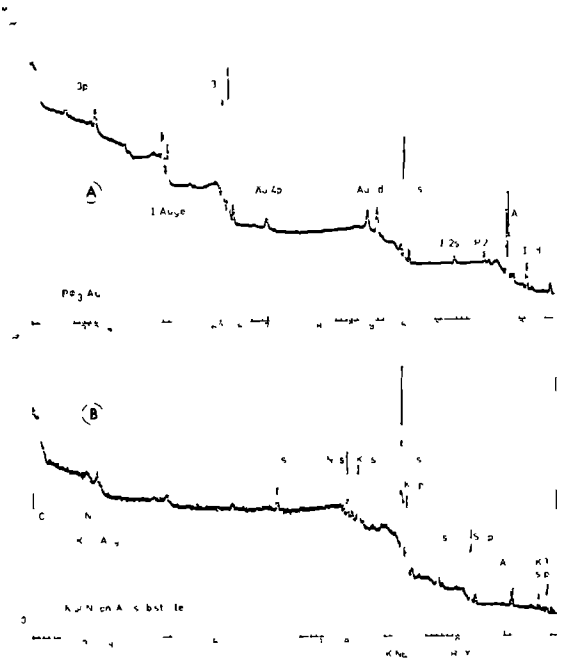

Figure 1.2 X-ray photoemission spectrum of $P(C_6H_5)_3AuI$ and KSCN. Along the horizontal axis the kinetic energy of the ejected electron is plotted. For each element at least one XPS line can be found that is well separated from all the others. This, identification of the elements in samples of unknown composition is possible with XPS. The Au(4f) lines in the KSCN spectrum are due to the gold substrate and the O(1s) line originates from a small surface contamination, which is appreciably amplified as a consequence of the surface sensitivity of XPS. Several Auger peaks are present: KVV transitions for C, N and O and $M_{4,5}N_{4,5}N_{4,5}$ transitions for I. The sequence of the 1s XPS lines and KVV Auger peaks is opposite for the series C, N and O. Since the binding energies of the I-shell electrons in the elements C, N and O are almost equal, it follows from Eq.(5) that when the binding energy of the 1s electron is higher (i.e. the kinetic energy of the photoelectron is lower) the kinetic energy of the Auger electron is also higher. The stepwise increase of the background intensity is due to inelastic scattering of photoelectrons after photoionization.

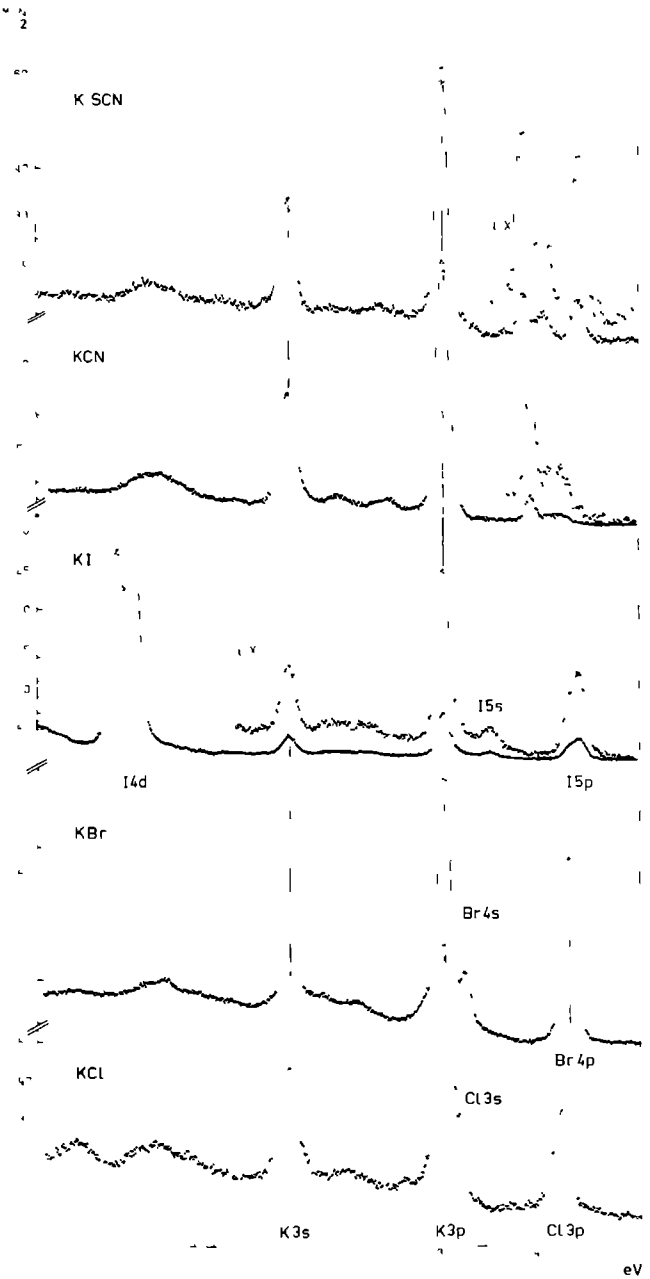

Figure 1.3 X-ray photoemission spectra of the highest orbitals of the potassium (pseudo)-halides, KX (X = Cl, Br, I, CN and SCN). The position of the K(3p) lines is aligned at a kinetic energy of 1231.6 eV to correct for differences in the charging of the samples. Apart from the main XPS lines extra structure is observed which is partly due to final state effects and partly to characteristic energy losses. The energy separation between the highest occupied level of the halogen ion and the K(3p) line increases from chlorine to iodine i.e. with decreasing ionicity. The valence bands of KCN and KSCN consist of two and three peaks, respectively. Pelms et al.[3] have analysed the energy levels in CN^- and SCN^-. From their analysis it can be concluded that the band with highest kinetic energy in KSCN has mainly S(3p) character.

$$P_{k\to i} = \frac{2\pi}{\hbar}\rho(E_k) \mid \langle \psi_k \mid V \mid \psi_i \rangle \mid^2 \qquad (4)$$

where $\rho(E_k)$ is the energy density of final states and V is the time dependent part of the Hamiltonian. In case of photoemission, the transitions are induced by the electromagnetic field. A more convenient quantity to study the intensity of photoelectron lines is the cross section for photoionization σ, which is defined as the total transition probability per unit time divided by the incident photon flux. The cross sections have dimensions of area. The differential cross section for ejection of an electron in a small solid angle, $d\Omega$, with respect to the electric field vector can be written as[4]:

$$\frac{d\sigma_{i\to k}}{d\Omega} = \frac{\pi\hbar^2 e}{m^2 c\omega}\rho(E_k) \mid \bar{u} \cdot \langle \psi_k \mid \exp(i\bar{q}.\bar{r})\bar{\nabla} \mid \psi_i \rangle \mid^2 \qquad (5)$$

where $\rho(E_k)$ is the density of final states corresponding to a given solid angle. The electromagnetic radiation is represented as a propagating plane wave with wave vector $\bar{q}$, frequency ω and polarisation $\bar{u}$. The differential cross section is proportional to the cross section σ[5]. The proportionality constant depends on the polarisation and energy of the photons and on the symmetry of the electron orbital studied. Scofield[6] has calculated the cross sections of the different orbitals in the elements for photon energies between 1 keV and 1.5 MeV. The values at a photon energy of 1253.64 eV (Mg Kα radiation) range from $10\text{-}10^6$ barn (1 barn = 10^{-28} m^2). In chapter 5 a more detailed analysis of the intensity of photoelectron lines will be given.

The linewidth of photoemission lines depends on the lifetime of the final state, which in turn is determined by the Auger and X-ray fluorescence transition rates. These two processes will be discussed in the next paragraph.

1.2 Processes occurring after photoionization and their effect on the spectrum

1.2.1 Secondary processes at the site of the hole

The initial event in the photoemission experiment is the ejection of an electron caused by the impinging X-rays. In Fig. 1.4a the ejection of a K-shell electron is depicted. The electronic configuration of the resulting ion with the vacancy in the K-shell is not stable and the vacancy will be

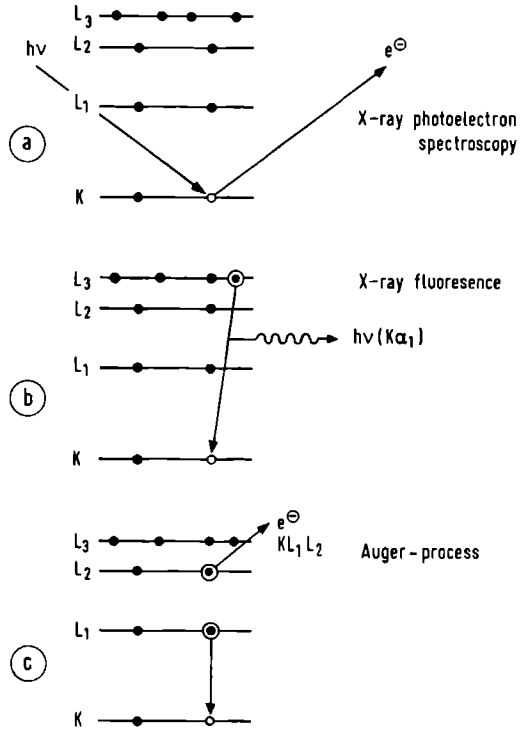

Figure 1.4 Two alternative modes of atomic de-excitation which follow upon the creation of an inner shell vacancy (a). In the X-ray fluorescence process (b) the inner vacancy is filled by an outer electron and the energy released is emitted as a photon. In the Auger process (c) the initial vacancy in the inner shell is filled by an outer electron and the available energy is transferred to another electron. The transition, as shown in the figure, where the initial hole in the K-shell is filled by an electron from the L_1-shell and the available energy is given to an electron in the L_2-shell, is designated KL_1L_2.

filled by one of the following two processes:

(i) radiationless transitions (Fig. 1.4c).

(ii) emission of characteristic X-ray radiation (Fig. 1.4b).

The first process leads to the so-called Auger emission. The vacancy (in level 3) is filled by an electron from a higher level (k) and the available energy is transferred to a third electron (in level 1), which is ejec-

ted, leaving behind a final state with two holes in outer orbitals. The Auger transitions are usually designated according to the three levels participating in the process. This is done with the aid of the X-ray level notation $K \rightarrow 1s$; $L_1 \rightarrow 2s$; $L_2 \rightarrow 2p_{1/2}$; $L_3 \rightarrow 2p_{3/2}$; etc. In the example depicted in Fig. 1.4c a vacancy in the K-shell is filled by an electron from the L_1-shell and the available energy is given to an electron in the L_2-shell. The resulting Auger electron is designated KL_1L_2. In several cases the energy splitting between different Auger transitions is too small to give resolved lines. In such cases, the notation of the transitions is combined (for instance $M_4N_{4,5}$ $N_{4,5}$). Fig. 1.2 contains the KLL Auger transitions of C, N and O and the $M_{4,5}N_{4,5}N_{4,5}$ Auger peaks of I.

The energy E(jkl;X) of the jkl Auger electron with final hole configuration X is given by

$$E(jkl;X) = E_B(j) - E_B(k) - E_B(l,k) \qquad (6)$$

where $E_B(l,k)$ is the binding energy of an electron in the l shell with a hole present in the k shell. The energy of the Auger electron is independent of the incoming radiation, provided the incident energy is large enough to create the initial hole. It has to be remarked that Auger spectroscopy can also be carried out using incident electrons to create the initial hole.

The lifetime width of XPS lines is dependent on Auger transition rates. When the primary vacancy is created in one of the inner subshells of the L, M, N, ... shells, the available energy is often sufficient to bring about a process in which one of the two final vacancies lies in an outer subshell of the primary vacancy's shell. Radiationless transitions of this type, for example $L_1L_3M_5$ are called Coster-Kronig processes. When all three orbitals involved in the Auger process are within the same shell one speaks of super Coster-Kronig processes. Because of the greater overlap between subshells of the same quantum number, Coster-Kronig transition rates are much faster than normal Auger rates. Consequently, very short lifetimes of holes in core levels i.e. very broad XPS lines occur when (super) Coster-Kronig processes are energetically possible[7,8]. As an example, Fig. 1.5 shows the 4s and 4p lines of Sb in the metallic state.

In the second mode of atomic de-excitation, X-ray fluorescence, the vacancy is again filled by an outer electron, but now the energy released is emitted as a photon. The emitted radiation is, of course, characteristic for

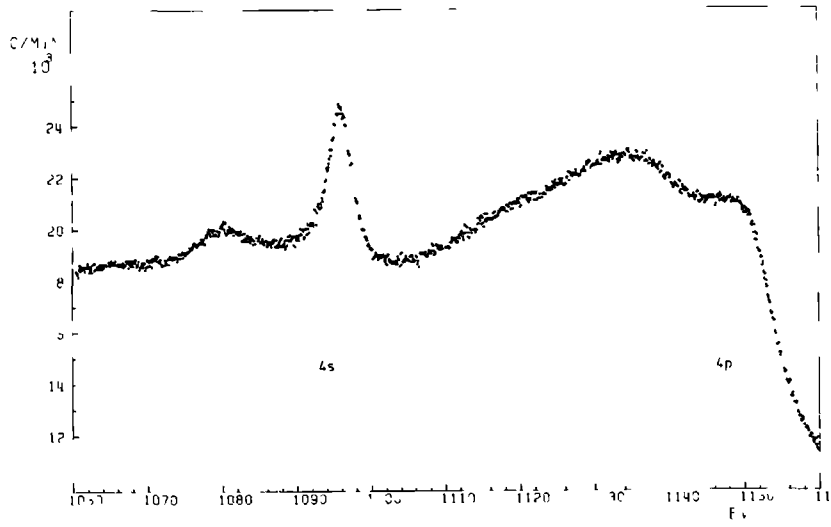

Figure 1.5 X-ray photoemission spectrum of the 4s and 4p levels of Sb in the metallic state. The energy scale is the kinetic energy of the ejected photoelectron. The width of the 4p level is very large due to the occurrence of (super) Coster-Kronig processes, that fill the hole in the 4p shell, which results in a very short lifetime of the hole. The peaks at about 10 eV below the 4s and 4p level are due to plasmon-loss satellites.

the sample. X-ray fluorescence is the more prominent decaying process for heavy elements.

1.2.2 Scattering of electrons after photoemission

In general, electrons originating deep in a solid will not escape without being inelastically scattered by interactions with the solid. The result is a loss of intensity from the peak of the unperturbed photoelectrons and the production of peaks and continua at lower kinetic energies, representing the energy losses. Examples of discrete energy losses are plasmon excitation (Fig. 1.6) - plasmons are collective oscillations of the electron density - and interband transitions (Fig. 1.8). The stepwise increase of the background after each XPS line is also due to (multiple) inelastically scat-

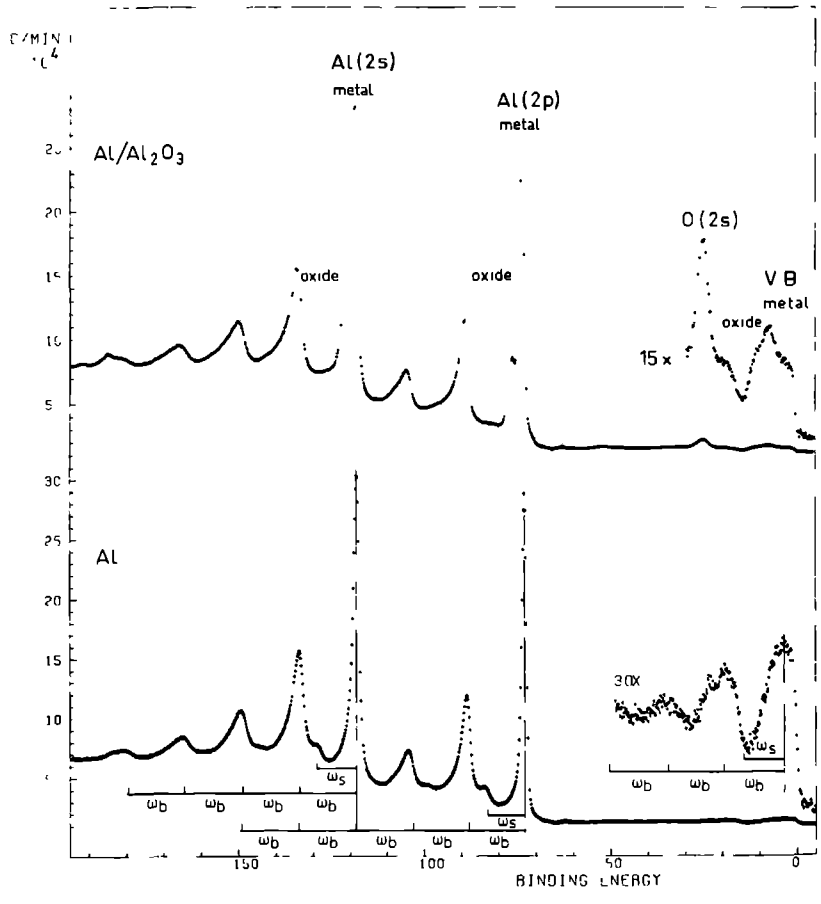

Figure 1.6 *Part of the X-ray photoemission spectrum of Al and Al/Al_2O_3. In the spectrum of Al metal several narrow lines are found to accompany the main 2s and 2p core lines and the valence band. The extra lines, plasmon-loss satellites, are due to photoelectrons, which have lost part of their kinetic energy by the excitation of one or several plasmons. The excitation can be both extrinsic and intrinsic. The plasmon-losses can be divided into bulk plasmons (separated by an energy $\hbar\omega_b$) and surface plasmons ($\hbar\omega_s$). Partial oxidation of the Al surface has a dramatic effect on the spectrum. The no-loss XPS lines split due to the presence of Al_2O_3: The binding energy of a 2s or 2p electron of Al in Al_2O_3 is different from that in Al metal. This difference in binding energy is called the chemical shift. Furthermore, an XPS line originating from O(2s) electrons is observed. The structure due to the bulk plasmon-losses remains the same and is characteristic for metallic Al, but the surface plasmon-loss satellite has disappeared.*

tered electrons (see for instance Fig. 1.2).

The depth from which an electron can escape with unimpaired energy is given by its mean free path length λ, and is dependent on the kinetic energy of the electron concerned. Experimental determinations of λ exist for a number of metals and compounds and for a number of different electron energies [9-11]. For electron energies between 10 and 2000 eV the values of λ vary from 5-25 Å (see Fig. 1.7). The absorption length of the incident photons is typi-

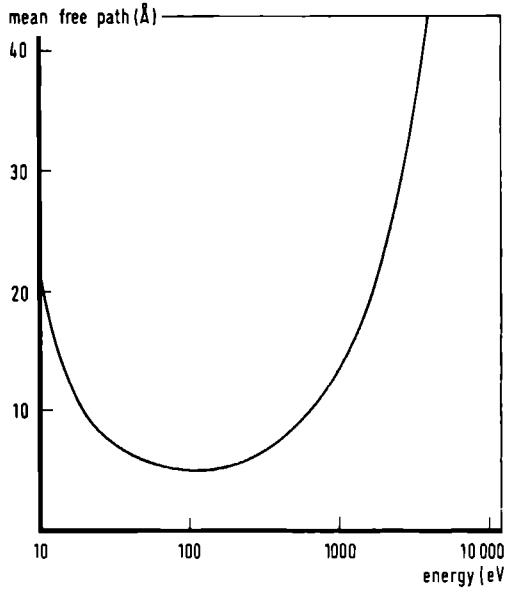

Figure 1.7 Electron mean free path, λ, as a function of the electron energy. The curve is determined from a number of experimental values of λ [9-11] for metals and compounds at several values of the electron energy.

cally in the order of 10^4 Å. As a result, the kinetic energy distribution of the photoelectrons in the vacuum is dominated by degraded electrons coming from deep inside the sample. The reason that the undegraded part can be observed in XPS is that it is narrow, while the degraded part is spread over a wide energy range.

Due to the small electron mean free path, XPS is a surface sensitive technique, and a small surface contamination can have a large effect on the

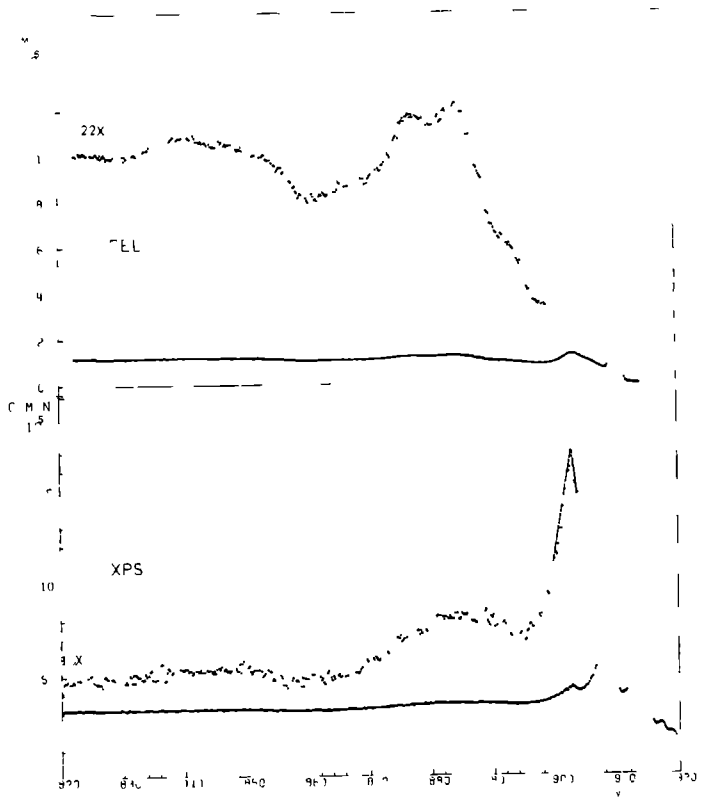

Figure 1.8 X-ray photoemission spectrum of the Pd(3d) levels and electron energy loss spectrum at a primary energy of 900 eV of Pd metal. The loss structure is mainly due to a surface plasron-loss and interband transitions. The loss structure of the EEL spectrum is very similar to that in the XPS spectrum.

experimental spectrum (see for instance Figs. 1.3 and 1.6). As a consequence, sample preparation is of major importance and will be discussed in section 1.4.

A more direct way to study energy losses is electron energy loss spectroscopy (EEL). Here the incident photons are replaced by electrons with a well defined (primary) energy, that can be varied. The EEL spectrum gives the distribution of the electrons that are scattered from the sample. A large peak is due to electrons that are scattered elastically. Peaks at lower energy are due to the characteristic energy losses in the sample. Fig. 1.8 compares the EEL spectrum of Pd metal at a primary energy of 900 eV with the

loss structure in the XPS spectrum of the 3d levels. The shape of the loss structure is similar in both spectra. In Fig. 1.9 the EEL spectra of Al and

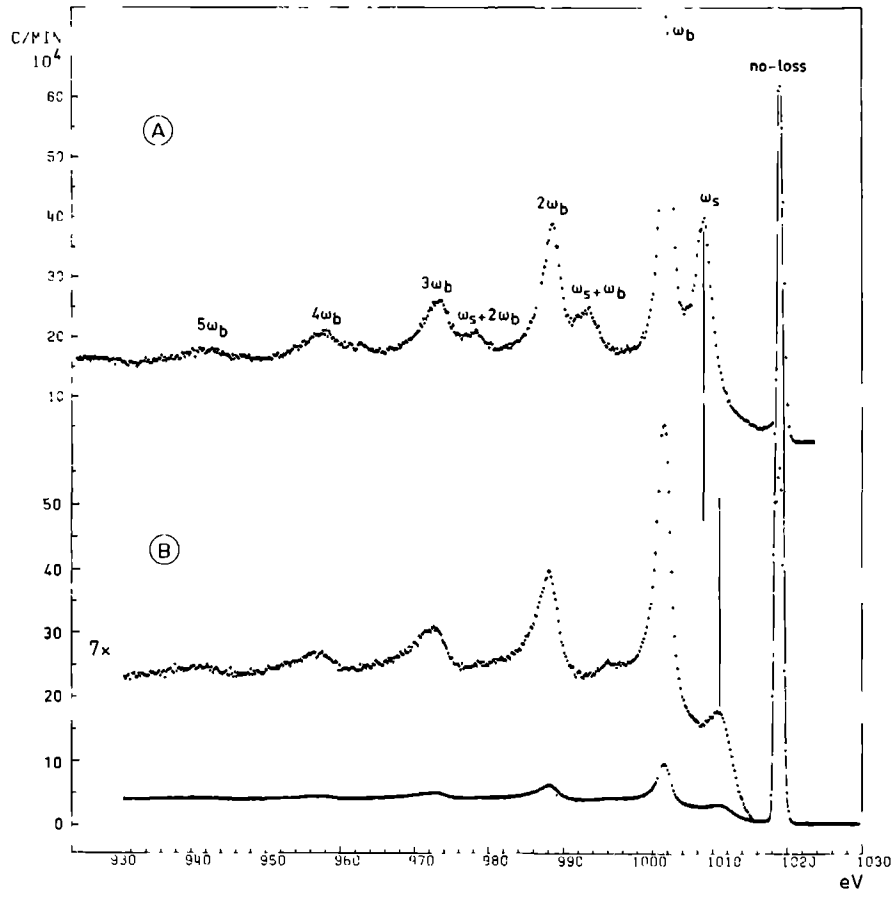

Figure 1.9 Electron energy loss spectrum of Al (A) and Al/Al_2O_3(B) at a primary energy of 1000 eV. In the spectrum of Al metal a rich structure is observed originating from extrinsic excitation of plasmons. The energy separation of the plasmon-loss satellites is the same as in the XPS spectrum (Fig. 1.8), but the lineshape is different. The surface plasmon-loss intensity in the spectrum of Al metal is increased compared with the XPS spectrum due to the fact that the electrons cross the surface twice and to the shorter information depth. Partial oxidation of the Al surface does not change the bulk plasmon-losses, but influences the surface plasmon-loss, which is less intense and displaced from its original position.

Al/Al_2O_3 is depicted. The plasmon-loss satellites should be compared with the satellites in the XPS spectrum (Fig. 1.6), especially for the surface plasmon-loss.

The inelastic scattering of the electrons has important consequences for the use of XPS in quantitative analysis. The theoretical values for the cross section of photoionization are calculated including all the possible final states (see section 1.3). The determination of the experimental intensity, however, is hampered by the occurrence of inelastically scattered electrons, that affect both the no-loss peak and hide other final states. Note that also in the case of Auger transitions inelastic scattering can occur.

1.3 Final state effects

Eq.(3) suggests a single peak to occur in the XPS spectrum for each electron orbital. The theoretical basis for this is Koopmans' Theorem[12] the binding energy of orbital j is equal to the negative of the orbital energy of orbital j in the initial state. This means that the final ionized state is described with the same one-electron wavefunctions as the initial state. Obviously this is not correct: the electrons in the ion will rearrange and the result of this relaxation is not necessarily unique. That is, several final states with different energy E_f are possible, resulting in more than one XPS line or, in some cases, in a broadening of the XPS line. The final state with the lowest energy (largest relaxation energy) is in general identified with the binding energy. In many cases this final state will have a much higher probability than the others. In the spectra of Figs. 1.1-3, for instance, this leads to the easily identifiable peaks. In solids the relaxation energy depends not only on the initial (atomic) configuration but also on the extra atomic electron distribution (see also chapter 5). Peaks ascribed to other final states (shake up satellites) can be seen in the spectra of the (pseudo)-halides (Fig. 1.3). However, it is not always possible to distinguish these "intrinsic" processes from characteristic energy losses ("extrinsic").

A more obvious example of different final states affecting the XPS spectrum is encountered when an electron is ejected from an orbital with angular momentum. In the case of gold, for instance, (Fig. 1.1) ejection of an electron from the filled 4f shell results in two final states $F_{5/2}$ and $F_{7/2}$ with a splitting given by the spin orbit coupling constant and an intensity ratio roughly equal to the multiplicity of each level. Ejection from an open shell

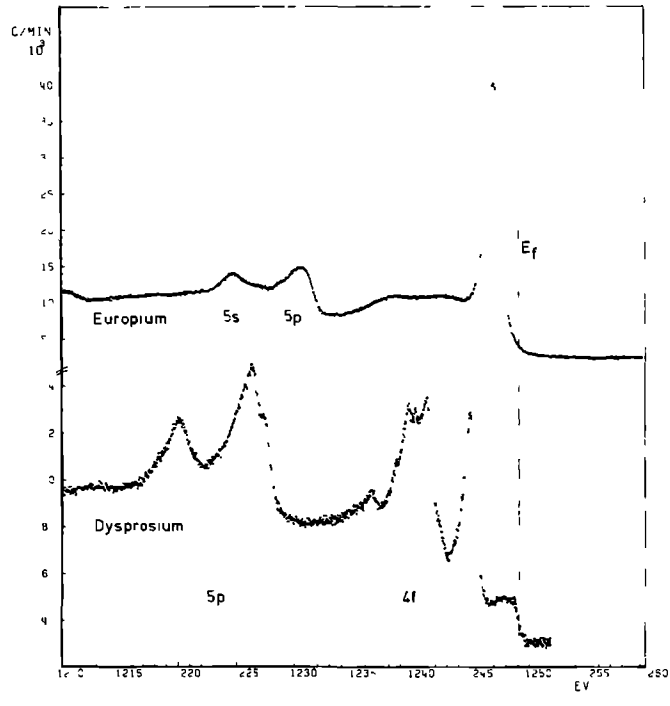

Figure 1.10 *Part of the X-ray photoemission spectrum of europium and dysprosium metal. Photoemission of an f electron produces an f shell with n-1 electrons not necessarily in its ground state. The probability with which the ground and excited states of $4f^{n-1}$ are occupied may be calculated by projecting the initial configuration on to the combination of the outgoing electron plus the manifold of final states[13]. In europium metal, Eu has the configuration $4f^7$ [$^8S_{7/2}$] i.e. all spins up (Hund's rule). Removal of an f electron results into the set of final states ^7F_J with J = 0,1,...6, which have only a very small splitting; thus only one single line is observed. In dysprosium metal (configuration $4f^9$) seven spins are up and two down. The removal of a spin-down electron leads to the ^7F state, the ground state of the $4f^8$ configuration. The peak at ~ 1245 eV has to be attributed to this final state. Removal of a spin-up electron leads to several quintet states[13] namely ^5L, ^5K, ^5I, ^5H, ^5G and ^5D all centered around 1241 eV. The final state analysis thus readily accounts for the observed structure in terms of configuration which does not exist in the initial state.*

can lead to a multitude of final states as examplified by the spectrum of dysprosium in Fig. 1.10. In metals the final state involves rearrangement of the conduction electrons around the hole created by photoemission. In alkali me-

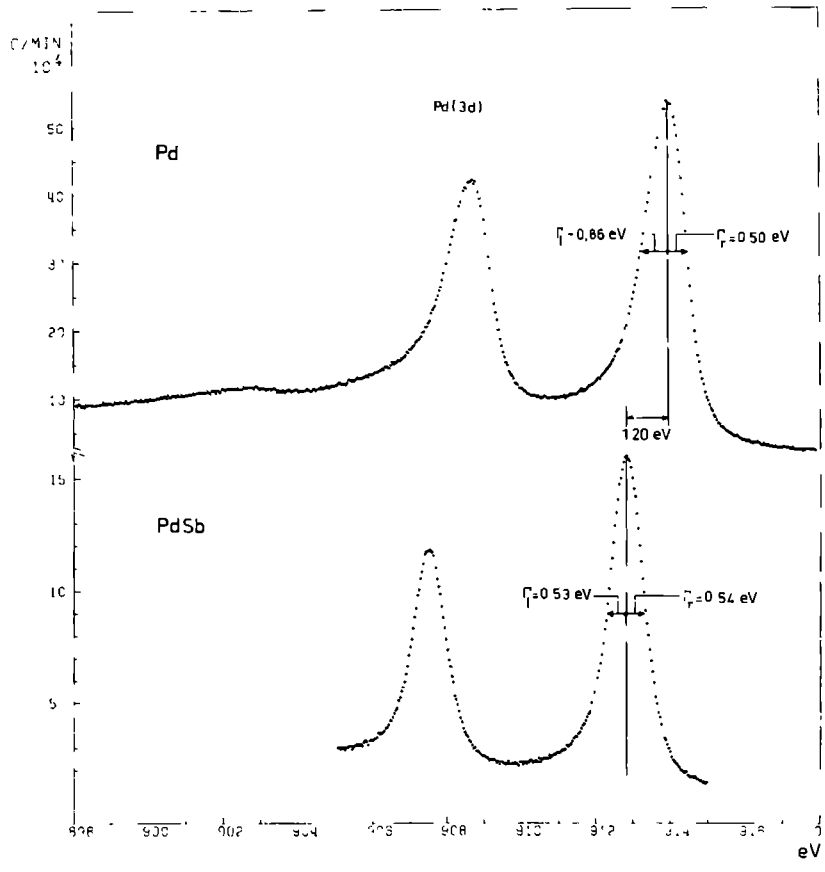

Figure 1.11 X-ray photoemission spectrum of the 3d levels of Pd in the metallic state and in the alloy PdSb. The asymmetry in the spectrum of Pd metal is due to electron hole excitations in the valence band, that accompany the ejection of the 3d electron. In PdSb the density of states at the Fermi energy is lower than in the metal (see Fig. 5.1) and as a consequence the asymmetry in the 3d lines is reduced. The shift in position between Pd and PdSb originates from the difference in electronic structure and in work function between both materials. A more detailed analysis is given in chapter 5.

tals this results in final states characterized by the loss of one or several plasmon energy units. This "intrinsic" plasmon-loss thus is of a totally dif-

ferent origin as the plasmon-losses due to inelastic scattering discussed in section 1.2.2 (extrinsic plasmon excitations). In chapter 4 an extensive study of plasmon-losses in Al and Mg metal is presented. In other metals notably those with high electron density at the Fermi level, electron hole excitations in the valence band can lead to a distribution of final states that show up as a strong asymmetry of the XPS lines. Fig. 1.11 illustrates this for the 3d levels of Pd. These lineshapes have been discussed extensively both theoretically[14] and experimentally[15].

1.4 Experimental aspects

In Fig. 1.12 the experimental set-up is shown. The spectrometer used in

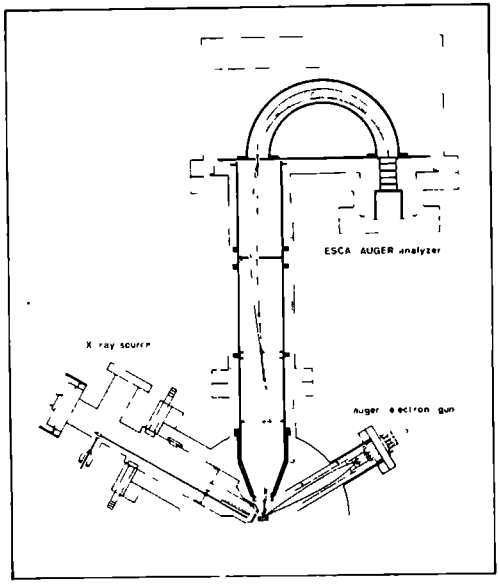

Figure 1.12 Experimental set-up of an X-ray photoemission or electron energy loss experiment. The spectrometer is a Leybold-Heraeus LHS-10 spectrometer. Details are given in the text.

the investigations discussed in this thesis is a Leybold-Heraeus LHS-10 photoelectron spectrometer. The radiation is generated in an X-ray tube of the Henke type. The copper anode has a magnesium or aluminum layer evaporated on it and consequently the energy of the photons is 1253.64 eV (Mg Kα radiation)

or 1486.65 eV (Al Kα radiation). The sample is a solid, that is mounted on the sample rod and is situated in the centre of the measurement chamber. The photoelectrons emitted at right angles to the plane of the sample are retarded and focussed by the electrostatic lens on an electrostatic hemispherical electron energy analyser, which has a variable pass energy. In recording a spectrum the retarding voltage is swept repeatedly through the desired energy range. The electrons transmitted through the analyser are detected by a venetian blind electron multiplier. The counts are stored in a multichannel analyser. The Auger electron gun emits electrons of well defined energy, and can

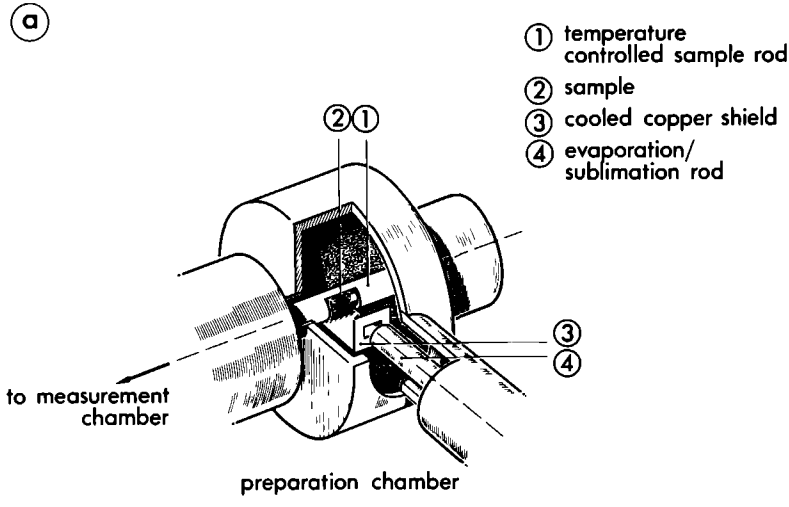

Figure 1.13 (a) Schematic view of the preparation chamber of the LHS-10 spectrometer. The sample can be heated or cooled. The sputtering gun and sample-manipulator are not included in the figure. (b) Evaporation/sublimation rod to sublime or evaporate samples in vacuum. In case of sublimation the compound is placed in a capillary and heated indirectly, while in case of evaporation the metal is placed in a tungsten coil. Since the pressure in the preparation chamber is in the order of 10^{-5} Pa clean samples can be obtained in this way.

be used both for electron energy loss spectroscopy and electron excited Auger spectroscopy as well. The vacuum in the measurement chamber and preparation chamber is maintained with the use of turbomolecular pumps. For samples with

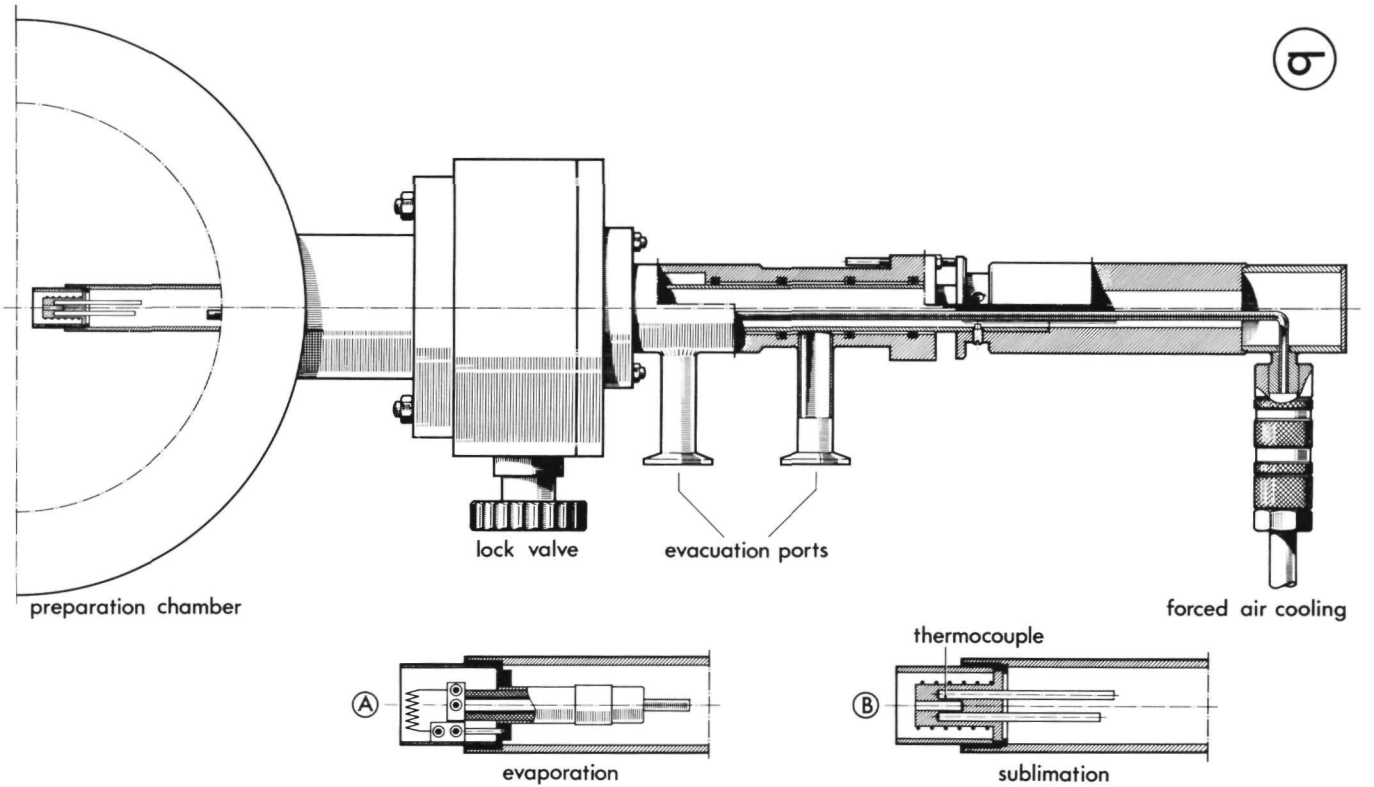
b
lock valve
evacuation ports
preparation chamber
forced air cooling
A
evaporation
thermocouple
B
sublimation

a low vapour pressure like metals and alloys the vacuum in the measurement chamber is in the order of 10^{-9} Pa. The calculations and the plotting of the spectra are done on an IBM 370/158 computer.

Since XPS is a surface sensitive technique, the preparation of the sample is important. For this reason, a separate sample preparation chamber with a separate vacuum system is attached to the measurement chamber (see Fig. 1.13a). Here the sample can be scraped, heated or cooled. An alternative sample preparation method is the sublimation or evaporation of the compound with a sublimation/evaporation rod as depicted in Fig. 1.13b. Another technique, often used with metals, is sputtering i.e bombarding the sample with high energy noble gas ions to remove surface layers.

However, many inorganic and organic compounds decompose during measurement. The decomposition rate can be reduced appreciably, at least for several gold compounds studied in chapters 6 and 7, by lowering the sample temperature and by using samples prepared by evaporation of dilute solutions on a graphite substrate.

In an actual experiment on a solid Eq.(3) for the kinetic energy of the photoelectrons has to be modified. The electron kinetic energy is measured with respect to ground potential of the analyser. However, if the solid sample is a conductor, there exists a contact potential between analyser and sample and the electron energy as measured by the analyser is

$$E_e = h\nu - E_B - e(\phi_{sp} - \phi_s) \tag{7}$$

where the contact potential $e\Delta\phi = e(\phi_{sp} - \phi_s)$ is the difference in workfunction ϕ between spectrometer and sample. Unfortunately ϕ_s is often unknown and correction for the contact potential is therefore impossible. For this reason binding energies are usually referenced to the Fermi level:

$$E'_B = E_B - e\phi_s \tag{8}$$

and Eq.(7) becomes

$$E_e = h\nu - E'_B - e\phi_{sp} \tag{9}$$

The spectrometer workfunction in our case is 4.49 eV (see chapter 3) so that

an electron originating from the Fermi level has an energy of 1249.15 eV in case of Mg Kα radiation. In Fig. 1.14 the different quantities are illustrated again.

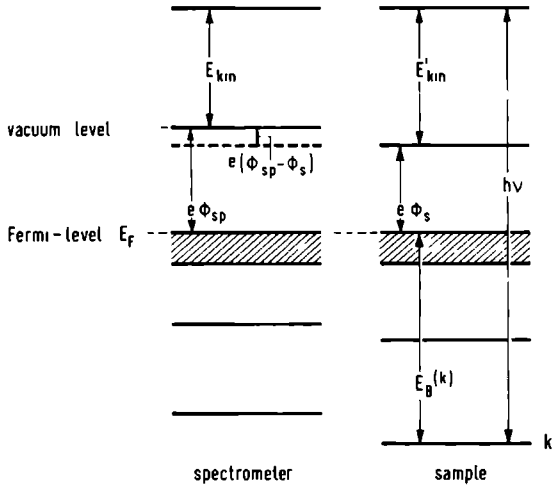

Figure 1.14 Illustration of the quantities involved in Eqs.(7-9). The contact potential, $e(\phi_{sp} - \phi_s)$ is given by the difference in work-function between the spectrometer (ϕ_{sp}) and sample (ϕ_s).

For insulators the situation is more complex because the potential difference between sample and spectrometer is not a physical constant, but is governed by experimental conditions. Photoemission leads to a positive charging of the sample and makes absolute measurements virtually impossible. In the literature various methods[16-20] have been proposed to provide the experimenter with some standard. The most wide-spread practice is the use of the C(1s) line as a reference, as carbon is almost always present as a surface contamination. However, we have used other methods, that will be detailed in chapters 6 and 7. It should be kept in mind that quoted binding energies of insulators refer to some fictitious Fermi level and never include the work-function.

In the foregoing, it was assumed, that the X-ray radiation is monochromatic. However, the X-ray spectrum of the Mg X-ray source consists in fact of the main $K\alpha_{1,2}$ doublet and a series of less intense lines at higher energy due to (multiple) ionized initial states [X-ray satellites or non-diagram

lines] superimposed on a continuous background [Bremsstrahlung]. In chapter 2 a method is described to remove from an experimental spectrum the lines due to the X-ray satellites. Fig. 1.15 shows an example.

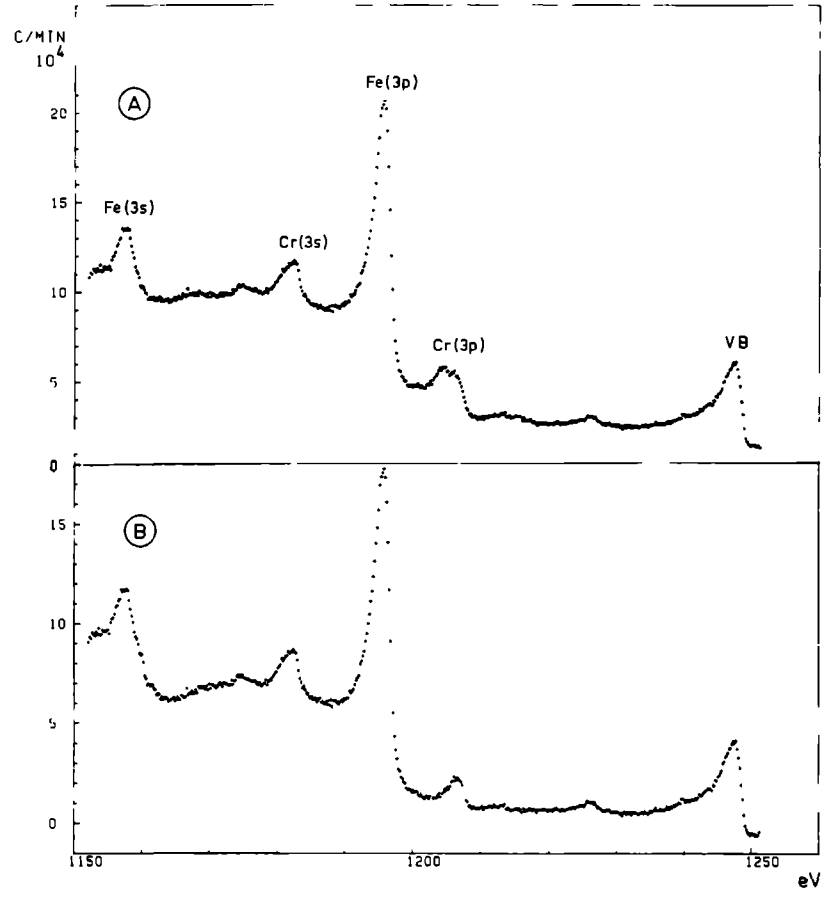

Figure 1.15 Part of the X-ray photoemission spectrum of Fe-Cr steel excited with Mg Kα radiation. The spectrum as measured (A) contains lines due to X-ray satellites. As a consequence the position of the Cr(3p) line cannot be determined. The lines due to X-ray satellites can be removed with a computer program detailed in chapter 2. The resulting spectrum (B) gives the real position and shape of the Cr(3p) line. XPS is very useful in the study of alloys, corrosion products etcetera.

Several textbooks are available on theory and applications of X-ray photoelectron spectroscopy[1,21-27] and the interested reader is referred to that literature.

1.5 References

1. K. Siegbahn, C. Nordling, A. Fahlman, R. Nordberg, K. Hamrin, J. Hedman, G. Johansson, T. Bergmark, S. Karlsson, I. Lindgren and B. Lindberg, Nova Acta Reg. Soc. Sci. Upsaliensis, 20 (1967) 1.
2. D.W. Turner, C. Baker, A.D. Baker and C.R. Brundle, Molecular Photoelectron Spectroscopy, Wiley & Sons, London (1969).
3. R. Prins and P. Biloen, Chem. Phys. Lett., 30 (1975) 340.
4. R.L. Martin and D.A. Shirley in "Electron Spectroscopy: Theory, Techniques and Applications" Ed. by C.R. Brundle and A.D. Baker, Academic Press, London (1977).
5. R.F. Reilman, A. Msezane, S.T. Manson, J. Electron Spectrosc. Relat. Phenom., 8 (1976) 389.
6. J.H. Scofield, J. Electron Spectrosc. Relat. Phenom., 8 (1976) 129.
7. S. Svensson, N. Mårtensson, E. Basilier, P.A. Målmquist, U. Gelius and K. Siegbahn, Physica Scripta, 14 (1976) 141.
8. L.I. Yin, I. Adler, T. Tsang, M.H. Chen, D.A. Ringers and B. Crasemann, Phys. Rev. A, 9 (1974) 1070.
9. C.J. Powell, Surf. Sci., 44 (1974) 29.
10. J.C. Tracy and J.M. Burkstrand, Crit. Rev. Solid State Sci., 4 (1974) 381.
11. J. Szajman, J. Liesegang, R.C.G. Leckey and J.G. Jenkin, Phys. Rev. B, 18 (1978) 4010.
12. T. Koopmans, Physica, 1 (1934) 104.
13. P.A. Cox, Y. Baer and C.K. Jörgensen, Chem. Phys. Lett., 22 (1973) 433.
14. S. Doniach and M. Sunjic, J. Phys. C: Solid State, 3 (1970) 285.
15. S. Hufner, G.K. Wertheim, J.H. Wernick, Solid State Commun., 17 (1975) 417.
16. G. Johansson, J. Hedman, A. Berndtsen, M. Klasson and R. Nilsson, J. Electron Spectrosc. Relat. Phenom., 2 (1973) 295.
17. L.J. Matienzo and S.O. Grim., Anal. Chem., 46 (1974) 2052.
18. Y. Mizokawa, H. Iwasaki, R. Nishitani and S. Nakamura, J. Electron Spectrosc. Relat. Phenom., 14 (1978) 129.
19. C.R. Ginnard and W.M. Riggs, Anal. Chem., 46 (1974) 1306.
20. A. Jaegle, A. Kalt, G. Nanse and J. Peruchetti, J. Electron Spectrosc. Relat. Phenom., 13 (1978) 175.

21. K. Siegbahn, C. Nordling, G. Johansson, J. Hedman, P.F. Hedén, K. Hamrin, U. Gelius, T. Bergmark, L.O. Werme, R. Manne and Y. Baer, ESCA applied to free molecules, North-Holland, Amsterdam (1969).
22. Electron Emission Spectroscopy, Ed. W. Dekeyser, L. Fiermans, G. Vanderkelen and J. Vennik, D. Reidel Publ. Co., Dordrecht (1973).
23. Th.A. Carlson, Photoelectron and Auger Spectroscopy, Plenum Press, New York (1975).
24. Electron Spectroscopy: Theory, Techniques and Applications, Vol. 1, Ed. C.R. Brundle and A.D. Baker, Academic Press, New York (1977).
25. D.A. Shirley, Adv. Chem. Phys., Vol. XXIII, Ed. I. Prigogine and S.A. Rice, John Wiley, New York (1973).
26. Electron Spectroscopy, Ed. R. Caudano and J. Verbist, Elsevier, Amsterdam (1974).
27. K. Siegbahn, Molecular Spectroscopy, Ed. A.R. West, Heyden and Son, London (1977).

CHAPTER 2

REMOVAL OF X-RAY SATELLITES FROM Mg Kα EXCITED PHOTOELECTRON SPECTRA*

P.M.Th.M. van Attekum and J.M. Trooster

Abstract - *A numerical method is described to remove X-ray satellite lines from photoelectron spectra excited with Mg Kα radiation. The satellite intensity is reduced to less than 0.25% of the $K\alpha_{1,2}$ line. An example is given of this method applied to the valence band spectrum of tin.*

2.1 Introduction

Although the use of monochromatized Al Kα X-rays as the excitation source in photoelectron spectroscopy is increasing, conventional Mg and Al Kα X-ray tubes are still widely used. In many applications the possibility of increasing the intensity at the expense of resolution is an advantage. Monochromatization results in a higher resolution (by a factor 3), removal of the X-ray satellites and Bremsstrahlung background. However, the X-ray satellites in a conventional X-ray source all have an energy higher than the main $K\alpha_{1,2}$ line and a fixed relation to this line. They can therefore be recognized as such in the photoelectron spectra. In a few papers, methods of removing the satellites[1] have been mentioned. In this paper a method is described of reducing the satellite amplitude in Mg Kα excited PES to less than 0.25% of the amplitude of the main line. An example is given of an application of this method.

2.2 Photoelectron spectrum of graphite

The X-ray emission spectra of Mg and Al have been studied by Krause and Ferreira[2]. Apart from the well known $K\alpha_3$ and $K\alpha_4$ satellites, there are a number of smaller lines with energies up to 50 eV larger than the $K\alpha_{1,2}$ line. Krause and Ferreira used the photoelectron spectrum of gaseous neon. In Fig. 2.1 the carbon 1s photoelectron spectrum of a single crystal of graphite excited with Mg Kα X-rays is given.

* *Published in: J. Electron Spectrosc. Relat. Phenom., 11 (1977) 339-347.*

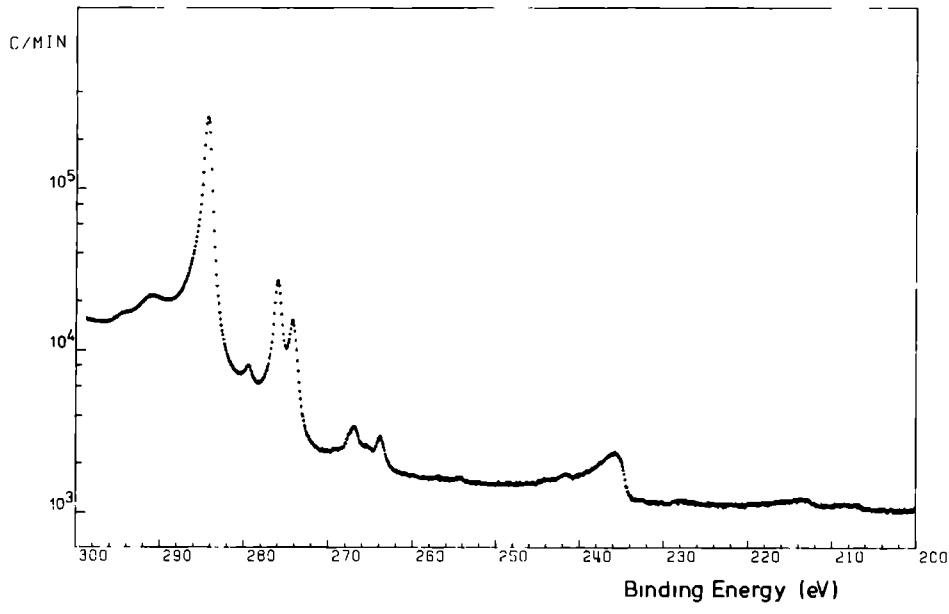

Figure 2.1 Carbon 1s photoelectron spectrum of a single crystal of graphite excited with Mg Kα radiation. The intensity is given on a logarithmic scale. The X-ray tube was operated at 200 W, number of channels 1024.

The spectrum was measured with a Leybold-Heraeus LHS-10 photoelectron spectrometer. The Henke-type X-ray tube has a copper anode with a Mg layer evaporated on it, and was operated at 10 keV and 20 mA. The photoelectrons emitted at right angles to the plane of the crystal are retarded and focussed by an electrostatic lens on an electrostatic hemispherical electron energy analyzer, which was set for a pass energy of 50 eV. In recording the spectrum the retarding voltage was swept repeatedly through the desired range with a period of 1 min. The electrons transmitted through the analyzer are detected by a venetian blind electron multiplier. The counts are stored in a multichannel analyzer. Total count in the C(1s) peak was ca. 10^6.

The linewidth of the main peak in Fig. 2.1 is 0.90 eV and the resolution in the spectrum is slightly better than in the spectrum of Krause and Ferreira, but otherwise there is excellent agreement on the high-energy side. The structure at the low-energy side is due to inelastic scattering of the photoelectrons in the graphite crystal.

2.3 Removal of the satellites

The X-ray satellites all occur at energies higher than that of the $K\alpha_{1,2}$ line and the energy as well as the intensity of the satellites have a fixed relation to the energy and intensity of the $K\alpha_{1,2}$ line. The method used to remove the satellites from the measured spectrum is based on the following assumptions: (1) the lineshape including the $K\alpha_{1,2}$ line of all X-ray lines is Lorentzian; (2) the linewidth of all satellites is not less than the linewidth of the $K\alpha_{1,2}$ line; (3) the observed photoelectron spectrum is a linear function of the X-ray spectrum. Specifically this means that the detection system should not show any dead-time effects.

The photoelectron spectrum is recorded as a digital, discrete energy signal Y(n) with n = 1, 2, ... N, and can be considered to be the response of a system S (= sample and spectrometer) to an input sequence X(n), which is the X-ray spectrum. Then Y(n) is given by the convolution sum of X(n) with the response function S(n) (ref. 3):

$$Y(n) = \sum_{k=-\infty}^{\infty} X(k)\, S(n-k) \equiv X(n) \star S(n) \qquad (1)$$

According to the first assumption, the continuous X-ray spectrum is described by a sum of Lorentzian lines

$$X(E) = \sum_{i=o}^{M} \frac{\Gamma_i^2 I_i}{\Gamma_i^2 + (E - E_i)^2} = \sum_{i=o}^{M} X_i(E) \qquad (2)$$

where i = 0 stands for the $K\alpha_{1,2}$ line.

If $E_n \leqslant E \leqslant E_n + \Delta E$ is the energy range corresponding to channel n of the MCA during a measurement, the discrete energy input is given by

$$X(n) = \sum_{i=o}^{M} X_i(n) \qquad (3)$$

with

$$X_i(n) = I_i \Gamma_i \tan^{-1}\left(\frac{E - E_i}{\Gamma_i}\right)\Bigg/ {}_{E = E_n}^{E = E_n + \Delta E} \qquad (4)$$

Then

$$Y(n) = \sum_{i=o}^{M} X_i(n) \star S(n) \tag{5}$$

According to the second assumption $\Gamma_i \geq \Gamma_o$ for all i, hence one can write

$$X_i(n) = X_i'(n) \star X_o(n) \tag{6}$$

with

$$X_i'(n) = I_i(\Gamma_i - \Gamma_o) \tan^{-1} \left(\frac{E - E_i}{\Gamma_i - \Gamma_o} \right) \Bigg/ \begin{matrix} E = E_n + \Delta E \\ E = E_n \end{matrix}$$

and $X_o'(n) = \delta(E_n - E_o)$ as the convolution of a Lorentzian with a Lorentzian is a Lorentzian.

Then

$$Y(n) = \sum_{i=o}^{M} X_i'(n) \star X_o(n) \star S(n) = \sum_{i=o}^{M} X_i'(n) \star S'(n) \tag{7}$$

where

$$S'(n) = X_o(n) \star S(n) \tag{8}$$

S'(n) is the photoelectron spectrum due to the $K\alpha_{1,2}$ line.

Because[3]

$$X_i'(n) \star S'(n) = \sum_{k=-\infty}^{\infty} X_i'(k) \cdot S'(n - k) = \sum_{k=-\infty}^{\infty} S'(k) \cdot X_i'(n - k)$$

$$= S'(n) \star X_i'(n) \tag{9}$$

the photoelectron intensity due to the X-ray satellites can now be calculated as the response to the input sequence S'(n).

In the following it is assumed that S'(n) is finite. Furthermore $X_i'(n)$ is made finite by putting $X_i'(n) = 0$ for $|E_n - E_i| > 10(\Gamma_i - \Gamma_o)$. As stated before, $E_i > E_o$ for all i and therefore if no photoelectron intensity is present in the energy range preceding the range being measured, the intensity Y(1) mea-

sured in the first channel is due to X'_o only and can be taken as equal to S'(1). The intensity at higher energies due to the satellites can then be calculated from Eq.(7) and subsequently subtracted. Thereafter, Y(2) = S'(2) and the process is continued to the last channel. In general, there is photoelectron intensity in the energy range preceding the range being measured and Y(1) is determined also by the X-ray satellites of the preceding energy range. Neglect of this would lead to discontinuities. Therefore Y(1) is corrected

$$Y_{corr}(1) = Y(1)/(1 + xsum)$$

where

$$xsum = \sum_{i=1}^{M} \sum_{n} X'_i(n)$$

This means that it is assumed that $Y(n) = Y_{corr}(1)$ for $n \leq 1$. The other channels can be corrected in a similar way.

The satellite response functions $X'_i(n)$ were determined from a spectrum as given in Fig. 2.1 with a least-squares minimalization program. The parameters E_i, I_i and $\Gamma'_i = \Gamma_i - \Gamma_o$ were determined such that the spectrum to the right of the main peak after subtraction of the satellites approached the tail of a Lorentzian with position E_B = 284.48 eV, $\Gamma/2$ = 0.38 eV, and an intensity given by the particular spectrum being analyzed.

2.4 Results

A total of twelve satellites was used to deconvolute the spectra. The parameters are given in Table 2.1. The result of a satellite subtraction using these parameters is given in Fig. 2.2. It can be seen that the remaining intensity variations are largest at the site of the α_3, α_4 satellites where they are of the order of 0.25% of the main peak. These remaining intensity variations can be traced to the assumption of Lorentzian lineshapes for the X-ray lines: the main line, for instance, is an unresolved doublet with intensity ratio 2 : 1.

The parameters given in Table 2.1 are a function of the X-ray source only and can be used also for other spectrometer functions. Figure 2.3 shows the 4d lines and valence band of Sn, before and after removal of the satellites. The

spectrum obtained after subtraction of the satellites should be compared with that obtained with monochromatized radiation by Pollak et al.[4]. The results are of comparable quality. From the shape of the spectrum at the Fermi edge of several metals the linewidth of the main line was determined to be 0.65 eV at most.

Although the aim of this research was the removal of the X-ray satellites from photoelectron spectra it is worthwhile to compare the satellite para-

Table 2.1 Position, relative intensity and linewidth difference with the $K\alpha_{1,2}$ line for X-ray satellites of Mg[+]

line	energy $E_i - E_o$ (eV)	peak-height I_i (% eV^{-1})	line width increase Γ_i' (eV)	area intensity A (%)
α'	4.90(2)	1.39	0.247	1.08(5)
α_3	8.40(1)	53.53	0.052	8.66(10)
α_3'	8.97(5)	11.05	0.021	0.72(5)
α_4	10.21(1)	6.31	0.310	6.14(10)
α_8	16.92(5)	0.20	1.30	0.80(5)
α_5	17.61(5)	0.79	0.15	0.37(5)
α_7	19.04(5)	0.23	0.50	0.36(5)
α_6	20.63(5)	0.60	0.29	0.55(5)
β_1	45.43	0.04	1.59	0.21(5)
β_2	46.78	0.02	1.05	0.06(1)
β_3	47.44	0.12	0.67	0.26(5)
β_4	48.74	0.28	0.67	0.60(5)

[+] *The numbering follows Krause and Ferreira[2] except for the β satellites, which have been artificially decomposed into four Lorentzians. The second column lists the energy distance to the $K\alpha_{1,2}$ line. The peak-height is given in percentage units of the $K\alpha_{1,2}$ line per ΔE, where ΔE is the energy increment per channel. The area intensity is listed in percentage units of the $K\alpha_{1,2}$ line and given by $A = \pi\Gamma_i' \cdot I_i$. Errors are given in units of the last decimal. No errors are given for the positions of the β satellites as this decomposition is rather arbitrary.*

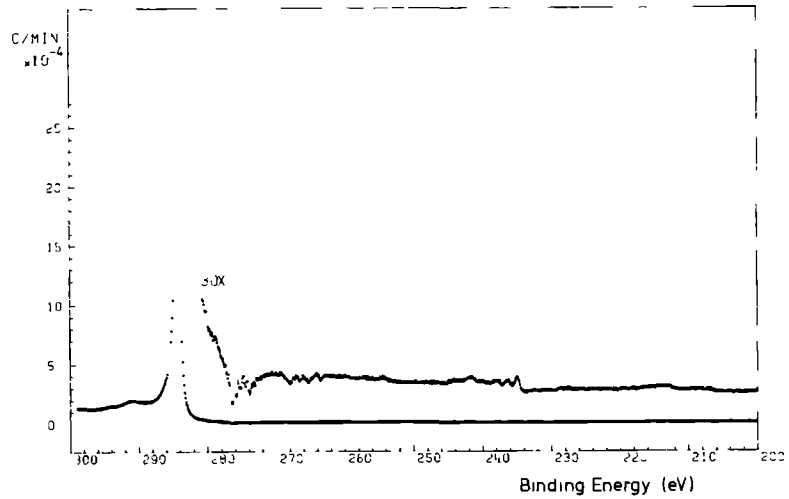

Figure 2.2 Same spectrum as given in Fig. 2.1 after subtraction of satellites with the intensity given on a linear scale.

Table 2.2 Position and relative intensity to the $K\alpha_{1,2}$ line for X-ray satellites of Mg according to Krause and Ferreira and this investigation

line	Krause and Ferreira (ref. 2)		this investigation	
	energy (eV)	intensity (%)	energy (eV)	intensity (%)
α''	3.6	0.3	-	-
α'	4.6	1.0	4.90	1.08
α_3	8.5	9.1	8.40	8.66
α_3'	-	-	8.97	0.72
α_4	10.1	5.1	10.21	6.14
α_8	15.7	0.12	16.92	0.80
α_5	17.4	0.76	17.61	0.37
α_7	19.2	0.29	19.04	0.36
α_6	20.6	0.48	20.63	0.55
β_1	-	-	45.43	0.21
β_2	-	-	46.78	0.06
β_3	-	-	47.44	0.26
$\beta=\beta_4$	48.6	0.55	48.74	0.60
$\beta_{1/2}$	49.9	1.7	-	-

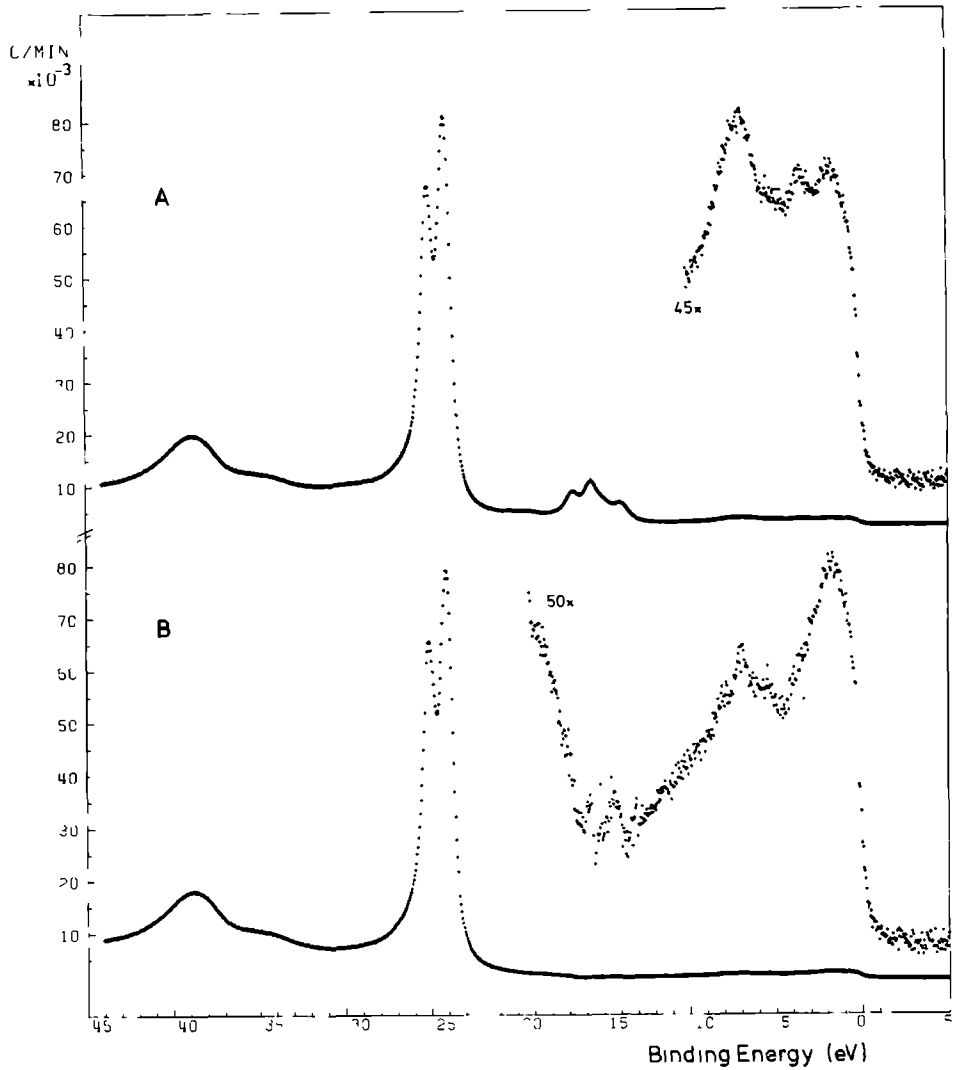

Figure 2.3 XPES spectrum of tin in the valence band region, excited with Mg Kα radiation. The X-ray tube was operated at 9kV, 30mA, number of channels 1024.

(A) As measured;

(B) After subtraction of satellite lines.

meters with those obtained by Krause and Ferreira[7]. This is done in Table 2.2. The intensities given are area intensities. There is good general agreement. It is known[2,5] that the positions and intensities of α_3 and α_4 are sensitive for oxidation of Mg. We have made an analysis as given above for four different anodes and only minor differences were observed. During the lifetime of the anode the intensities of the α_3 and α_4 lines change slightly. The differences are up to a few tenths of a percent of the intensity of the $K\alpha_{1,2}$ line over a four-month period.

2.5 Conclusions

With the method described, the X-ray satellite lines can be almost completely removed. The remaining signal has mainly a derivative character. This means that for broader lines the remaining signal is even smaller than 0.25%. Thus one of the disadvantages of unfiltered X-rays can be largely overcome in a simple way.

2.6 References

1. N. Beatham and A.F. Orchard, J. Electron Spectrosc. Relat. Phenom., 9 (1976) 129.
2. M.O. Krause and J.G. Ferreira, J. Phys. B, 8 (1975) 2007.
3. A.V. Oppenheim and R.W. Schafer, Digital Signal Processing, Prentice-Hall, Englewood Cliffs, New Jersey, 1975.
4. R.A. Pollak, S.P. Kowalczyk, L. Ley and D.A. Shirley, Phys. Rev. Lett., 29 (1972) 274; R.A. Pollak, L. Ley, F.R. McFeely, S.P. Kowalczyk and D.A. Shirley, J. Electron Spectrosc. Relat. Phenom., 3 (1974) 381.
5. W.L. Baun and D.W. Fischer, Advan. X-Ray Anal., 8 (1965) 371.

CHAPTER 3

ON THE RESOLUTION OBTAINABLE IN X-RAY PHOTOELECTRON SPECTROSCOPY WITH UNMONOCHROMATIZED Mg Kα RADIATION*

P.M.Th.M. van Attekum and J.M. Trooster

3.1 Introduction

In this paper we discuss the resolution obtainable in photoelectron spectra excited with unmonochromatized Mg Kα radiation. In section 3.2 we consider the various contributions to the instrumental resolution function and give theoretical estimates. In section 3.3 we discuss experimental results and compare them with theory.

3.2 Theory

The lineshape S(E) in an X-ray photoelectron spectrum is the result of a convolution of the lifetime lineshape of the level studied, I(E), and an instrumental resolution function, R(E):

$$S(E) = \int_{-\infty}^{\infty} I(E')\, R(E - E')\, dE' \equiv I(E) \star R(E) \qquad (1a)$$

The instrumental resolution function in turn is the result of a convolution of the lineshape of the exciting X-rays, $R_X(E)$, and the spectrometer function, $R_S(E)$:

$$R(E) = R_X(E) \star R_S(E) \qquad (1b)$$

For a magnesium X-ray tube $R_X(E)$ consists of the strong $K\alpha_{1,2}$ doublet (E = 1253.64 eV) and a number of weak lines at higher energy. The contributions of these weak X-ray satellites can be removed from the photoelectron spectrum using a method discussed elsewhere[1] and only the $K\alpha_{1,2}$ radiation

Submitted to: J. Electron Spectrosc. Relat. Phenom.

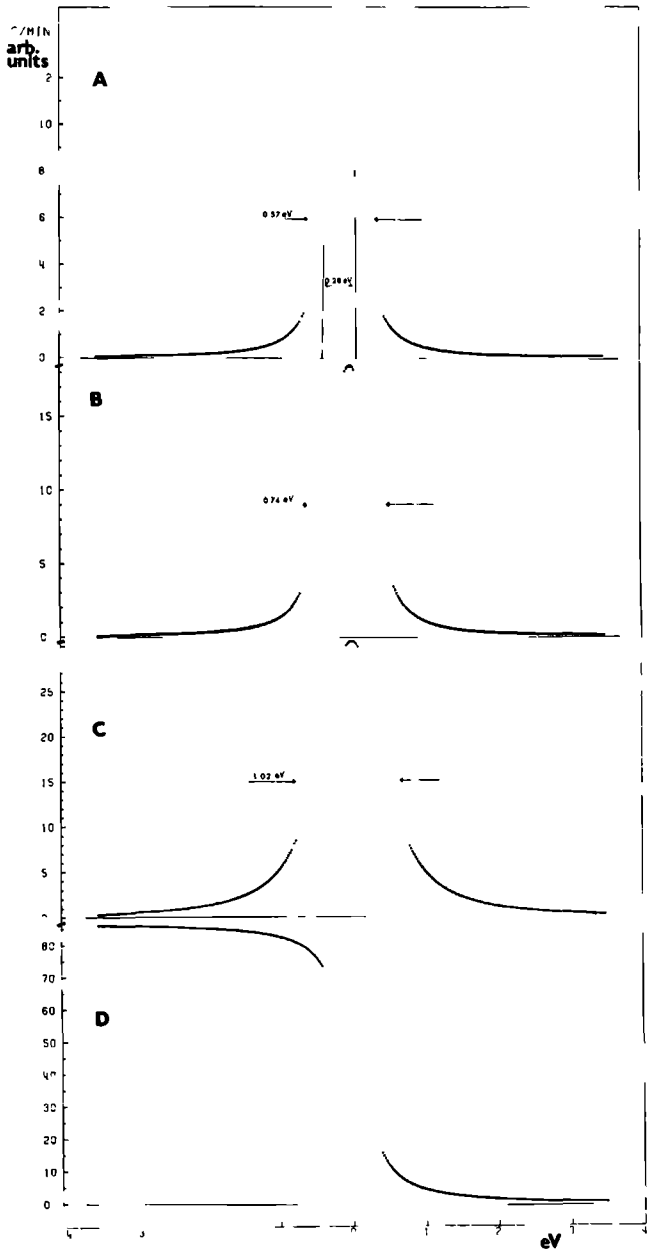

Figure 3.1 Calculation of experimental lineshapes from theoretical estimates.

A X-ray excitation spectrum of Mg calculated from[2]: $\Delta F_{LS}(2p) = 0.28$ eV, $\Gamma(1s) = 0.35$ eV and $\Gamma(2p) = 0.03$ eV. The intensity ratio of the constituent Lorentzians was ? : 1.

B Instrumental resolution function obtained by convoluting the result of (A) with a triangular function with F.W.H.M. = 0.40 eV.

C Convolution of (B) with a Lorenizian with F.W.H.M. = 0.38 eV, corresponding with the lifetime width of the $Ag(3d_{5/2})$ core level.

D Integral of (B).

will be considered in the following discussion. The lineshape of the $K\alpha_{1,2}$ line of Mg can be calculated using the results of Citrin et al.[2]. These authors determined the spin-orbit coupling of the 2p level as well as the lifetime width of the 1s and 2p levels using high resolution photoelectron spectroscopy $\Delta E_{LS}(2p) = 0.28$ eV, $\Gamma(1s) = 0.35 + 0.03$ eV and $\Gamma(2p) = 0.03 \pm 0.02$ eV. The $K\alpha_{1,2}$ X-ray lineshape can thus be calculated as the sum of two Lorentzians of intensity ratio 2 : 1, linewidth 0.38 ± 0.04 eV and splitting 0.28 eV. The result is shown in Figure 3.1A.

The spectrometer function $R_S(E)$ of the Leybold-Heraeus electron spectrometer used in this study has been discussed by Polaschegg[3]. $R_S(E)$ can be approximated by a triangular function with a full width at half maximum intensity (F.W.H.M.) equal to E/120 - quoted by the manufacturer -, where E is the pass energy of the hemispherical analyser. A numerical convolution of $R_X(E)$ of Figure 3.1A, with $R_S(E)$ for E = 50 eV gives R(E) as shown in Figure 3.1B. The F.W.H.M. of R(E) is 0.74 eV.

To compare with experiment the instrumental resolution function of Figure 3.1B has to be convoluted with the lifetime lineshape of the level studied, I(E). We discuss here two cases.

(i) Photoelectron lines of core levels of metals often have an asymmetrical lineshape; however, according to Hufner and Wertheim[4] the $3d_{5/2}$ line of Ag is an almost symmetrical Lorentzian with F.W.H.M. = 0.38 eV. Convoluting a Lorentzian of F.W.H.M. 0.38 eV with the resolution function of Figure 3.1B results in a lineshape as given in Figure 3.1C, with F.W.H.M. equal to 1.02 eV.

(ii) The lineshape at the Fermi-edge of the valence band of a metal with high d-density at the Fermi energy is essentially a step function. According to Eq.(1a) the experimental spectrum is therefore given by the integral of the instrumental resolution function. The result is shown in Figure 3.1D.

3.3 Experiment and discussion

The experiments were carried out with a Leybold-Heraeus LHS-10 photoelectron spectrometer described elsewhere[5]. The spectrometer was equipped with a preparation chamber in which Pd- or Ag metal was evaporated onto a stainless steel substrate at a pressure less than 10^{-6} Pa. Immediately after the evaporation the samples were transferred into the measurement chamber

through a valveless lock. The pressure in the measurement chamber was better than 10^{-8} Pa. The spectra were stored in a multichannel analyser and after completion of the measurement the X-ray satellite lines were removed from the spectrum[1]. Results for the 3d core levels of Ag and the valence band of Pd are given in Figure 3.2.

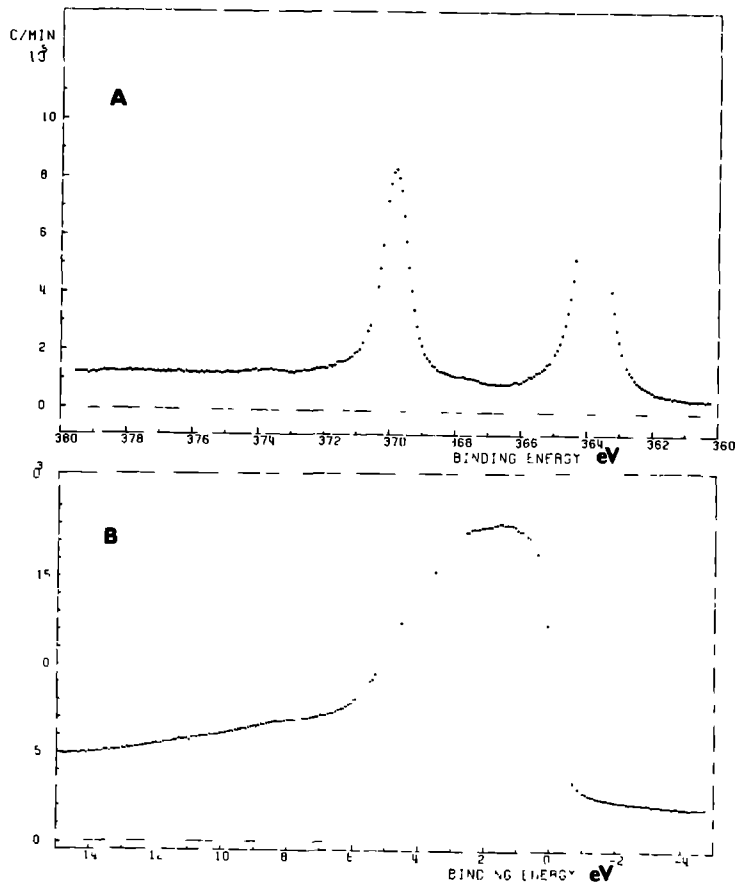

Figure 3.2 A Experimentally measured Ag 3d core lines at a pass energy of the electron spectrometer of 50 eV after removal of lines due to X-ray satellites.

B experimentally measured valence band of Pd metal at a pass energy of the electron spectrometer of 50 eV after removal of the intensity due to X-ray satellites.

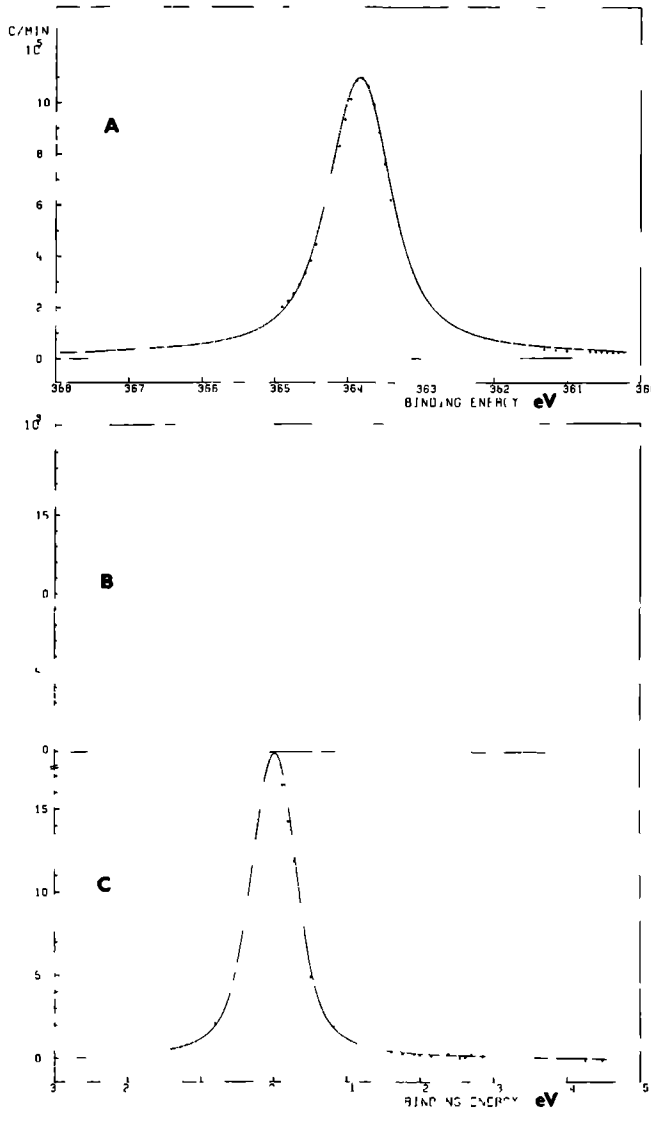

Figure 3.3 A $Ag(3d_{5/2})$ *photoelectron line of Figure 3.2A compared with the calculated lineshape of Figure 3.1C.*

B *Fermi-edge as measured with a pass energy of the electron spectrometer equal to 50 eV, on an expanded scale.*

C *Difference spectrum derived from Figure 3.3B compared with the calculated resolution function of Figure 3.1B.*

In Figure 3.3A we compare on an expanded scale the Ag($3d_{5/2}$) lineshape with the calculated lineshape of Figure 3.1D. The comparison is hampered by the presence of inelastically scattered electrons on the high energy side of the measured spectrum, but the measured spectrum is clearly ~ 0.1 eV narrower than predicted.

The measured spectrum of the Fermi-edge is a direct measure of the integrated instrumental resolution function. However, it is not very well suited to determine the instrumental resolution. This is because the resolution is defined as the width for a specified INTENSITY change (in our case F.W.H.M.), whereas the valence band spectrum at the Fermi-edge measures the integrated intensity and the width (or slope) of the Fermi-edge in the spectrum is therefore given by the change in AREA. Only for a Lorentzian line is the F.W.H.M. the same as the halfwidth (i.e. ΔE for $I = 3/4\ I_{max}$ to $I = 1/4\ I_{max}$) of the slope of the integrated spectrum. For all other conceivable experimental lineshapes the halfwidth of the integrated spectrum is less than the F.W.H.M. When the spectrometer function is not known the relation between the F.W.H.M. and the slope of the Fermi-edge can only be conjectured. However, the resolution function can be obtained directly from the Fermi-edge spectrum by numerical differentiation of the measured spectrum, i.e. by plotting the difference in intensity between adjacent channels.

In Figures 3.3B and 3.3C we give the measured Fermi-edge spectrum on an expanded scale together with the numerically differentiated spectrum. The latter is to be compared with the calculated spectrometer function: As in case of the Ag($3d_{5/2}$) line the measured F.W.H.M. is smaller than predicted by 0.1 eV.

The origin of the difference in predicted and measured F.W.H.M. of the resolution function probably is to be found in the spectrometer function $R_S(E)$. Using a formula for the resolution given by Polaschegg[3], we calculate F.W.H.M. = 0.31 eV instead of the value of 0.40 eV used. The calculated width of the resolution function however can be reduced with 0.1 eV if we reduce the width of the triangular spectrometer function $R_S(E)$ by 0.20 eV. It should be kept in mind, that the assumed triangular shape is only an approximation of $R_S(E)$.

Results for other pass energies of the hemispherical analyser of our photoelectron spectrometer are shown in Table 3.1.

The calculated electron density of states of bulk Pd contains a rather pronounced peak at the Fermi level[6-8] which could possibly result in an apparent narrowing of the measured Fermi-edge. However, XPS spectra taken with

Table 3.1 Full width at half maximum (F.W.H.M.) of the Ag($3d_{5/2}$) core level (A) and differentiated experimental Fermi-edge of Pd (B) as function of the pass energy of the hemispherical analyser. In (C) the halfwidth of the slope of the Fermi-edge of Pd is given. All values are in eV. The errors are estimates.

	pass energy 50 eV	pass energy 100 eV	pass energy 150 eV
A	0.90(3)	1.13(3)	1.33(3)
B	0.64(3)	0.82(5)	1.04(7)
C	0.46(3)	0.56(3)	0.76(3)

monochromatic Al Kα radiation do not show appreciable difference between the Fermi-edges of Pd and Pt on the one hand and Rh and Ir on the other hand[6] even though in the latter metals the Fermi-edge lies below the peak in the density of states. Also, calculation of the band structure of the (111) surface of Pd does not show this peak and in view of the surface sensitivity of XPS spectra this should result in a considerable reduction of the peak to the measured spectrum.

A measurement of the Fermi-edge of Ag is hampered due to the long Lorentzian tail of the d-band, but gives essentially the same width as Pd. Moreover, the results obtained above from the Fermi-edge of Pd are consistent with the measured linewidth of the Ag($3d_{5/2}$) core line.

In conclusion, we find that the instrumental resolution is 0.64 eV for a pass energy of 50 eV. The lower limit is 0.57 ± 0.03 eV due to the width of the exciting Mg $K\alpha_{1,2}$ radiation.

The measured resolution is not much less than values quoted for spectrometers equipped with a monochromator. This is also apparent from Figure 3.4, where we show the 4f- and valence band spectrum of dysprosium metal. This spectrum should be compared with that obtained with a monochromator as given by McFeely et al.[9].

3.4 Appendix

We have made a number of attempts to fit the measured Fermi-edge with an integrated Lorentzian, and the differentiated spectrum with a single Lorentz-

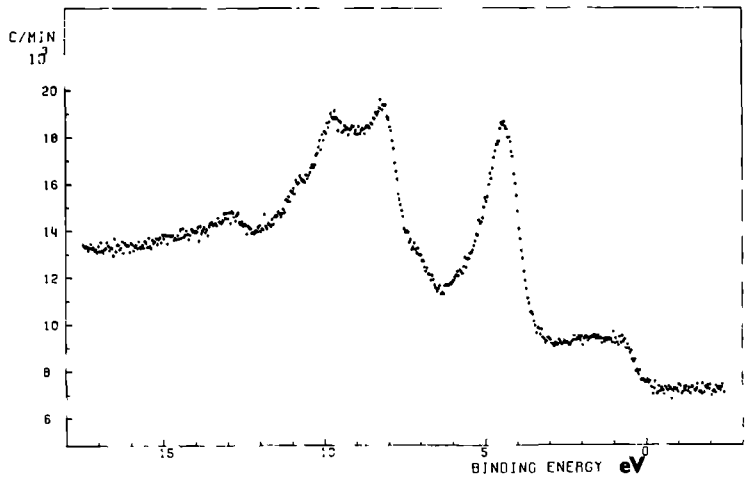

Figure 3.4 Experimentally measured 4f and valence band region of dysprosium metal at a pass energy of the electron spectrometer of 50 eV after correction for X-ray satellites.

ian. Representative results are shown in Figures 3.5A and 3.5B and in Table 3.2 the fitted F.W.H.M. of both the Lorentzian and $\tan^{-1}$ are listed as a function of the pass energy of the analyser. The F.W.H.M. of the fitted Lorentzians is only slightly less than the values obtained directly from the dif-

Table 3.2 Full width at half maximum (F.W.H.M.) of the Lorentzians used to fit the differentiated Fermi-edge of Pd-metal (A) and of $\tan^{-1}$ used to fit the experimental Fermi-edge (B) as function of the pass energy of the analyser. All values are in eV and the errors are estimates.

	pass energy 50 eV	pass energy 100 eV	pass energy 150 eV
A	0.58(3)	0.78(5)	0.96(7)
B	0.47(4)	0.59(4)	0.71(4)

ferentiated spectrum. Figure 3.5A shows that a Lorentzian is a reasonable approximation of the instrumental resolution function at a pass energy of 50 eV. However, the linewidths of $\tan^{-1}$ fitted to the Fermi-edge are too small for

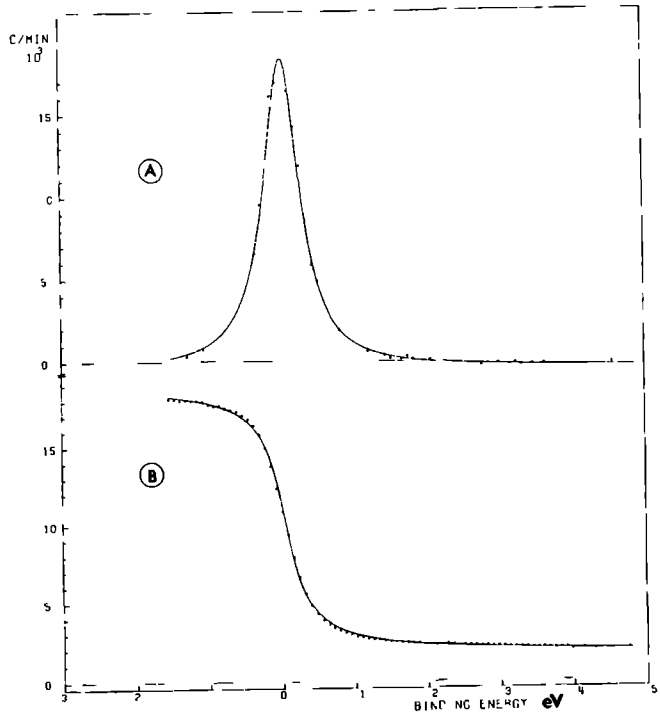

Figure 3.5 A *Fit to the differentiated spectrum of Figure 3.3C with a single Lorentzian (solid line) of F.W.H.M. = 0.58 eV.*
B *Fit to the experimental Fermi-edge of Pd metal of Figure 3.3B with* $\tan^{-1}$ *(solid line) of F.W.H.M. = 0.47 eV.*

the reasons explained in section 3.3. Fits with doublets of Lorentzians or $\tan^{-1}$ subject to the same constraints as used to calculate the X-ray spectrum gave only minor differences. Nevertheless, the fits have been useful as they result in an accurate determination of the photoelectron energy of electrons ejected from the Fermi level - i.e. 1249.15 ± 0.03 eV - and the intensity as function of the pass energy - i.e. 1.0 ± 0.1, 3.6 ± 0.1, 9.0 ± 0.1 for 50, 100 and 150 eV, respectively.

3.5 References

1. P.M.Th.M. van Attekum and J.M. Trooster, J. Electron Spectrosc. Relat. Phenom., 11 (1977) 363.
2. P.H. Citrin, G.K. Wertheim and Y. Baer, Phys. Rev. B, 16 (1977) 4256.
3. H.D. Polaschegg, Appl. Phys., 9 (1976) 223.
4. S. Hüfner and G.K. Wertheim, Phys. Rev. B, 11 (1975) 678.
5. H.G. Nöller, H.D. Polaschegg and H. Schillalies, J. Electron Spectrosc. Relat. Phenom., 5 (1974) 705.
6. N.V. Smith, G.K. Wertheim, S. Hüfner and M.M. Traum, Phys. Rev. B, 10 (1974) 3197.
7. S.G. Louie, Phys. Rev. Lett., 40 (1978) 1525.
8. S.G. Das, D.D. Koelling and F.M. Mueller, Solid State Commun., 12 (1973) 89.
9. F.R. McFeely, S.P. Kowalczyk, L. Ley and D.A. Shirley, Phys. Lett., 45A (1973) 227.

CHAPTER 4A

BULK AND SURFACE PLASMON-LOSS INTENSITIES IN PHOTOELECTRON, AUGER AND ELECTRON ENERGY LOSS SPECTRA OF Al METAL*

P.M.Th.M. van Attekum and J.M. Trooster

Abstract - *The intensities of plasmon-loss satellites of core lines and the valence band in X-ray photoemission spectra, as well as of Auger lines of Al are determined by convoluting the no-loss spectra with an asymmetric Lorentzian lineshape. Intrinsic processes contribute 25% of the total plasmon intensity of XPS core lines. For the valence band the intrinsic process is noticeably less and contributes approximately 12%. For the KLL and KLV Auger lines the intrinsic processes have the same contribution as for the XPS core lines. The extrinsic plasmon-loss intensity is measured independently on electron energy loss spectra. The lineshape of the plasmon-losses in the latter is different from that in XPS and Auger spectra, and both are different from theoretical plasmon energy distribution functions. The importance of intrinsic processes is confirmed by the observation of a plasmon-gain line in the KLL Auger spectrum.*

4A.1 Introduction

The existence of collective electron density oscillations (plasmons) is known since the theoretical work of Pines and Bohm[1-3]. Since that time many experimentalists using different techniques have studied these plasmons, especially in the free electron metals, where the plasmons manifest themselves most clearly. For Al metal many studies have been published using optical-[4], energy loss-[5,6] and electron transmission[7-9] techniques. In all these experiments the excitation of the plasmon occurs during the transport of the electron through the solid - the so-called extrinsic plasmon excitation. In X-ray photoemission a second kind of plasmon excitation is possible -the so-

*Published in Solid State Commun. 23, 187 (1977) 469-473.

called intrinsic process- where the excitation of the plasmon takes place simultaneously with the creation of the hole. Both contributions can be separated by an analysis of the area intensity of the subsequent plasmon-loss lines[10,11]. Since the intrinsic process is believed to contribute only a minor part to the plasmon intensity a careful analysis is necessary. In the present study on Al metal the plasmons accompanying the 2s and 2p core levels, the valence band and the X-ray excited KLL and KLV Auger lines will be discussed. Furthermore results of electron energy loss experiments will be given. The plasmon-losses of the core and valence band photoelectron spectra have been studied earlier[10-14] and we will comment on this work in connection with our results in section 4A.4.

In section 4A.2 the experimental aspects of our investigation are given. In section 4A.3 the experimental results are analysed. Finally the results are discussed in section 4A.4.

4A 2 Experimental

X-ray photoelectron, Auger and Electron Energy Loss (EEL) spectra were measured in a Leybold-Heraeus LHS-10 spectrometer. The excitation source for the XPS and Auger spectra was a Henke type X-ray tube with Mg anode operated at 200 watts. The $K\alpha_{1,2}$ line of Mg has too low energy for photoionization of the Al K-shell, but the Bremsstrahlung background proved to be of sufficient intensity to enable the study of the KLL and KLV Auger transitions. The X-rays illuminate the sample under an angle of 60° with the normal to the surface. Electrons escaping from the sample along the normal to the surface are retarded and focussed by an electron lens on the entrance slit of a hemispherical analyser set for a constant pass energy[15]. The spectra were measured by repeated scans of one minute and stored in a multichannel analyser. The X-ray satellite lines in the photoelectron spectra were removed with a computer program described elsewhere[16]. The EEL spectra were measured with primary electrons impinging on the surface under an angle of 60° with the normal. The energy width of the primary electrons was less than 0.5 eV.

The samples were prepared in a preparation chamber by evaporation on a polished stainless steel plate at a pressure of $\sim 10^{-6}$ Pa. Immediately after the evaporation the sample was slid into the measuring chamber through a valveless lock. The pressure during the measurements was less than 10^{-9} Pa. The samples were free of impurities, no carbon or oxygen could be detected.

4A 3 Results and analysis

4A 3 1 XPS core lines

The XPS spectrum of the 2s and 2p levels of Al metal with accompanying plasmon-loss lines is shown in Figure 4A.1A. This spectrum was measured with a transmission energy of 50 eV, which results in an instrumental lineshape which is Lorentzian with a linewidth of 0.60 eV [17]. Apart from the bulk plasmon-loss lines, a surface plasmon-loss line can be clearly discerned. In judging the intensity of the surface plasmon-loss line, it should be kept in mind, that electrons are measured, that escape at right angles to the surface. The binding energies are: 118.1 ± 0.1 eV for the 2s and 73.0 ± 0.1 eV for the 2p line. These values are the mean of three independent measurements and in good agreement with those published earlier[18-20]. The asymmetric lineshape of the no-loss lines is a consequence of electron-hole excitations and has been extensively discussed by Citrin et al.[21]. The plasmon-loss peaks are also markedly asymmetric. The shape of the plasmon-loss lines has been discussed by Hedin[22] and Penn[12-14]. However, we found that the theoretical lineshape of Hedin or Penn could only reproduce the main features of the measured spectra (see below). Therefore and for computational reasons a simpler analytical expression was used to describe the asymmetric plasmon-loss lines, using the following assumptions:

a) The n-th bulk plasmon-loss line P_n is given by the convolution of the no-loss line P_o with the plasmon-loss energy distribution function $D_n(E)$:

$$P_n(E) = P_o(E) \star D_n(E) \tag{1}$$

b) $D_n(E)$ is given by an asymmetric Lorentzian:

$$D_n(E) = \frac{I_n}{1 + \left(\frac{E - E_n}{\Gamma_n(E)}\right)^2} \tag{2}$$

Asymmetry is obtained by taking $\Gamma_n(E) = \Gamma_n^R$ for $E < E_n$ and $\Gamma_n(E) = \Gamma_n^L$ for $E > E_n$.

c) To reduce the number of parameters the following relations were assumed

to hold:

$$\Gamma_n^{R,L} = n\,\Gamma^{R,L} \tag{3a}$$

$$E_n = n\,E_B \tag{3b}$$

E_B is the bulk plasmon energy.

d) The surface plasmon energy distribution function is similarly described by:

$$P_S(E) = P_o(E) \star D_S(E) \tag{4}$$

with $D_S(E)$ also given by an asymmetric Lorentzian with parameters I_S, Γ_S^L, Γ_S^R and E_S.

e) Lines due to a combination of bulk and surface plasmon-losses are given by:

$$P_{S,n}(E) = P_o(E) \star D_{S,n}(E) \tag{5}$$

where $D_{S,n}$ is an asymmetric Lorentzian for which

$$\Gamma_{S,n}^{R,L} = \Gamma_n^{R,L} + \Gamma_S^{R,L} \tag{6a}$$

$$E_{S,n} = n\,E_B + E_S \tag{6b}$$

$$I_{S,n} = I_n \times I_S \tag{6c}$$

f) Multiple surface plasmon-losses are neglected.

In ref. 16 a method was given to determine the positions and intensities of the X-ray satellite lines in an XPS spectrum. With the assumptions given above the same method can be used to determine the parameters I_n, Γ^R, Γ^L, E_B, I_S, Γ_S^R, Γ_S^L, E_S. Starting from the right in Figure 4A.1A we can remove from the spectrum the intensity due to plasmon excitations using the algorithm des-

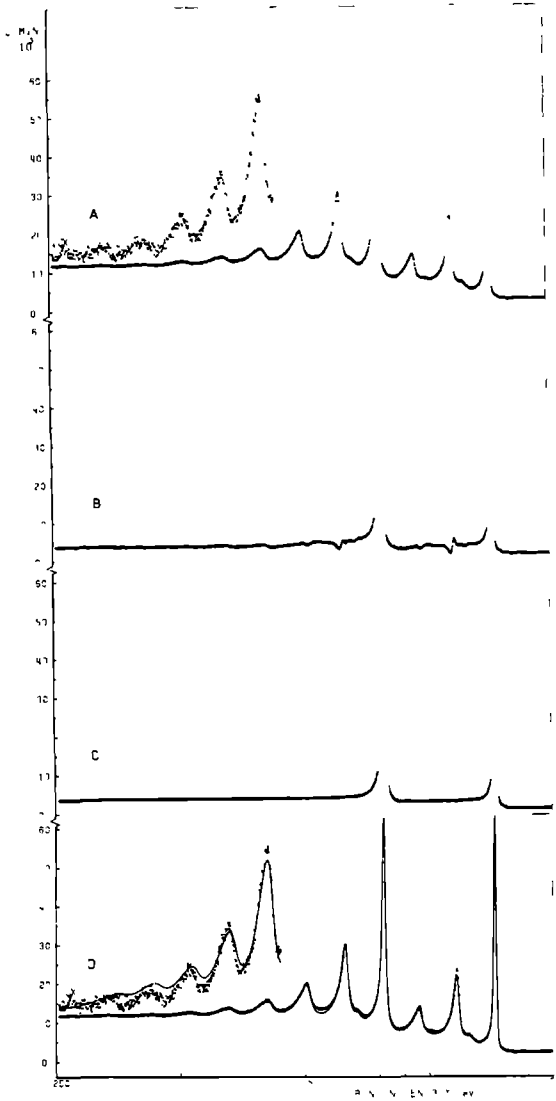

Figure 4A.1 Photoemission spectrum of the 2s and 2p core levels of Al metal. The spectrometer transmission energy was 50 eV, number of channels 1024.

A experimental spectrum after correction for X-ray satellites.

B after removal of the contributions of the plasmon-loss lines using the parameters of Table 4A.1.

C the same as (B) after baseline smoothing.

D comparison between experimental (points) and calculated plasmon-loss spectrum (solid line) using the parameters of Table 4A.1 and (C) as no-loss spectrum.

cribed in ref. 16. The best values of the parameters were determined with a least-squares fitting procedure[23] with the requirement that the spectrum to the left of the 2s line should approach the tail of a Lorentzian of linewidth 1.75 eV and intensity 55000 counts/min, superimposed on an adjustable constant term. Although the least-squares fitting was restricted to the part of the spectrum left of the 2s line the contributions in this region of the plasmon-loss lines associated with the 2p line were taken into account. Seven plasmon-loss lines of each XPS line have been included in the fitting procedure. Fits have been made to three independent measurements. Figure 4A.1B gives the spectrum obtained after removal of the plasmon-loss lines using the parameters given in Table 4A.1. Smoothing the spectrum of Figure 4A.1B, one

parameter	value	units
I_1	24.6 (5)	$\%eV^{-1}$
I_2	8.4 (3)	$\%eV^{-1}$
I_3	3.6 (2)	$\%eV^{-1}$
I_4	1.6 (1)	$\%eV^{-1}$
I_5	0.8 (1)	$\%eV^{-1}$
I_6	0.4 (1)	$\%eV^{-1}$
I_7	0.2 (1)	$\%eV^{-1}$
I_S	5.0 (2)	$\%eV^{-1}$
Γ^L	1.52(5)	eV
Γ^R	0.60(5)	eV
Γ^L_S	1.4 (1)	eV
Γ^R_S	0.5 (1)	eV
E_B	15.32(5)	eV
E_S	10.41(5)	eV

Table 4A.1 Best parameter values for the plasmon-losses in Al metal. The peak intensity (I_n, I_S) is given in percentage units of the no-loss peak per ΔE, where ΔE is the energy increment per channel. Errors are given in units of the last decimal.

obtains the spectrum of Figure 4A.1C which was used to generate the calculated plasmon-loss spectrum shown in Figure 4A.1D together with the measured data. A good fit is obtained up to the fourth plasmon-loss line. The value of E_B is in good agreement with the results of Williams et al.[24] who found E_B = 15.2 eV, but somewhat smaller than found by Pollak et al.[19] (E_B = 15.7 (2) eV) and Flodstrom et al.[20] (E_B = 15.7 eV). The ratio E_B/E_S = 1.47 is close to the theoretical value 1.41.

The following points should be noted:

a) The plasmon-loss lines are calculated as a convolution with the no-loss line. The parameters of $D_n(E)$ are therefore a direct measure of the shape, area intensity and position of the plasmon-loss lines relative to the no-loss line and are independent of the shape of the latter.

b) The 'misfit' as apparent in Figure 4A.1B is of a derivative character. Hence the area intensities of the calculated lines are a better measure of the intensity than is suggested by the absolute deviations present in Figure 4A.1B.

c) The inclusion in the fit of a constant term which raises the baseline on the left of the 2s line introduces an uncertainty in the intensities of the plasmon-loss lines. This baseline presumably is due to inelastic scattering of the photoelectrons other than plasmon excitation. The reliability of the results however, is supported by the good fit obtained for the first two plasmon-loss lines of the 2p line, which were not included in the sum of least-squares. Note that the 2p line is considerably narrower than the 2s line.

d) To a very good approximation the 2s and 2p lines in Figure 4A.1C can be described with a Doniach-Sunjic lineshape over the same range as used by Citrin et al.[21].

e) The intensity between the first and second bulk plasmon-loss line could not be fitted appropriately with the constraints described above. It appears that the intensity of the first bulk-surface plasmon-loss is higher as given by Eqs.(5,6).

Following Pardee et al.[10] the area intensity of the n-th plasmon-loss line is given by:

$$A_n = \alpha^n \sum_{m=0}^{n} \frac{(\beta/\alpha)^m}{m!} \qquad (7)$$

where $\alpha = (1 + \ell/L)^{-1}$, ℓ is the mean free path for extrinsic plasmon excitation, L is the mean attenuation length for electrons due to processes other than plasmon excitation. The parameter β is a measure for the probability $P_i(n)$ for intrinsic excitation of n plasmons:

$$P_i(n) = \frac{\beta^n}{n!} e^{-\beta} \qquad (8)$$

By least-squares fitting Eq.(7) to the experimental area intensities A_n as derived from the parameters listed in Table 4A.1, we found $\alpha = 0.62$ and $\beta = 0.21$. In Table 4A.2 both measured and calculated values of A_n are given.

parameter	experiment	theory
	%	%
A_1	82 ± 2	83
A_2	56 ± 2	54
A_3	36 ± 2	34
A_4	21 ± 2	21
A_5	13 ± 3	13
A_6	8 ± 3	8
A_7	5 ± 3	5
A_S	15 ± 3	-

Table 4A.2 Experimental area intensities of the bulk and surface plasmon-losses compared with theoretical values from Eq.(7) with $\alpha = 0.62$ and $\beta = 0.21$. The area intensity is listed in percentage units of the no-loss line and given by $A_n = \frac{\pi}{2}(\Gamma_n^L + \Gamma_n^R)I_n$.

With these values the total intensity in the bulk plasmon-loss lines is 2.3 times the intensity in the no-loss line and the intrinsic process contributes 25% of the total plasmon intensity. An estimate of the effect of the baseline on α and β was made by correcting the peak intensities of the plasmon-loss lines with the value of the baseline constant: either α or β changed by about 10%.

The surface plasmon-loss intensity A_S is very close to the theoretical estimate[25]. This is an indication of the high purity of the surface: even very slight oxidation reduces the surface plasmon intensity appreciably. The ratio $A_S/A_1 = 0.18$ is larger than the value which was found by Williams et al.[24] through extrapolation of angle dependent measurements. It should be remarked, that the area intensity of the third plasmon-loss line of the 2p line is approximately 25% of the 2s line, with which it nearly coincides. Therefore neglect of this line in analyzing the lineshape of the 2s line, as is done by Citrin et al.[21], is not allowed.

4A 3 2 XPS valence band

As mentioned before, the determination of the plasmon parameters is independent of the lineshape of the no-loss line. The same algorithm as was used to obtain the difference spectrum of Figure 4A.1B can therefore be used to remove the plasmon-loss peaks of the valence band spectrum.

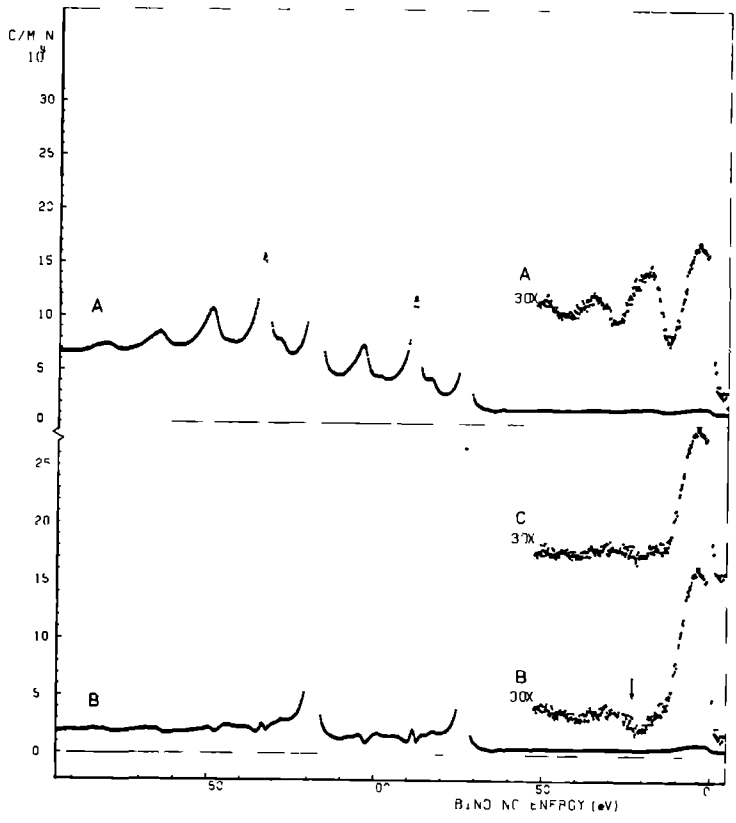

Figure 4A.2 Photoemission spectrum of the 2s and 2p core levels and valence band of Al metal. The spectrometer transmission energy was 150 eV.

A experimental spectrum after correction for X-ray satellites.

B after removal of the contribution of the plasmon-loss lines using the parameters of table 4A.1 (e.g. β = 0.91).

C after removal of the plasmon-loss lines with β = 0.10, for the valence band region.

Figure 4A.2A shows again the spectrum of the 2s and 2p lines but this time including the valence band. This spectrum was measured with a lower resolution than that of Figure 4A.1A, which results in a higher countrate. Figure 4A.2B is obtained by removing the plasmon-loss lines using the parameters given in Table 4A.1. The spectrum to the left of the 2s and 2p lines closely

resembles that of Figure 4A.1B. This demonstrates the lineshape independence of the method. However, for the valence band the subtracted plasmon intensity is too high. At the site of both the first and second plasmon-loss line the intensity in Figure 4A.2B is too low. This effect was observed in two independent measurements. Oxidation of the sample can be excluded as the cause. The bulk plasmon intensity is not very sensitive to oxidation and even a slightly oxidized sample should give an O(2s) line at the site of the arrow in Figure 4A.2B. Therefore, we believe that this is evidence of the fact that for valence band electrons the intrinsic plasmon intensity is less than for core electrons Using intensities calculated with $\beta = 0.1$ the spectrum given in Figure 4A.2C is obtained. This method of removing plasmon-loss intensity gives also better insight in the true shape of the valence band XPS spectrum.

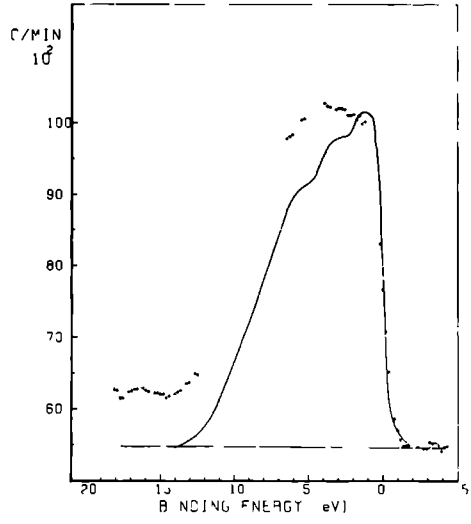

Figure 4A.3 Valence band of Al metal after removal of plasmon-loss lines. The solid line is taken from the work of Baer and Busch[26]. Spectrometer transmission energy was 150 eV.

In Figure 4A.3 we compare the shape of the valence band as determined by us with that of Baer and Busch[26] which has been used in many discussions. Especially at the high binding energy side there is considerable difference, which is due to the fact, that Baer and Busch have made no correction for surface- or bulk plasmon-loss lines but simply subtracted a slanted baseline from the

measured spectrum.

4A.3.3 Auger spectrum

In Figure 4A.4 we give the Auger lines in the region from 1300 to 1500 eV. This covers all but one of the KLL and all KLV transitions. Table 4A.3

Table 4A.3 Kinetic energies (in eV), corrected for the workfunction, of the KLL and KLV Auger levels in Al metal. The values given in the second column are the mean of at least three measurements. Errors are given in units of the last decimal.

peak	this work	Dufour et al[27] experiment	Dufour et al[27] theory
$KL_1L_1(^1S)$	1302.0(2)	1302.0	1304.0
$KL_1L_{2,3}(^1P)$	1341.2(2)	1341.4	1342.3
$KL_1L_{2,3}(^3P)$	1356.8(2)	1357.2	1358.5
$KL_{2,3}L_{2,3}(^1S)$	1387.1(2)	1387.2	1386.6
$KL_{2,3}L_{2,3}(^1D)$	1393.2(2)	1393.2	1393.5
$KL_{2,3}L_{2,3}(^3P)$	-	-	1398.1
KL_1M_1 $KL_1M_{2,3}$	1436.0(5)	-	-
$KL_{2,3}M_1$ $KL_{2,3}M_{2,3}$	1483.2(2)	-	-

lists our values for the kinetic energies (corrected for the workfunction) together with theoretical and experimental data by Dufour et al.[27]. For the KLL transitions there is good agreement. No literature data are available for the KLV transitions.

In Figure 4A.4-II we have subtracted the plasmon-loss lines, again using the parameters of Table 4A.1. For the KLL transitions the deviations from a smooth line are of similar shape and magnitude as in Figure 4A.1B. We conclude therefore, that the intensities of the plasmon-loss peaks are the same for XPS core lines and KLL Auger lines. The same appears to be true for the KLV lines: there is much less need for adjustment of the parameter β in this case. However it should be pointed out, that the noise prevents an accurate

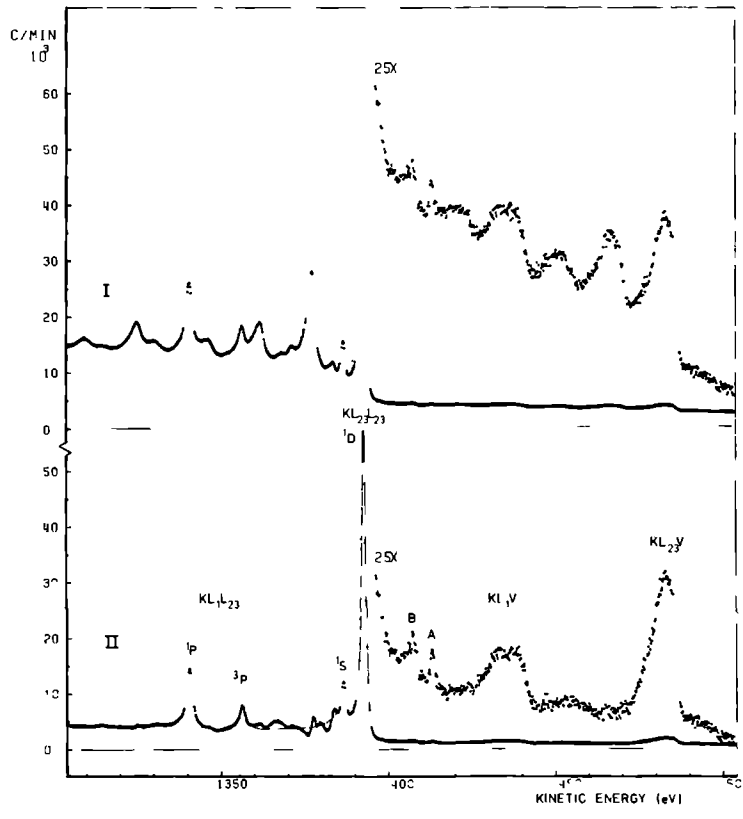

Figure 4A.4 X-ray excited KLL and KLV Auger spectrum of Al metal. The kinetic energy scale is corrected for the workfunction. (I) as measured. (II) after removal of the plasmon-loss lines using the parameters of Table 4A.1. A is the internal photo-emission Al 2p line, B a plasmon-gain peak of the $KL_{2,3}L_{2,3}(^1D)$ Auger line.

determination of the plasmon-loss intensities for these lines.

Figure 4A.4-II reveals in a beautiful way the structure of the KLV Auger lines. A striking difference with the XPS valence band can be observed. The differences are similar to those observed in Mg[28,29] and due to the fact that in the KLV Auger process emission occurs from the valence band as modified by the presence of the K-hole. In extreme cases this can result in atomic-like Auger spectra[30].

The Auger spectrum contains two more features which merit attention

a) The small peak marked A in Figure 4A.4-II has an energy of 1413.7 eV and is due to internal photoemission from the Al 2p level in the sample Al Kα X-rays of 1486.6 eV are generated through fluorescence decay of the holes in the K-shell. These X-rays, in turn, can lead to photoemission out of the 2s and 2p level. With a binding energy of 73.0 eV of the 2p electrons this results in a peak at ~ 1413.7 eV. The corresponding 2s line is difficult to discern because of the plasmon-losses or what is left of those after their removal.

b) The peak B has an energy of 1408.6 + 0.5 eV and is broader than peak A. The energy difference with the $KL_{2,3}L_{2,3}(^1D)$ Auger transition is 15.4 + 0.5 eV. This suggests that B is due to a plasmon-gain peak. This interpretation is supported by the observation of a similar line in the Auger spectra of Mg with an energy distance of 10.3 eV which is the plasmon energy for Mg[31]. The peak intensity of peak B is ~ 0.5% of the $KL_{2,3}L_{2,3}$ (^1D) Auger line. Plasmon-gain peaks have been reported for the LVV Auger peaks[32-34], but were later attributed to double ionization[35,36]. Double ionization can be excluded in our case because of the energy of the satellite and because low intensity X-rays were used as exciting radiation. According to Watts[37] and Almbladh[38] plasmon-gain satellites are possible for Auger lines and connected with the intrinsic plasmon-losses occurring on the creation of the primary hole. According to Almbladh[38], the shorter lifetime of the K-hole makes the occurrence of plasmon-gain satellites more probable in KLL Auger spectra than in the LVV spectra studied up to now. Although the noise prevents an accurate determination of the lineshape of the plasmon-gain peak, the linewidth seems comparable to that of the plasmon-loss lines.

4A 3 4 Electron Energy Loss spectra

EEL spectra were measured to obtain an independent determination of the parameter α in Eq.(7) In the EEL spectra intrinsic processes play no role and hence the area intensity ratio of successive plasmon-loss lines should be equal to α. Spectra were measured for primary energies ranging from 500 to 1500 eV. The intensity analysis of the EEL spectra is complicated by a background intensity due to inelastic scattering other than plasmon-losses. This background increases in intensity with decreasing primary energy.

There is a striking difference in the shape of the plasmon-loss lines of the EEL and XPS spectra: The lines appear to be more symmetrical and for primary energies greater than 750 eV narrower in the EEL spectra. This is partly due to the difference in shape of the no-loss line, but spectra calculated by convoluting the measured no-loss peak of the EEL spectrum with the lineshapes of the plasmon-loss lines derived from the XPS spectrum result in broader plasmon-loss lines than observed. We have, therefore, fitted the measured EEL spectra with symmetrical Lorentzians. The background was approximated by $B(E) = b(1 - a \exp(-(E - E_o)/c))$, E_o is the primary energy, b, a and c are parameters to be fitted. Within each pair of bulk and surface plasmon-loss lines, P_n and $P_{S,n-1}$, the linewidth was kept equal: $\Gamma_n = \Gamma_{S,n-1}$ (see section 4A.3.1 for definition symbols). Also the ratio $R = I_{S,n-1}/I_n$ was taken the same for all n, except for n = 1 because of the large uncertainty in the background under the first pair. The area intensity A_n of the n-th bulk plasmon-loss line was assumed to be given by $A_n = \alpha A_{n-1}$ for $n > 1$. Furthermore, a small peak corresponding with excitation of two surface plasmons was included in the fit. The peak intensity of this line (I_S^2) was used as a parameter, while the linewidth was fixed at $2\Gamma_1$. Thus, the following adjustable parameters were used in the fit: I_1, I_S/I_1, R, I_S^2/I_1, α, Γ_n (n = 1 to 5), E_S, E_B, and the baseline parameters a, b and c.

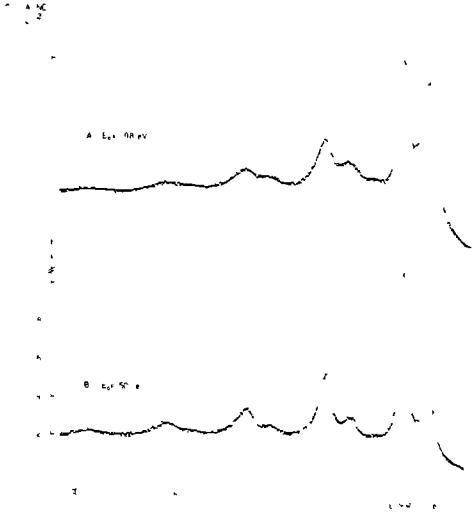

Figure 4A.5 Electron Energy Loss spectra of Al metal.

A Fit of experimental spectrum (points) with symmetrical Lorentzians at a primary energy of 498 eV. The baseline is indicated with a solid line. The zero of the energy scale corresponds with the position of the maximum of the no-loss line.

B Same as A at a primary energy of 1500 eV.

Table 4A.4 Best parameter values for the plasmon-losses in the EEL spectra of Al metal as a function of the primary energy E_o. Meaning of the symbols is given in the text. Errors are estimates based on several fits and given in units of the last decimal.

	E_o = 498 eV	E_o = 751 eV	E_o = 1000 eV	E_o = 1252 eV	E_o = 1500 eV
E_B(eV)	15.7 (1)	15.6 (1)	15.6 (1)	15.5 (1)	15.5 (1)
E_S(eV)	10.8 (1)	10.6 (1)	10.6 (1)	10.6 (1)	10.6 (1)
I_S/I_1	0.99(5)	0.75(5)	0.60(5)	0.55(5)	0.47(5)
R	0.53(5)	0.40(5)	0.36(5)	0.30(5)	0.28(5)
I_S^2/I_1	0.19(3)	0.11(3)	0.08(3)	0.06(3)	0.04(3)
α	0.62(2)	0.61(2)	0.63(2)	0.63(2)	0.61(2)
Γ_1(eV)	2.6 (1)	2.1 (1)	2.0 (1)	1.9 (1)	1.7 (1)
Γ_2(eV)	4.5 (1)	3.6 (1)	3.4 (1)	3.2 (1)	2.9 (1)
Γ_3(eV)	6.9 (2)	5.5 (2)	5.1 (2)	4.5 (2)	4.2 (2)
Γ_4(eV)	8.4 (3)	7.7 (3)	6.7 (3)	6.0 (3)	5.2 (3)
Γ_5(eV)	10.4 (4)	11.2 (4)	8.0 (4)	8.0 (4)	7.0 (4)
a	1.27(3)	1.21(3)	1.30(3)	1.40(3)	1.35(3)
c(eV)	11.0 (3)	10.1 (3)	9.6 (3)	10.2 (3)	11.4 (3)
I_1/b	9.4 (1)	10.6 (1)	13.0 (1)	13.1 (1)	13.2 (1)

Figs. 4A.5A and 4A.5B give the best fit for primary energies of 498 and 1500 eV and Table 4A.4 lists the parameter values obtained.

The following points should be noted:

a) The value of α is constant for primary energies ranging from 500 to 1500 eV and has the value 0.62 + 0.02. This value of α is in excellent agreement with the value of α determined from the XPS spectra.

b) The linewidth of the n-th plasmon-loss line is given by $\Gamma_n = n\Gamma + \Gamma_o$, where $\Gamma_o \simeq 0.5$ eV is the linewidth of the no loss line. Γ changes from 2.1 eV at 498 eV to 1.2 eV at 1500 eV.

c) The linewidth of corresponding plasmon-loss lines increases with decreasing primary energy.

d) The shape of the baseline is the same over the whole range (a and c are constant), but the intensity of the baseline relative to the intensity of the first plasmon-loss line (b/I_1) increases with decreasing primary energy.

e) The surface plasmon-loss intensity is much higher than in the XPS spectrum This is due to the short penetration depth of the primary electrons and to the fact that the detected electrons have crossed the surface twice.

4A 4 Discussion

This is not the first attempt to determine the intensities of plasmon-loss peaks in XPS spectra and before discussing our results we comment briefly on some of the recent papers on this subject. The first attempt to determine the plasmon-loss intensities was made by Pardee et al.[10]. These authors neglected the asymmetry of the plasmon-loss lines and fitted with Gaussians. Moreover, the fact that the plasmon-loss lines are a convolution of the no-loss line with the plasmon energy distribution function was not taken into account. The same approach was used by Williams et al.[24] in a study of the angular dependence of the plasmon intensities. A rough analysis was made by Fuggle et al.[39]. More recently Steiner et al.[11] have published results on Be, Na, Mg and Al. For Al these authors find $\alpha = 0.67$ and $\beta = 0.10$. However, no details of the fitting procedure are given. According to the same authors the same parameters as used for the core lines give good results for the valence band spectra of Be, Na and Mg[40]. However, these good fits are obtained including a background correction, which assumes a background proportional to the integrated intensity. As pointed out recently by Citrin et al.[21] there is no experimental basis for this correction.

In all these cases Al Kα radiation was used. However, the plasmon-loss intensities are not expected to depend much on the kinetic energy of the photoelectrons. A comparison between spectra obtained by us with Mg Kα and Al Kα radiation did not reveal marked differences.

In a series of papers Penn has used a fundamental approach, calculating intensities and lineshapes from theory[12-14]. The bulk plasmon lineshape, P(E,E'), was derived from the Lindhard dielectric function $\varepsilon(q,\omega)$.

$$P(E,E') = \frac{v(E)}{\pi a_o E} \int \frac{dq}{q} \operatorname{Im}\left[\frac{1}{\varepsilon(q,E-E')}\right] \tag{9}$$

with

$$\operatorname{Im}\left[\frac{1}{\varepsilon(q,\omega)}\right] = \frac{\omega_p^2 \omega \tau_q}{\left[(\omega^2 - \omega_q^2)^2 + (\omega\tau_q)^2\right]} \tag{10}$$

ω_p is the plasmon frequency for wavevector q = 0, τ_q is a measure for the lifetime broadening, which is related to the linewidth of the plasmons. Gibbons et al.[41] determined experimentally the linewidth of the plasmons in Al as a function of the wavevector:

$$\Gamma(\omega_q) = 0.9 + 3.25\ q^2 \tag{11}$$

where $\Gamma(\omega_q)$ is expressed in eV and q in $Å^{-1}$. The relation between the plasmon energy $\hbar\omega_q$ and q is given by[9,41]

$$\hbar\omega_q = \hbar\omega_p + 3.01\ q^2 \tag{12}$$

We have calculated numerically the lineshape resulting from Eq.(9). The result is shown in Figure 4A.6. In two consecutive papers Penn was able to ob-

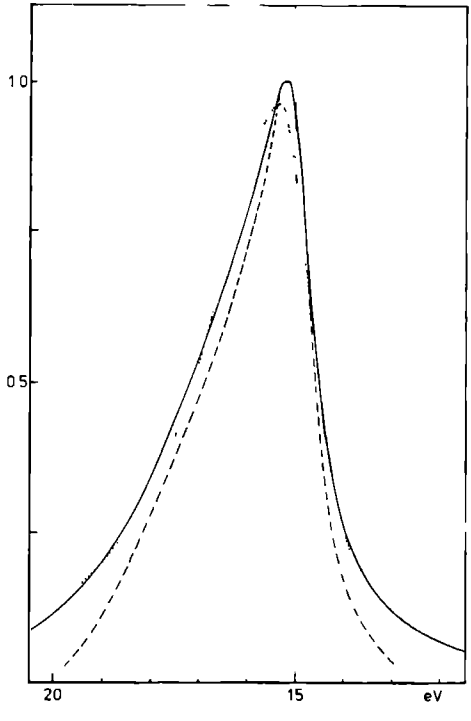

Figure 4A.6 The plasmon energy distribution function calculated with the model of Penn [Eq.(9)] (----), the model of Hedin [Eq.(13)] (——). In both cases $\hbar\omega_p$ = 15.0 eV. Also given is the asymmetric Lorentzian (····) fitted to the curve of Hedin. This line has Γ^L = 1.88 eV and Γ^R = 0.76 eV.

tain good fits to experimental data with[13] and without[12] inclusion of intrin-

sic processes. In a recent paper the plasmon-losses of the valence band were analysed[14]. However, using the lineshape of Figure 4A.6 we were not able to reproduce the measured spectrum very well. This is illustrated in Figure 4A.7A. To obtain the calculated spectrum self-convolutions of the lineshape from

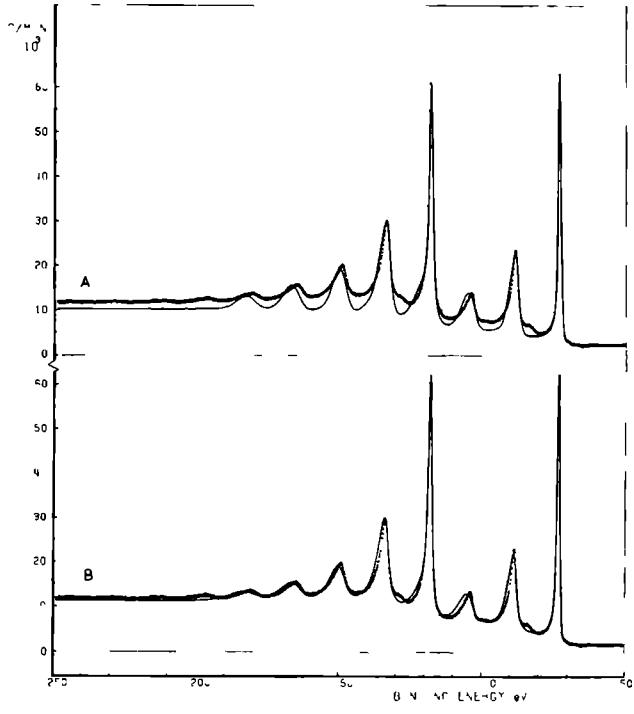

Figure 4A.7 Comparison between experimental spectrum and theoretical models of Penn (A) and Hedin (B). The drawn lines are convolutions of Figure 4A.1C with the theoretical lineshapes given in Figure 4A.6 and self-convolutions thereof. The peak intensity ratio I_2/I_1 was taken equal to the value resulting from Table 4A.1 and I_1 was scaled to give reasonable fit to the first plasmon-loss line. Only bulk plasmon-loss contributions were taken into account.

Eq.(9) were calculated numerically and convoluted with the spectrum of Figure 4A.1C. Obviously the main cause for the discrepancy is a too low intensity in the wings of the lineshape of Eq.(9), but two other points are noteworthy: the lineshape of the second and higher plasmon-loss peaks is more

symmetric than measured and the maxima of the plasmon-loss peaks are shifted to the left.

Hedin[22] has given a different expression for the plasmon energy distribution function:

$$g(\omega) = \frac{e^2}{\pi} \left(\frac{m}{2}\right)^{1/2} \frac{\omega_p^2 0(\omega - \omega_p)}{\omega^3(\omega - \omega_p)^{1/2}} \qquad (13)$$

To include lifetime effects this function was convoluted with a Lorentzian with linewidth depending on ω_q as given by Eqs.(11) and (12). The result of a numerical calculation of Hedin's function is also given in Figure 4A.6. The main difference with Penn's function is the larger intensity in the wings, which is the result of the more realistic Lorentzian lifetime broadening as compared to Eq.(9). Also shown in Figure 4A.6 is an asymmetric Lorentzian lineshape as used in our analysis, which gives the best fit to Hedin's function. It is clear that the asymmetric Lorentzian is a good approximation of Hedin's function. In the same way as described above the plasmon-loss spectrum was calculated with Hedin's function. Figure 4A.7B shows the result; there is better agreement with the measured spectrum than with Penn's approach. However, again the lineshape of the second and higher plasmon-loss peaks is too symmetric and the maxima are shifted to the left as compared with the experimental data. As can be seen in Figure 4A.1D such a shift is indeed observed but becomes appreciable only in the fifth and higher plasmon-loss lines (Remember that the fitted spectrum of Figure 4A.1D was constrained to have equidistant plasmon-loss lines).

It is important to note, that the plasmon energy distributions $D_n(E)$, which we have used to fit the second and higher plasmon-loss lines, are not self-convolutions of the energy distribution of the first plasmon-loss line $D_1(F)$, as expected from theory when spatial redistribution on scattering is neglected. This is assumed to be valid for the XPS and Auger spectra because the initial direction of the unscattered electron is undetermined and for the EEL spectra because they are obtained on polycrystalline materials. Similarly unexplained is the observation that the plasmon-loss lineshape is different for EEL and XPS spectra.

The XPS and EEL measurements give two independent determinations of α, which are in excellent agreement with each other. The fact that α is constant

for the energy range 500-1500 eV is in agreement with results by Flodstrom et al.[20] who measured the bulk plasmon intensities for kinetic energies between 30 and 330 eV. The plasmon intensity appears to be constant above 200 eV. The same authors give a theoretical estimate of $\alpha = (1 + \ell/L)^{-1}$ which for energies larger than 200 eV results in $\alpha = 0.64$ again in excellent agreement with our results.

The value of β obtained is in fact an effective number. As shown by Langreth[42] and Gadzuk[43] the intrinsic plasmon satellites are weakened by the presence of interference effects between intrinsic and extrinsic plasmon excitations. However, as shown by these authors, Eq.(7) can still be used. The relatively large intrinsic contribution for core electrons found in our analysis is supported by the observation of a plasmon-gain satellite of the $KL_{2,3}L_{2,3}(^1D)$ transition. The smaller intrinsic plasmon excitation in the case of the valence band is not unexpected for delocalized electrons. Penn[14] has discussed mechanisms which can lead to intrinsic plasmon-losses of the valence electrons, but in the light of our results his calculation overestimates the importance of these effects. It is surprising that for Auger lines and XPS core lines essentially the same intensities are found for the plasmon-loss lines. The fact, that there seems to be no need for reduction of the intrinsic contribution in case of the KLV Auger lines, may be understood by the polarization of the valence electrons by the K-hole.

4A 5 Conclusions

The results of this investigation can be summarized as follows

(i) Using asymmetric Lorentzians to describe the lineshape of the plasmon-losses good fits to the experimental XPS core level spectra could be obtained. From the area intensities of the plasmon-loss lines we derive for the extrinsic (α) and intrinsic (β) contribution to the plasmon excitations $\alpha = 0.62$ and $\beta = 0.21$. This means, that the intrinsic plasmon excitation contributes at least 25% to the total of the plasmon excitations.

(ii) The theoretical lineshape of Penn can only reproduce the main features of the measured spectra, Hedin's function gives better agreement. The experimental lineshape of the second and higher plasmon-loss lines cannot be described with self-convolutions of the lineshape of the first plasmon-loss line.

(iii) The same parameters as in case of the core levels describe the plasmon-losses of the KLL and KLV Auger lines.

(iv) The intrinsic plasmon excitation in case of photoemission from the valence band is markedly less: $\beta \approx 0.10$.

(v) In the Auger spectrum a plasmon-gain peak of the $KL_{2,3}L_{2,3}(^1D)$ line is observed, again indicating a large contribution of the intrinsic plasmon excitation.

(vi) The width of the plasmon-loss lines in EEL spectra decreases with increasing energy of the primary electrons. At 1200 eV the width of EEL plasmon-loss lines is considerably smaller than in the XPS spectra. α is constant for the energy range 500-1500 eV and equal to $\alpha = 0.62 \pm 0.02$.

4A.6 Acknowledgement

We gratefully acknowledge the technical assistance of Mr. A.E.M. Swolfs.

4A.7 References

1. D. Pines and D. Bohm, Phys. Rev., 85 (1952) 338.
2. D. Bohm and D. Pines, Phys. Rev., 92 (1953) 609.
3. D. Pines, Elementary excitations in solids, W.A. Benjamin Inc., New York (1964).
4. H. Ehrenreich, H.R. Philipp and B. Segall, Phys. Rev., 132 (1963) 1918.
5. C.J. Powell and J.B. Swan, Phys. Rev., 115 (1959) 869.
6. R.E. Burge and D.L. Misell, Phil. Mag., 18 (1968) 261.
7. N. Swanson, J. Opt. Soc. Am., 54 (1964) 1130.
8. Osamu Sueoka, J. Phys. Soc. Japan, 20 (1965) 2203.
9. Tetsuji Aiyama and Keiji Yada, J. Phys. Soc. Japan, 36 (1974) 1554.
10. W.J. Pardee, G.D. Mahan, D.E. Eastman, R.A. Pollak, L. Ley, F.R. McFeely, S.P. Kowalczyk and D.A. Shirley, Phys. Rev. B, 11 (1975) 3614.
11. P. Steiner, H. Höchst, S. Hüfner, Phys. Lett., 61A (1977) 410.
12. D.R. Penn, J. Vac. Sci. Technol., 14 (1977) 300.
13. D.R. Penn, Phys. Rev. Lett., 38 (1977) 1429.
14. D.R. Penn, Phys. Rev. Lett., 40 (1977) 568.
15. H.G. Nöller, H.D. Polaschegg and H. Schillalies, J. Electron Spectrosc. Relat. Phenom., 5 (1974) 705.

16. P.M.Th.M. van Attekum and J.M. Trooster, J. Electron Spectrosc. Relat. Phenom., 11 (1977) 363.
17. P.M.Th.M. van Attekum and J.M. Trooster, to be published.
18. J.C. Fuggle, E. Källne, L.M. Watson and D.J. Fabian, Phys. Rev. B, 16 (1977) 750.
19. R.A. Pollak, L. Ley, F.R. McFeely, S.P. Kowalczyk and D.A. Shirley, J. Electron Spectrosc. Relat. Phenom., 3 (1974) 381.
20. S.A. Flodstrom, R.Z. Bachrach, R.S. Bauer, J.C. McMenamin and S.B.M. Hagström, J. Vac. Sci. Technol., 14 (1977) 303.
21. P.H. Citrin, G.K. Wertheim and Y. Baer, Phys. Rev. B, 16 (1977) 4256.
22. L.H. Hedin in X-ray spectroscopy, Ed. L.V. Azaroff, McGraw Hill, 226 (1974).
23. F. James and M. Roos, Comp. Phys. Comm., 10 (1975) 343.
24. R.S. Williams, S.P. Kowalczyk, P.S. Wehner, G. Apai, J. Stöhr and D.A. Shirley, J. Electron Spectrosc. Relat. Phenom., 12 (1977) 477.
25. G.D. Mahan, Phys. Stat. Sol. B, 55 (1973) 703.
26. Y. Baer and G. Busch, Phys. Rev. Lett., 30 (1973) 280.
27. G. Dufour, J.-M. Mariot, P.-E. Nilsson-Jatko and R.C. Karnatak, Physica Scripta, 13 (1976) 370.
28. L. Ley, F.R. McFeely, S.P. Kowalczyk, J.G. Jenkin and D.A. Shirley, Phys. Rev. B, 11 (1975) 600.
29. J.C. Fuggle, L.M. Watson, P.R. Norris and D.J. Fabian, J. Phys. F, 5 (1975) 590.
30. G.A. Sawatzky, Phys. Rev. Lett., 39 (1977) 504.
31. P.M.Th.M. van Attekum and J.M. Trooster, to be published.
32. G. Dufour, H. Guennou and C. Bonnelle, Surf. Sci., 32 (1972) 731.
33. L.H. Jenkins and M.F. Chung, Surf. Sci., 33 (1972) 159.
34. M. Suleman and E.B. Pattinson, J. Phys. F, 1 (1971) L21.
35. H. Löfgren and L. Walldén, Solid State Commun., 12 (1973) 19.
36. J.E. Rowe and S.B. Christman, Solid State Commun., 13 (1973) 315.
37. C.M.K. Watts, J. Phys. F, 2 (1972) 574.
38. C.O. Almbladh, Nuovo Cim., 23B (1974) 75.
39. J.C. Fuggle, D.J. Fabian and L.M. Watson, J. Electron Spectrosc. Relat. Phenom., 9 (1976) 99.
40. H. Höchst, P. Steiner and S. Hüfner, J. Phys. F, 7 (1977) L309.
41. P.C. Gibbons, S.E. Schnatterly, J.J. Ritsko and J.R. Fields, Phys. Rev. B, 13 (1976) 2451.

42. D. Langreth in "Collective Properties of Physical Systems", ed. by B. and S. Lundqvist, Academic Press (1974).
43. J.W. Gadzuk, J. Electron Spectrosc. Relat. Phenom., 11 (1977) 355.

CHAPTER 4B

BULK AND SURFACE PLASMON-LOSS INTENSITIES IN PHOTOELECTRON, AUGER AND ELECTRON ENERGY LOSS SPECTRA OF Mg METAL*

P.M.Th.M. van Attekum and J.M. Trooster

Abstract - *The intensities of plasmon-loss satellites in X-ray photoelectron (XPS) and electron energy loss (EEL) spectra of Mg metal have been determined. The method used, has been described earlier in a similar study of aluminum*[1]*. Intrinsic processes contribute 22% of the total plasmon intensity in case of XPS core lines. The probability for extrinsic plasmon excitations is* $\alpha = 0.67$*, in good agreement with the value* $\alpha = 0.63$ *derived from the EEL spectra with primary electron energies ranging from 300 to 1500 eV. For KLL and KLV Auger lines we find the same contributions of intrinsic and extrinsic processes to the plasmon intensities as for the XPS core lines. The lineshapes of plasmon-loss lines are different in XPS and EEL spectra, and cannot be described as self-convolutions of the plasmon energy distribution function.*

4B.1 Introduction

Following our investigation of plasmon-losses in X-ray photoelectron (XPS), Auger, and Electron Energy Loss (EEL) spectra of aluminum[1], we report here on a similar study of magnesium metal.

The method used to determine the intensities of the plasmon-loss lines has been extensively described in ref. 1. Here we reiterate the most important features.

a) The n-th bulk plasmon-loss line, P_n, is calculated as a convolution of the measured no-loss line, $P_o(E)$, with a plasmon-loss energy distribution function $D_n(E)$:

$$P_n(E) = P_o(E) \star D_n(E) \qquad (1)$$

*Submitted to: Phys. Rev. B

b) The plasmon-loss energy distribution function $D_n(E)$ is given by an asymmetric Lorentzian:

$$D_n(E) = \frac{I_n}{1 + \left(\frac{E - F_n}{\Gamma_n(E)}\right)^2} \qquad (2)$$

where $E_n = nE_B$, with E_B is the bulk plasmon energy, and $\Gamma_n(E) = n\Gamma^R$ for $E < E_n$ and $\Gamma_n(E) = n\Gamma^L$ for $E > E_n$.

c) Similar expressions are used for the surface plasmon-loss line and for lines due to loss of one surface plasmon-loss and one or more bulk plasmon-losses. Altogether this results in the following parameters: E_B, E_S, Γ^R, Γ^L, Γ_S^R, Γ_S^L, I_n and I_S.

The experiments were carried out on a Leybold-Heraeus LHS-10 spectrometer. XPS spectra were measured with Mg Kα radiation, Auger spectra with Al Kα radiation. The EEL spectra were measured with primary electron energies ranging from 300 to 1500 eV. The energy width of the primary electrons was 0.5 eV.

4B 2 Analysis and results

4B 2 1 XPS core lines and valence band

Fig. 4B.1A presents a typical photoelectron spectrum, excited with Mg Kα radiation, used in the analysis. To obtain a high countrate the electron energy analyser was set for a pass energy of 150 eV, resulting in an instrumental resolution of 1.0 eV. The KLL and KLV Auger lines, which are present in the experimentally measured spectrum because of the Bremsstrahlung background from the X-ray source, were subtracted using the Auger spectrum measured with Al Kα radiation given in Fig. 4B.2-I. Lines due to X-ray satellites were removed with a procedure described elsewhere[2]. The binding energy of the 2s and 2p electrons is 88.6 ± 0.1 eV and 49.6 ± 0.1 eV respectively in good agreement with results of other authors[3,4].

Starting from the right in the spectrum the plasmon-loss intensity is calculated for each datapoint and subtracted from the measured intensity (see ref. 1 for a detailed description of this method). If the method was perfect the result should be the two no-loss core lines, each with Doniach-Sunjic

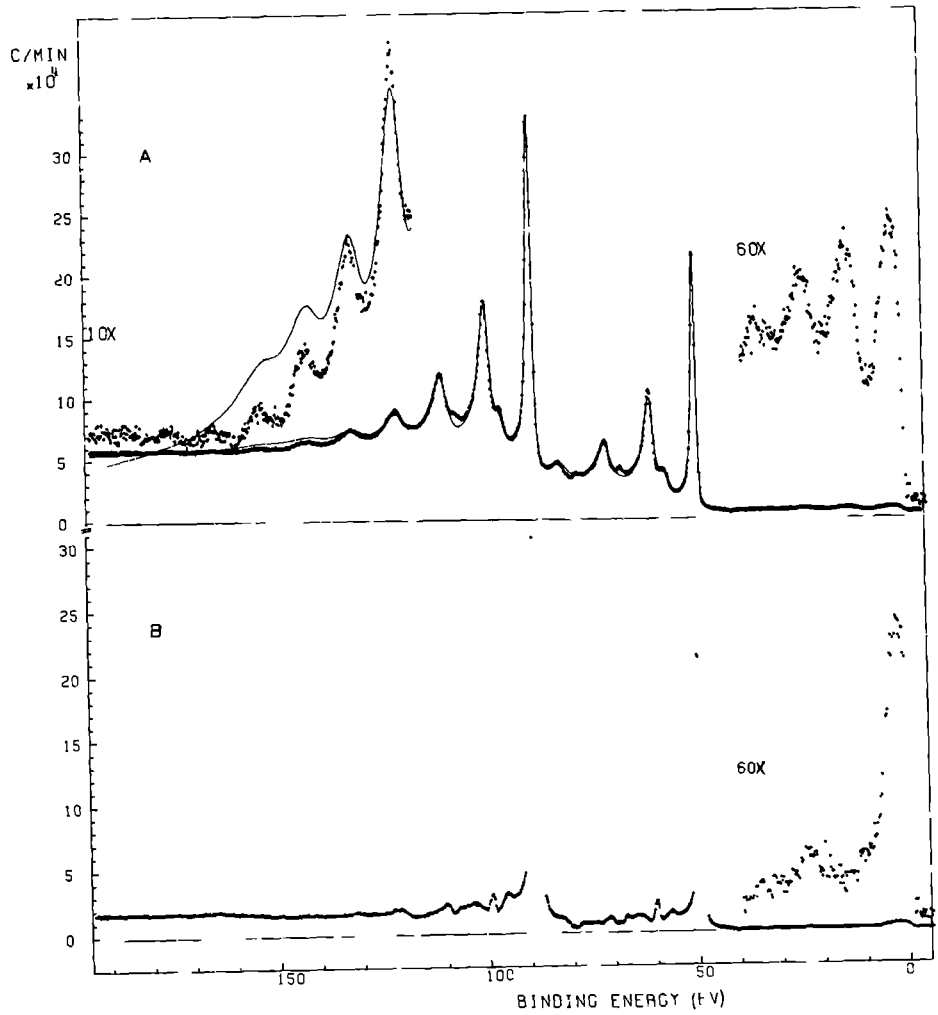

Figure 4B.1 A Photoemission spectrum of the 2s and 2p core levels and valence band of Mg metal after removal of the Auger lines and X-ray satellites. The solid line is the calculated spectrum (see text).

B After the removal of the plasmon-loss lines using the parameters of Table 4B.1.

lineshape as discussed by Citrin et al.[5], modified by the instrumental resolution. However, as in the case of Al[1], it was necessary to allow for a con-

parameter	value	units
E_B	10.63(5)	eV
E_S	7.23(5)	eV
Γ^L	1.07(5)	eV
Γ^R	0.65(5)	eV
Γ^L_S	1.25(5)	eV
Γ^R_S	0.70(5)	eV
I_1	31.3 (5)	$\%eV^{-1}$
I_2	11.5 (3)	$\%eV^{-1}$
I_3	4.5 (2)	$\%eV^{-1}$
I_4	2.2 (2)	$\%eV^{-1}$
I_5	1.3 (2)	$\%eV^{-1}$
I_6	0.6 (1)	$\%eV^{-1}$
I_7	0.3 (1)	$\%eV^{-1}$
I_S	5.8 (2)	$\%eV^{-1}$

Table 4B.1 Best parameter values for the plasmon-losses in Mg metal. The peak intensity (I_n, I_S) is given in percentage units of the no-loss peak per ΔE, where ΔE is the energy increment per channel. Errors are given in units of the last decimal.

stant background to the left of the core lines. A least-squares fitting method[6] was used to determine the parameters given above, using seven bulk plasmon-loss lines for each XPS line. The parameter values are listed in Table 4B.1. The values of E_B and E_S are in good agreement with results of Ley et al.[3] and 0.1 - 0.2 eV lower than found by Fuggle et al.[4,7] and Tejada et al.[8]. The ratio E_B/E_S = 1.47 is close to the theoretical value 1.41. The optimum result after removal of the plasmon-loss lines is shown in Fig. 4B.1B. A reasonable fit could be obtained only up to the third plasmon-loss line. This is most clearly apparent in Fig. 4B.1A, where the spectrum is calculated as a convolution of $D_n(E)$ with the no-loss spectrum obtained from Fig. 4B.1B by smoothing. For higher order plasmon-losses the constraints used in the fit result in too large linewidths. The measured linewidths of the higher order plasmon-losses are also much smaller than one would expect if the lineshapes were given by self-convolutions of the first plasmon-loss energy distribution function. The same result was obtained for plasmon-losses in aluminum, but is more pronounced in the present case. An attempt to fit the spectrum with independent linewidths did not result in an appreciable improvement.

In our method the area intensities A_n of the successive plasmon-loss lines are directly obtained as fraction of the area intensity of the no-loss

line, without actually determining the lineshape and intensity of this no-loss line. The probability for extrinsic and intrinsic plasmon excitation can be derived using the expression[9,10]:

$$A_n = \alpha^n \sum_{m=0}^{n} \frac{(\beta/\alpha)^m}{m!} \qquad (3)$$

where the probability for extrinsic plasmon excitation $\alpha = (1 + \ell/L)^{-1}$, ℓ is the mean free path for extrinsic plasmon excitation, L is the mean attenuation length for electrons due to processes other than plasmon excitation. The parameter β is a measure of the probability of intrinsic excitation of plasmons modified by interference effects between intrinsic and extrinsic plasmon excitations. From the first three experimental area intensities A_1, A_2, A_3, we find $\alpha = 0.67 \pm 0.05$ and $\beta = 0.19 \pm 0.05$. In Table 4B.2 the measured and

Table 4B.2 Experimental area intensities of the bulk and surface plasmon-losses compared with calculated values from Eq.(3). Experimental values in brackets are less reliable. The area intensity is listed in percentage units of the no-loss line and given by $A_n = \frac{\pi}{\ell}(\Gamma_n^L + \Gamma_n^R)I_n$ *(see Table 4B.1). The errors are estimates based on several fits.*

parameter	experiment %	theory % $\alpha = 0.67$, $\beta = 0.19$
A_1	84 ± 3	86
A_2	62 ± 3	60
A_3	37 ± 3	40
A_4	(24)	27
A_5	(17)	18
A_6	(10)	12
A_7	(6)	8
A_S	18 ± 3	-

calculated values of A_n are given. Note that with these values the total intensity for bulk plasmon excitation is about two times the intensity in the no-loss line and that the contribution of intrinsic processes is about 22% of

the total plasmon intensity.

The valence band spectrum is of similar shape as found by Ley et al.[3] and Hochst et al.[11]. The small increase in intensity at 24 eV binding energy is possibly due to a small oxygen impurity, O(2s). This precludes any determination of β for the valence band. In the case of Al we found β to be smaller for the valence band.

4B 2 2 Auger spectrum

In Fig. 4B.2 the KLL and KLV Auger spectrum of Mg metal is shown. Table 4B.3 lists the values for the kinetic energies corrected for the workfunction, together with experimental data of Fuggle et al.[7] and Ley et al.[3] and with theoretical results of Hoogewijs et al.[12]. There is good agreement with theoretical values.

Table 4B.3 Kinetic energies (in eV), corrected for the workfunction, of the KLL and KLV Auger lines in Mg metal. Errors are given in units of the last decimal.

peak	this work	Fuggle et al[7] experiment	Ley et al[3] experiment	Hoogewijs[12] theory
$KL_1L_1(^1S)$	1106.4(2)	1106.2(2)	1106.0(3)	1109.3
$KL_1L_{2,3}(^1P)$	1140.2(2)	1140.1(1)	1139.8(2)	1141.3
$KL_1L_{2,3}(^3P)$	1154.2(2)	1154.1(3)	1154.3(6)	1155.8
$KL_{2,3}L_{2,3}(^1S)$	1180.5(2)	1180.5(1)	1179.8(2)	1180.4
$KL_{2,3}L_{2,3}(^1D)$	1185.9(2)	1185.5(1)	1185.3(2)	1186.4
$KL_{2,3}L_{2,3}(^3P)$	-	-	-	1190.4
KL_1M_1	1209.5(3)	1208.8(5)	-	-
$KL_1M_{2,3}$	1212.6(3)	1212.8(5)	-	-
$KL_{2,3}M_1$ $KL_{2,3}M_{2,3}$	1251.9(2)	1251.7(4)	-	-

In Fig. 4B.2-II we show the same spectrum after subtraction of the plasmon-loss lines using the parameters in Table 4B.1. Both for the KLL and KLV transitions the deviations from a smooth line are of similar magnitude and shape as for the 2s and 2p XPS core lines (Fig. 4B.1B). This implies, that

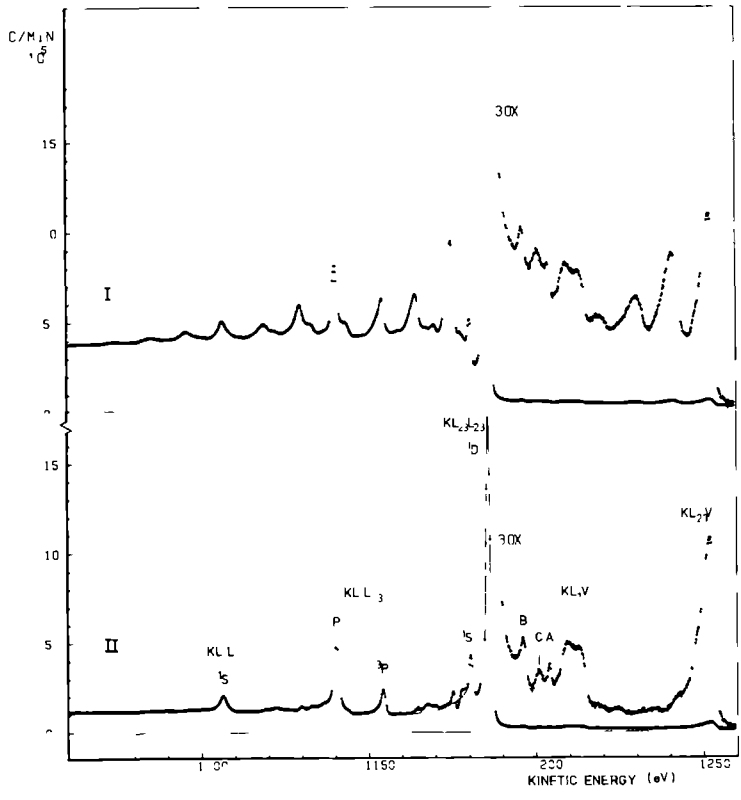

Figure 15.2 X-ray excited (Al Kα) KLL and KLV Auger spectrum of Mg metal. The kinetic energy scale is corrected for the workfunction. (I) As measured. (II) After removal of the plasmon-loss lines using the parameters of Table 15.1. A is the internal photoemission Mg 2p line, B a plasmon-gain peak of the $KL_{2,3}L_{2,3}(^1D)$ Auger line, C a small carbon impurity.

the intrinsic plasmon intensity is the same for the Auger and XPS lines. A similar conclusion was obtained for Al[1].

The small peaks labelled A, B and C are due to internal photoemission from the 2p core level [A], a plasmon-gain satellite of the $KL_{2,3}L_{2,3}(^1D)$ Auger transition [B] and a small carbon impurity [C], and have been discussed elsewhere[13]. The occurrence of the plasmon-gain satellite confirms the importance of intrinsic plasmon excitations.

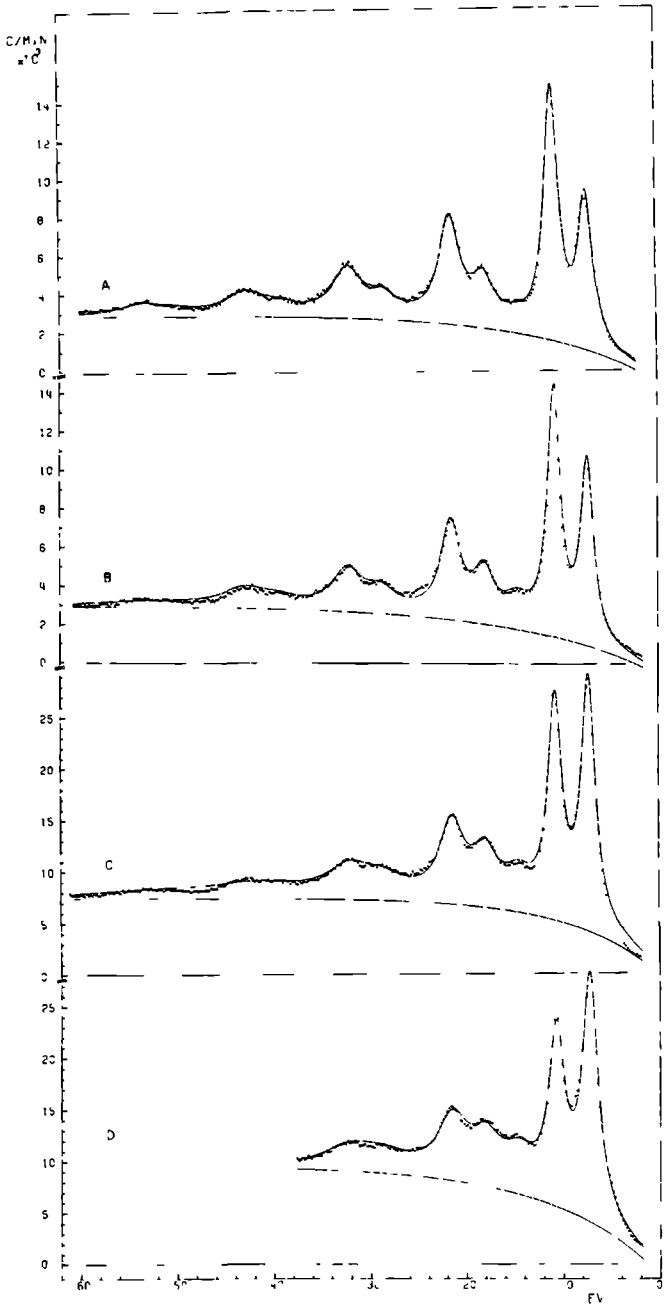

Figure 4B.3 Electron Energy Loss spectra of Mg metal (points) fitted with symmetrical Lorentzians at different values of the primary energy (E_O). The baseline is indicated with a solid line.

A E_O = 1595 eV
B E_O = 1008 eV
C E_O = 433 eV
D E_O = 333 eV

In EEL spectra intrinsic processes cannot occur and hence the area ratio of successive plasmon-loss lines should be equal to α, the probability for extrinsic plasmon excitation (see Eq.(3)). The primary energy E_o was varied from 300 to 1500 eV and the dependence of α on the primary energy was examined. Fig. 4B.3 gives the FEL spectra of Mg metal at primary energies of 336, 499, 1008 and 1505 eV. Note the increase in surface plasmon intensity going to lower primary energies and the presence of a peak due to the excitation of two surface plasmons. This peak occurs as the scattered electron crosses the surface twice. The intensity analysis is hampered by a background, which increases with increasing energy loss. As in the case of Al metal[1] the plasmon-loss lines could be described with symmetrical Lorentzians. The background was approximated by $B(E) = b(1 - a \exp(-(E - E_o)/c))$. In fitting the spectra, the same constraints were used as in ref. 1. The most important features are: Within each pair of bulk and surface plasmon-loss lines, the linewidth was kept equal. Similarly, the intensity ratio within each pair was kept constant except for the first pair. The area intensity ratio of successive bulk plasmon-loss lines was set equal to α. The fits are shown in Fig. 4B.3 and the parameters are tabulated in Table 4B.4

The following points should be noted:

a) The value of α is constant in the primary energy range studied and has the value 0.63 ± 0.04, in good agreement with the value determined for the XPS core lines.

b) After subtraction of the linewidth of the no-loss line (0.5 eV) the linewidth of the first plasmon-loss line is markedly smaller than in the XPS spectra.

c) The linewidths increase with decreasing primary energy and with increasing order of the loss line.

d) The assumed shape of the baseline appears to be a good approximation. The ratio of the baseline intensity to the intensity of the first plasmon-loss line increases with decreasing primary energy.

e) The fact that the ratio of surface to bulk plasmon intensity in the first pair is different from that in the second and higher order pairs indicates, that an appreciable fraction of the electrons scatters from the surface without entering the (bulk) metal and has therefore none or little probability for exciting bulk plasmons as well. This fraction obviously increases

with decreasing primary energy.

Table 4B.4 Best parameter values for the plasmon-losses in the REL spectra of Mg metal as function of the primary energy E_o. E_B and E_S are the bulk and surface plasmon energy, I_1, I_S and I_S^2 are the peak heights of the first bulk plasmon-loss, and the first and second surface plasmon-loss, respectively. R is the ratio between the bulk/surface and bulk peak-height in the second and higher order pairs, and α is the ratio between successive area intensities. Γ is the linewidth and a, b and c are the baseline parameters. Errors are estimates based on several fits and given in units of the last decimal.

	E_o = 336 eV	E_o = 499 eV	E_o = 1008 eV	E_o = 1505 eV
E_B(eV)	10.8 (1)	10.7 (1)	10.7 (1)	10.7 (1)
E_S(eV)	7.3 (1)	7.3 (1)	7.3 (1)	7.2 (1)
I_S/I_1	1.47(5)	1.17(5)	0.74(5)	0.60(5)
R	0.70(5)	0.62(5)	0.49(5)	0.40(5)
I_S^2/I_1	0.36(5)	0.26(5)	0.18(5)	0.05(5)
α	0.65(2)	0.63(2)	0.61(2)	0.62(2)
Γ_1(eV)	2.0 (1)	1.7 (1)	1.6 (1)	1.8 (1)
Γ_2(eV)	3.8 (1)	3.1 (1)	2.5 (1)	2.6 (1)
Γ_3(eV)	6.9 (2)	5.5 (2)	3.7 (2)	3.7 (2)
Γ_4(eV)	-	10.9 (3)	5.4 (3)	5.0 (3)
Γ_5(eV)	-	15.0 (5)	14.6 (3)	6.0 (3)
a	1.11(3)	1.03(3)	1.28(3)	1.30(3)
c(eV)	10.9 (2)	8.9 (2)	14.4 (2)	12.3 (2)
I_1/b	5.0 (1)	7.3 (1)	10.4 (1)	12.0 (1)

4B.3 Conclusions

The results of this investigation are similar to those found on Al[1] and are detailed below.

a) Intrinsic plasmon excitations are important and contribute for XPS core lines about 22% to the total of the plasmon excitations. A similar result

was found by Steiner et al.[14], who gave, however, no details of the fitting procedure.

b) For the KLL and KLV Auger lines the same parameter values as for the core lines are obtained. The occurrence of a plasmon-gain satellite of the $KL_{2,3}L_{2,3}(^1D)$ Auger line confirms the importance of intrinsic processes.

c) Electron energy loss spectra for primary energies ranging from 300 to 1500 eV are analysed with symmetrical Lorentzians. From this a value of $\alpha = 0.63$ is found, in good agreement with the value determined for the XPS core lines.

d) The lineshape of plasmon-loss lines depends on the energy of the primary electrons in EEL spectra and at the same primary energy is different for XPS and EEL spectra. Also, successive plasmon-loss lines cannot be described as self-convolutions of the plasmon-loss energy distribution function.

4B 4 Acknowledgement

We gratefully acknowledge the technical assistance of Mr. A.E.M. Swolfs.

4B 5 References

1. P.M.Th.M. van Attekum and J.M. Trooster, Phys. Rev. B, 18 (1978) 3872.
2. P.M.Th.M. van Attekum and J.M. Trooster, J. Electron Spectrosc. Relat. Phenom., 11 (1977) 363.
3. L. Ley, F.R. McFeely, S.P. Kowalczyk, J.G. Jenkin and D.A. Shirley, Phys. Rev. B, 11 (1975) 600.
4. J.C. Fuggle, Surf. Sci., 69 (1977) 581.
5. P.H. Citrin, G.K. Wertheim and Y. Baer, Phys. Rev. B, 16 (1977) 4256.
6. F. James and M. Roos, Comp. Phys. Comm., 10 (1975) 343.
7. J.C. Fuggle, L.M. Watson, D.J. Fabian and S. Affrossman, J. Phys. F, 5 (1975) 375.
8. J. Tejada, M. Cardona, N.J. Shevchik, D.W. Langer and E. Schonherr, Phys. Stat. Sol. (b), 58 (1973) 189.
9. D. Langreth in "Collective Properties of Physical Systems", ed. B. and S. Lundqvist, Academic Press (1974).
10. W.J. Pardee, G.D. Mahan, D.E. Eastman, R.A. Pollak, L. Ley, F.R. McFeely, S.P. Kowalczyk and D.A. Shirley, Phys. Rev. B, 11 (1975) 3614.

11. H. Höchst, P. Steiner and S. Hüfner, J. Phys. F, 7 (1977) L309.
12. R. Hoogewijs, L. Fiermans and J. Vennik, J. Electron Spectrosc. Relat. Phenom., 11 (1977) 171.
13. P.M.Th.M. van Attekum and J.M. Trooster, J. Phys. F, 8 (1978) L169.
14. P. Steiner, H. Höchst and S. Hüfner, Phys. Lett., 61A (1977) 410.

CHAPTER 4C

A PLASMON GAIN SATELLITE IN THE KLL AUGER SPECTRUM OF Mg AND Al METAL*

P.M.Th.M. van Attekum and J.M. Trooster

Abstract - *We report the observation of a plasmon-gain satellite of the $KL_{2,3}L_{2,3}(^1D)$ Auger line in Mg and Al metal. For both metals the integrated intensity of this satellite is ~ 1.2% of the parent line; this is in good agreement with an estimate based on a theory presented by Almbladh and supports the importance of intrinsic plasmon-losses as derived from intensity measurements of the plasmon-loss lines.*

In X-ray photoelectron spectroscopy plasmons can be excited both by extrinsic (during the transport of the emitted electron through the solid) and intrinsic processes (on the creation of a hole in a core level). The importance of intrinsic processes is well established now (Penn 1977, van Attekum and Trooster 1978), but little attention has been given to a phenomenon related to the intrinsic plasmon excitation, which is the possibility of the occurrence of a plasmon-gain satellite in Auger spectra. Plasmon-gain satellites in $L_{2,3}VV$ Auger spectra have been reported for a number of elements by Suleman and Pattinson (1971), Chung and Jenkins (1971), Dufour et al (1972) and Jenkins and Chung (1972). In most cases, however, the energy difference between satellite and parent line deviated considerably from the plasmon energy. Watts (1972) and Almbladh (1974) showed that the observed intensity was much too high for plasmon-gain satellites and the satellites were shown to be due to double ionisation in the L shell by Lōfgren et al (1973) and Rowe et al (1973). Fuggle et al (1975) observed a plasmon-gain satellite in the KLL Auger spectrum of Mg. However, interference with plasmon-loss satellites of the KLV Auger lines makes the assignment less clear.

The intensity of a plasmon-gain satellite is determined by the ratio of the relaxation time of the disturbance in the free electron density to the lifetime of the core hole and Almbladh (1974) has pointed out that due to the

*Published in: J. Phys. F: Metal Phys., 8 (1978) L169-L173.

shorter lifetime of K holes, KLL Auger transitions are better candidates for the observation of plasmon-gain satellites than $L_{2,3}VV$ transitions. According to this author the intensity of the plasmon-gain satellite is to a good approximation given by:

$$S = \frac{1}{4\pi\omega_p \alpha} \lg \frac{\omega_p}{\Gamma} \qquad (1)$$

where l is the lifetime of the core hole, ω_p the plasmon energy and α is given by the dispersion relation

$$\omega(q) = \omega_p + \alpha q^2 \qquad (2)$$

where $\omega(q)$ is the plasmon frequency at wave vector q. The linewidth of K holes was recently accurately determined by Citrin et al (1977) who found 0.35 and 0.47 eV for Mg and Al, respectively. With a bulk plasmon energy of 10.6 and 15.3 eV and α = 0.46 (Aiyama and Yada 1974) this results in an integrated intensity of 2% for the plasmon-gain peaks of the KLL transitions.

As part of a study of plasmon-losses in Al and Mg (van Attekum and Trooster 1978) we have measured the KLL and KLV Auger spectra of these metals. The spectra as measured are shown in the upper half of Figures 4C.1 and 4C.2. The Al Auger spectrum was measured using an X-ray tube with a magnesium anode as primary radiation source. The Mg $K\alpha_{1,2}$ X-rays have too low an energy for ionising the 1s shell of Al, but the Bremsstrahlung background had sufficient intensity to result in reasonably intense KLL Auger lines. This source has the advantage, that no photoemission lines are present above 1253 eV. For the Mg Auger spectrum an X-ray tube equipped with an aluminum anode was used. Consequently XPS lines can be present up to 1486 eV and interfere with the Auger spectrum.

To reveal the small peaks labelled A, B and C more clearly and to make an unambiguous assignment possible we have removed from the spectrum the intensity due to plasmon-losses, see the lower half of Figures 4C.1 and 4C.2. The plasmon intensities were calculated as a convolution of the parent line with an asymmetric Lorentzian. Intensities and widths were determined by a least-squares fitting of the X-ray photoelectron spectra. An extensive treatment of the procedure used, is given elsewhere (van Attekum and Trooster 1978) and here we concentrate on the result. The Auger lines are identified in Fi-

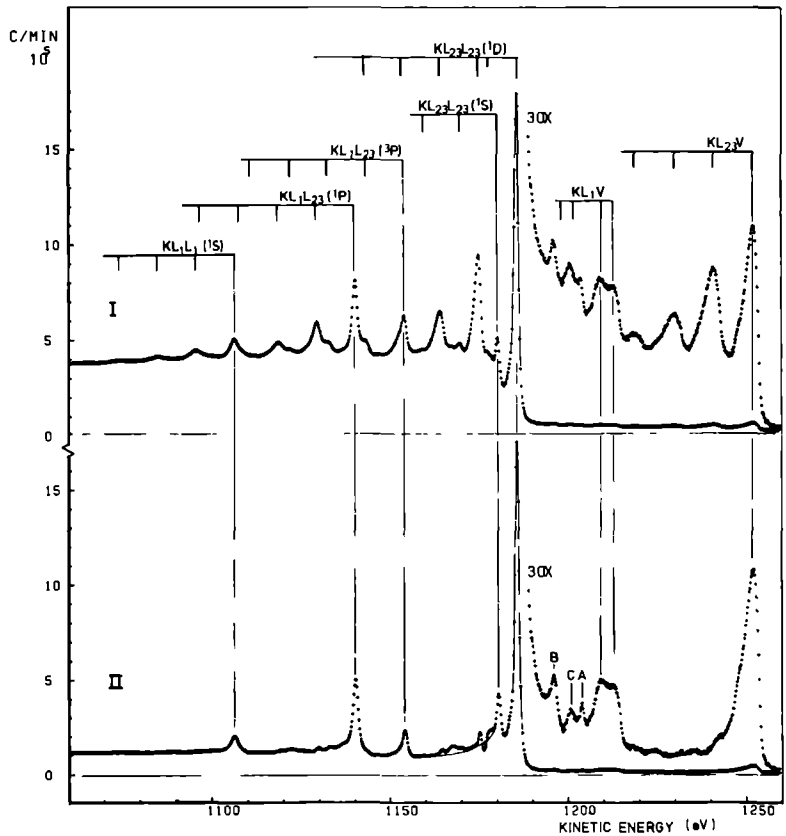

Figure 4C.1 X-ray excited KLL and KLV Auger spectrum of Mg metal. The kinetic energy scale is corrected for the workfunction: (I) as measured. Plasmon-losses are indicated for each Auger line. (II) after removal of the plasmon-loss satellites. The plasmon-gain satellite of the $KL_{2,3}L_{2,3}(^1D)$ Auger line is the peak labelled B. line A is due to internal photoemission and C is the photoelectron peak of the C 1s level of a carbon impurity on the surface of the Mg.

gures 4C.1 and 4C.2 and the energies (corrected for the workfunction) are given in Table 4C.1. There is good agreement with previous experimental and theoretical results of Ley et al (1975) and Dufour et al (1976).

The features labelled A, B and C, which are also present in the untreated spectra cannot be identified as Auger transitions. A is due to internal photoemission from the metal 2p core level, B is the plasmon-gain sa-

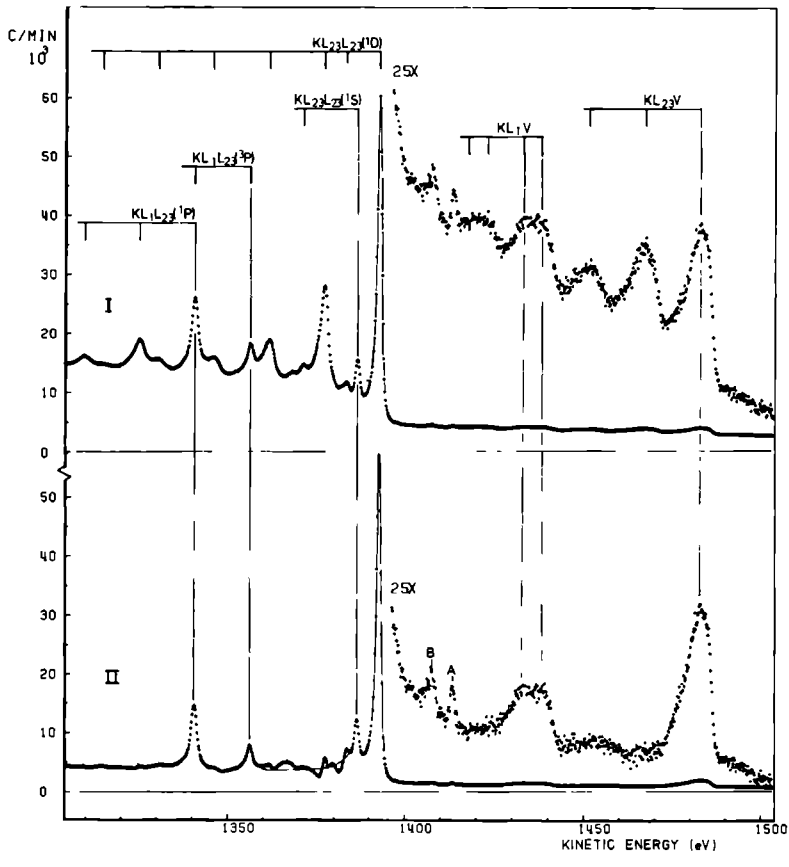

Figure 4C.2 X-ray excited KLL and KLV Auger spectrum of Al metal. The kinetic energy scale is corrected for the workfunction (I) as measured. Plasmon-losses are indicated for each Auger line. (II) after removal of the plasmon-loss satellites. The plasmon-gain satellite of the $KL_{2,3}L_{2,3}(^1D)$ Auger line is the peak labelled B. Line A is due to internal photoemission.

tellite and C, in the spectrum of Mg, is due to a small carbon impurity.

(i) Fluorescence decay of the hole in the K shell leads in the sample to the generation of X-rays (1253.64 eV for Mg and 1486.65 eV for Al), which in turn can result in photoemission from the 2s and 2p level. The energies of peaks A (see Table 4C.1) correspond with binding energies of 49.7(5) and 72.9(5) eV in Mg and Al respectively, very close to the values of

Table 4C.1 Kinetic energies (in eV) corrected for the workfunction of the KLL and KLV Auger lines in Mg and Al metal. Errors are given in units of the last decimal. The meaning of A, B and C is given in the text.

peak	Mg	Al
$KL_1L_1(^1S)$	1106.5(2)	1302.0(2)
$KL_1L_{2,3}(^1P)$	1140.2(2)	1341.2(2)
$KL_1L_{2,3}(^3P)$	1154.3(2)	1356.8(2)
$KL_{2,3}L_{2,3}(^1S)$	1180.6(2)	1387.1(2)
$KL_{2,3}L_{2,3}(^1D)$	1185.9(2)	1393.2(2)
KL_1M_1	1209.6(3)	1436.0(5)
$KL_1M_{2,3}$	1212.8(3)	
$KL_{2,3}M_1$	1252.0(2)	1483.2(2)
$KL_{2,3}M_{2,3}$		
A	1203.9(5)	1413.7(5)
B	1196.2(5)	1408.6(5)
C	1200.6(5)	-

49.6 and 73.0 eV (van Attekum and Trooster 1978) for the binding energy of the 2p core levels in Mg and Al respectively. The corresponding 2s lines cannot be observed due to the plasmon-loss lines or what is left of those after their removal.

(ii) The energy difference between peaks B and the $KL_{2,3}L_{2,3}(^1D)$ Auger line is 10.3(5) and 15.4(5) eV for Mg and Al, respectively. This is within experimental accuracy equal to the bulk plasmon energy of 10.6 eV for Mg and 15.3 eV for Al (van Attekum and Trooster 1978) and leaves little doubt for the assignment of peak B as a plasmon-gain satellite of the $KL_{2,3}L_{2,3}(^1D)$ Auger line. The peak intensity of B is ~ 0.5% of that of the $KL_{2,3}L_{2,3}(^1D)$ Auger line, which is lower than the calculated intensity given above, but of the right order of magnitude. If we assume the linewidth of B to be equal to that of the first plasmon-loss satellite, the integrated intensity is ~ 1.2%, in good agreement with the calculated value.

(iii) Peak C in the Auger spectrum of Mg is probably due to a carbon impurity at the surface of the magnesium sample. The observed energy results in a binding energy of 286.0(5) eV, which must be compared to 284.5 eV for

the carbon 1s level in graphite.

In conclusion we have observed unambiguously the occurrence of a plasmon-gain satellite of the $KL_{2,3}L_{2,3}(^1D)$ Auger line both of Al as well as Mg. This confirms the importance of intrinsic plasmon excitation in these metals.

We thank Dr. C.E. Johnson for his comments on this paper.

4C.1 References

Aiyama Tetsuji and Yada Keji, 1974, J. Phys. Soc. Japan, 36, 1554.
Almbladh C.O., 1974, Nuovo Cim., 23B, 75.
van Attekum P.M.Th.M. and Trooster J.M., 1978, to be published.
Chung M.F. and Jenkins L.H., 1971, Surf. Sci., 26, 649.
Citrin P.H. Wertheim G.K. and Baer Y., 1977, Phys. Rev. B, 16, 4256.
Dufour G.,Guennou H and Bonnelle C., 1972, Surf. Sci., 32, 731.
Dufour G., Mariot J.-M., Nilsson-Jatko P.-E. and Karnatak R.C., 1976, Phys. Scr., 13, 370.
Fuggle J.C., Watson L.M., Fabian D.J. and Affrossmann S., 1975, J. Phys. F: Metal Phys., 5, 375.
Jenkins L.H. and Chung M.F., 1972, Surf. Sci., 33, 159.
Ley L., McFeely F.R., Kowalczyk S.P., Jenkin J.G. and Shirley D.A., 1975, Phys. Rev. B, 11, 600.
Löfgren H. and Walldén L., 1973, Solid St. Commun., 12, 19.
Penn D.R., 1977, Phys. Rev. Lett., 38, 1429.
Rowe J.E. and Christman S.B., 1973, Solid St. Commun., 13, 315.
Suleman M. and Pattinson E.B., 1971, J. Phys. F: Metal Phys., 1, L21.
Watts C.M.K., 1972, J. Phys. F: Metal Phys., 2, 574.

CHAPTER 5

AN X-RAY PHOTOELECTRON SPECTROSCOPY STUDY OF PdSb, PtBi AND AuSn*

P.M.Th.M. van Attekum and J.M. Trooster

Abstract - *The alloys PdSb, PtBi and AuSn as well as the pure constituent metals have been studied with X-ray photoelectron spectroscopy (XPS). The d-bands of Pd, Pt and Au reduce in width and shift to higher binding energy on alloying. A relatively high electron density of states (DOS) at the Fermi level persists in PtBi, indicating an important contribution of the Pt 5d electrons to the DOS at the Fermi level. Relating XPS and Auger shifts on alloying, we have derived values for the screened two hole Coulomb interaction in Pd, Sn and Sb. Both for the pure metals and the alloys the measured intensities of the XPS lines are compared with theoretical cross sections. In general, good agreement is found except for the outer electron levels for which the theoretical cross sections are too low.*

5.1 Introduction

Recently several papers have been published on the electronic structure of compounds with NiAs structure (Allen and Mikkelsen, 1977; Bongi et al, 1974; Castelijns and de Vroomen, 1978; Franzen and Sawatzky, 1975; Höchst et al, 1976; Myron and Mueller, 1978). Castelijns and de Vroomen (1978) used optical techniques to study the valence band of AuSn and PdSb. X-ray photoelectron spectroscopy (XPS) enables a direct measurement of the electron density of states (DOS) in the valence band, facilitating the comparison with theoretical calculations. An XPS study of a series of Au_{1-x} Sn_x alloys has been reported earlier (Friedman et al, 1973), but it is likely that in that study the composition of the alloys deviated strongly from the assumed value (see section 5.3.1). This paper presents an XPS study of the alloys PdSb, PtBi and AuSn

*Submitted to: J. Phys. F: Met al Phys.

together with measurements on the pure constituent metals. Valence bands as well as core levels and Auger transitions have been measured. Although accurate theoretical cross sections for photoionization are available (Scofield, 1976), their use in XPS is hampered because the measured intensities are strongly affected by secondary processes and inelastic scattering of the photoelectrons. We will show that although high accuracy cannot be obtained deviations from nominal composition larger than 10% can be detected.

5 2 Experimental

The measurements were performed with a Leybold-Heraeus LHS-10 spectrometer described elsewhere (Noller et al, 1974). The Henke-type X-ray tube has a copper anode with a magnesium layer evaporated on it, and was operated at 10 keV and 20 mA. Most measurements were made with a constant analyser potential of 50 eV, which results in a resolution function, that is nearly Lorentzian with a full width at half maximum of 0.64 eV (van Attekum and Trooster, 1979).

The pure metal samples Au, Sn, Pd, Sb and Pt were studied in the form of thin evaporated films. The Bi sample was a platelet, that was cleaned by heating to 250 ^{o}C in a vacuum of 10^{-6} Pa. The alloys were prepared by L.W.M. Schreurs (Research Institute of Materials, University of Nijmegen) and studied in the form of platelets of 10 × 5 × 1 mm. Clean surfaces of the alloys were made by scraping the sample in vacuum. Argon ion sputtering could not be used as it was found, that this results in preferential removal of one of the constituents. The amount of either oxygen or carbon present on the samples during measurement is estimated to be less than 0.1 of a monolayer. The pressure during the measurements was of the order of 10^{-8} Pa.

The spectra were recorded by sweeping repeatedly through the desired energy range and storing the data in a multichannel analyser. Lines due to X-ray satellites were removed from the spectra with a method described earlier (van Attekum and Trooster, 1977).

5 3 Results

5 3 1 Core levels, valence bands and Auger peaks positions

In Tables 5.1-3 a compilation is given of the experimental line positions of the samples studied. For each XPS line the binding energy (in eV) relative

Table 5.1 Experimental data on Pd and Sb in the pure metals and the alloy PdSb. The errors in the binding energy of the XPS lines (relative to the Fermi level) and in the kinetic energy of the Auger lines (corrected for the workfunction) are given in units of the last decimal. The estimated error in the experimental relative cross sections is 10%, and the values between square brackets are from the calculations of Scofield (1976).

level	position			relative cross section		
	Pd	PdSb	Sb	Pd	PdSb	Sb
Pd($3p_{1/2}$)	559.9 (1)			0.28 [0.33]		
Pd($3p_{3/2}$)	532.1 (1)	533.3 (1)		0.56 [0.66]		
Pd($3d_{3/2}$)	340.45(5)	341.60(5)		0.65 [0.69]	0.65 [0.69]	
Pd($3d_{5/2}$)	335.18(5)	336.31(5)		1.00 [1.00]	1.00 [1.00]	
Pd(4s)	87.5 (2)	88.3 (2)		0.07 [0.05]		
Pd(4p)	51.4 (2)	52.6 (2)		0.24 [0.17]	0.25 [0.17]	
Pd(VB)	2.35(10)			0.22 [0.13]		
Pd($M_{V}N_{4,5}N_{4,5}$)	327.4 (1)	326.3 (1)				
Pd($M_{IV}N_{4,5}N_{4,5}$)	332.3 (1)	331.1 (1)				
Sb($3p_{1/2}$)		812.3 (3)	812.7(1)		0.35 [0.39]	
Sb($3p_{3/2}$)		766.1 (3)	766.4(1)		0.90 [0.82]	0.39 [0.49]
Sb($3d_{3/2}$)		537.50(5)	537.7(1)		1.12 [1.17]	0.70 [0.69]
Sb($3d_{5/2}$)		528.14(5)	528.2(1)		1.68 [1.69]	1.00 [1.00]
Sb(4s)		153.1 (2)	153.5(1)		0.06 [0.08]	0.03 [0.04]
Sb(4p)		100.1 (4)	100.1(4)			
Sb($4d_{3/2}$)		33.24(5)	33.5(1)		0.44 [0.31]	0.25 [0.19]
Sb($4d_{5/2}$)		32.07(5)	32.3(1)			
Sb(5s)		10.5 (2) 9.0 (2)	10.0(1)			0.01 [0.005]
Sb(5p)			2.7(1)			0.01 [0.006]
Sb($M_{V}N_{4,5}N_{4,5}$)		455.5 (3) 458.0 (3)	455.1(2) 457.5(2)			
Sb($M_{IV}N_{4,5}N_{4,5}$)		464.9 (3)	464.5(2)			

to the Fermi level is listed, and for the Auger peaks the kinetic energy, corrected for the workfunction. In case of Sb and Sn metal strong plasmon-loss satellites accompany the XPS lines. The intensity and position of these plasmon-losses are in agreement with XPS results (Pollak et al, 1974), electron energy loss measurements (Robins, 1962) and electron transmission experiments (Sueoka, 1965). In Figures 5.1-3 the valence bands of PdSb, PtBi and AuSn are shown, together with the valence bands of the constituent metals.

Table 5.2 Experimental data on Pt and Bi in the pure metals and the alloy PtBi. The errors in the binding energies (relative to the Fermi level) are given in units of the last decimal. The estimated error in the experimental relative cross sections is 10% and the values between square brackets are from the calculations of Scofield (1976).

level	position (eV)			relative cross section		
	Pt	PtBi	Bi	Pt	PtBi	Bi
Pt($4d_{3/2}$)		331 25(20)			0 54 [0 70]	
Pt($4d_{5/2}$)		314 5 (2)			0 79 [1 03]	
Pt($4f_{5/2}$)	74 41(5)	74 53(3)		0 79 [0 78]	0 79 [0 78]	
Pt($4f_{7/2}$)	71 07(5)	71 21(5)		1 00 [1 00]	1 00 [1 00]	
Pt($5p_{3/2}$)	51 7 (2)			0 06 [0 09]		
Pt(VB)	4 25(5) 1 75(5)			0 20 [0 14]		
Bi($4d_{3/2}$)		463 9 (2)	463 7 (2)		0 67 [0 80]	0 41 [0 51]
Bi($4d_{5/2}$)		440 4 (2)	440 3 (2)		0 91 [1 20]	0 79 [0 76]
Bi($4f_{5/2}$)		162 43(5)	162 21(5)		0 98 [1 23]	0 78 [0 78]
Bi($4f_{7/2}$)		157 14(5)	156 88(5)		1 33 [1 57]	1 00 [1 00]
Bi($5d_{3/2}$)		27 25(5)	26 97(5)		0 12 [0 11]	0 08 [0 07]
Bi($5d_{5/2}$)		24 14(5)	23 86(5)		0 17 [0 16]	0 11 [0 10]
Bi(6s)		11 05(20)	10 9 (3)		0 008 [0 008]	0 005 [0 005]
Bi(VB)			3 45(30) 1 15(10)			0 005 [0 005]

The results on Pd, Pt, Sb and Bi metal are in good agreement with literature (Baer et al, 1970; Baer and Myers, 1977; Friedman et al, 1973, Hochst et al, 1976; Hüfner et al, 1974; Hufner et al, 1975; Ley et al, 1973; Pollak et al, 1974, Siegbahn, 1977; Smith et al, 1974; Wertheim and Hüfner, 1975; Wertheim and Walker, 1976; Wertheim and Buchanan, 1977) except for the binding energy of the $3d_{5/2}$ level in Sb metal. The value given by Pollak et al (1974) is clearly erroneous and was propagated in the position of the corresponding plasmon-losses. For Pd metal a plasmon energy of 6.0 eV is obtained in reasonable agreement with earlier results (Baer et al, 1970).

For Au and Sn metal our results are in agreement with literature values. Values for Au and Sn core levels given by Friedman et al (1973) are based on an unusual reference and all have to be shifted by 0.6 eV to obtain the present values. Friedman et al (1973) have studied AuSn alloys in a number of compositions. There is no agreement between the present results and those ob-

Table 5.3 Experimental data on Au and Sn in the pure metals and the alloy AuSn. The errors in the binding energy of the XPS lines (relative to the Fermi level) and in the kinetic energy of the Auger lines (corrected for the workfunction) are given in units of the last decimal. The estimated error in the experimental relative cross sections is 10% and the values between square brackets are from the calculations of Scofield (1976).

level	positions (eV)			relative cross sections		
	Au	AuSn	Sn	Au	AuSn	Sn
Au($4d_{3/2}$)	352.9 (1)	353.8 (1)			0.58 [0.66]	
Au($4d_{5/2}$)	334.7 (1)	335.8 (1)			0.75 [0 97]	
Au($4f_{5/2}$)	87.67(5)	88.57(5)		0.80 [0.81]	0.81 [0.81]	
Au($4f_{7/2}$)	83.97(5)	84.89(5)		1.00 [1.00]	1.00 [1.00]	
Au($5p_{3/2}$)	57.25(20)			0.07 [0.09]		
Au(VB)	6.3 (1) 3.9 (1)			0.26 [0.15]		
Sn($3p_{1/2}$)		756.8 (1)	756.5 (2)		0 22 [0.37]	0.23 [0.25]
Sn($3p_{3/2}$)		714.8 (1)	714.6 (2)		0.43 [0.78]	0.47 [0.52]
Sn($3d_{3/2}$)		493.47(5)	493.2 (1)		0.73 [1.07]	0.68 [0.69]
Sn($3d_{5/2}$)		485.10(5)	484.8 (1)		1.05 [1.49]	1.00 [1.00]
Sn(4s)			136.8 (1)			0.03 [0.04]
Sn(4p)			85.2 (3)			
Sn($4d_{3/2}$)		25.27(5)	25.02(5)		0.24 [0.26]	0.27 [0.18]
Sn($4d_{5/2}$)		24.34(5)	24.04(5)			
Sn(5s)			7.0 (1)			0.02 [0.01]
Sn(VB)			1.45(5)			
Sn($M_V N_{4,5} N_{4,5}$)		424.7 (2) 428.7 (1)	424.5 (2) 429.0 (1)			
Sn($M_{IV} N_{4,5} N_{4,5}$)		430.9 (1) 437.2 (1)	431.2 (1) 437.5 (1)			

tained by Friedman et al (1973) on AuSn. However, samples studied by these authors were cleaned by argon ion sputtering and we have observed, that such treatment results in a considerable depletion of Sn from the surface layer. Thus the valence band of $AuSn_4$ as presented by Friedman et al (1973) resembles our results obtained on AuSn.

5.3.2 Intensities of core level lines

In the limit of an infinitely thick homogeneous sample the total inten-

sity I_i of the photoelectron line at kinetic energy ε_i due to atoms of the type i is (Fadley et al, 1974):

$$I_i = I_{h\nu} N_i \left(\frac{d\sigma(\varepsilon_i)}{d\Omega}\right)_i T(\varepsilon_i)\lambda(\varepsilon_i) \tag{1}$$

where $I_{h\nu}$ is the photon flux impinging on the sample, N_i the number of atoms emitting electrons from level i, $(d\sigma(\varepsilon_i)/d\Omega)_i$ the differential cross section for ejection of an electron from level i in the solid angle $d\Omega$, $T(\varepsilon_i)$ the sensitivity of the spectrometer and $\lambda(\varepsilon_i)$ the mean free path in the specific sample of an electron with energy ε_i. For unpolarized light $(d\sigma(\varepsilon_i)/d\Omega)_i$ can be written as (Reilman et al, 1976):

$$\left(\frac{d\sigma(\varepsilon_i)}{d\Omega}\right)_i = \frac{\sigma_i(\varepsilon_i)}{4\pi}\left[1 - \frac{\beta_i(\varepsilon_i)}{2} P_2(\cos\theta)\right] \tag{2a}$$

where $\sigma_i(\varepsilon_i)$ is the cross section for photoionization of an electron from the i-th level, $\beta_i(\varepsilon_i)$ is the angular anisotropy parameter, which characterizes the angular distribution and is a function of the angular momentum and energy of the photoelectron, $P_2(x) = (3x^2 - 1)/2$ and θ is the angle between photon and photoelectron direction. In the LHS-10 spectrometer $\theta = 60^o$ (manual LHS-10 spectrometer) so:

$$\left(\frac{d\sigma(\varepsilon_i)}{d\Omega}\right)_i = \frac{\sigma_i(\varepsilon_i)}{4\pi}\left[1 + \frac{\beta_i(\varepsilon_i)}{16}\right] \tag{2b}$$

From Eqs.(1,2) it follows, that the ratio of intensities of two different photoelectron lines from the same sample is:

$$\frac{I_i}{I_j} = \frac{N_i}{N_j}\,\frac{\sigma_i(\varepsilon_i)}{\sigma_j(\varepsilon_j)}\,\frac{[1 + \beta_i(\varepsilon_i)/16]}{[1 + \beta_j(\varepsilon_j)/16]}\,\frac{T(\varepsilon_i)}{T(\varepsilon_j)}\,\frac{\lambda(\varepsilon_i)}{\lambda(\varepsilon_j)} \tag{3}$$

For our spectrometer, operated at a constant analyser potential $T(\varepsilon_i)$ is inversely proportional to the kinetic energy of the photoelectrons (Nõller et al, 1974). Thus for the ratio of cross sections $\sigma_i(\varepsilon_i)/\sigma_j(\varepsilon_j)$ we obtain:

$$\frac{\sigma_i(\varepsilon_i)}{\sigma_j(\varepsilon_j)} = \frac{I_i}{I_j}\,\frac{N_j}{N_i}\,\frac{[1+\beta_j(\varepsilon_j)/16]}{[1+\beta_i(\varepsilon_i)/16]}\,\frac{\varepsilon_i}{\varepsilon_j}\,\frac{\lambda(\varepsilon_j)}{\lambda(\varepsilon_i)} \qquad (4)$$

The values of $\beta_i(\varepsilon_i)$ can be obtained from Reilman et al (1976). The dependence of the mean free path on the kinetic energy is not well known. Recently, Penn (1976) calculated the mean free paths of the elements as a function of the kinetic energy, and presented a method to calculate the mean free path in compounds.

Using Eq.(4) and Penn's results for $\lambda(\varepsilon_i)$ we have calculated relative cross sections for the various levels in the metals from the measured area intensities. In Tables 5.1-3 these results are compared with Scofield's (1976) theoretical ratios. In determining the area intensities only the primary XPS line was used assuming the losses due to plasmons, shake-up satellites et cetera to be the same for all levels of a given element. In Tables 5.1-3 we compare also the experimentally determined cross sections with the theoretical values of Scofield (1976) for the alloys assuming $N_i = N_j$ in Eq.(4).

5 4 Discussion

5 4 1 Cross sections

The relative cross sections of the different core levels of a given element in general agree with the theoretical values of Scofield (1976) both in the pure metals and in the alloys. Deviations, that occur for deep lying core levels resulting in wide lines such as Pd(3p), Au(4d) must be ascribed to less accurate experimental values. However, this is not the case for the experimental cross sections of the valence band of Pd, Pt and Au, which are 40% larger than the calculated values. The same is true for the Sb and Sn 4d levels. These discrepancies presumably reflect the difficulty in calculating cross sections for outer shells. Experimental and theoretical cross sections of the two elements in the alloy are consistent with the nominal composition for PdSb. The PtBi alloy appears to be slightly enriched in Bi. A very large deviation from the nominal composition occurs in AuSn from the measured cross sections a composition $Au_{0.6}\,Sn_{0.4}$ is derived. In view of the surface preparation technique this is a surprisingly large deviation probably due to a surface enrichment in Au. The Au(4f) lines have a shoulder on the high kinetic energy side, which can be ascribed to such an enriched layer.

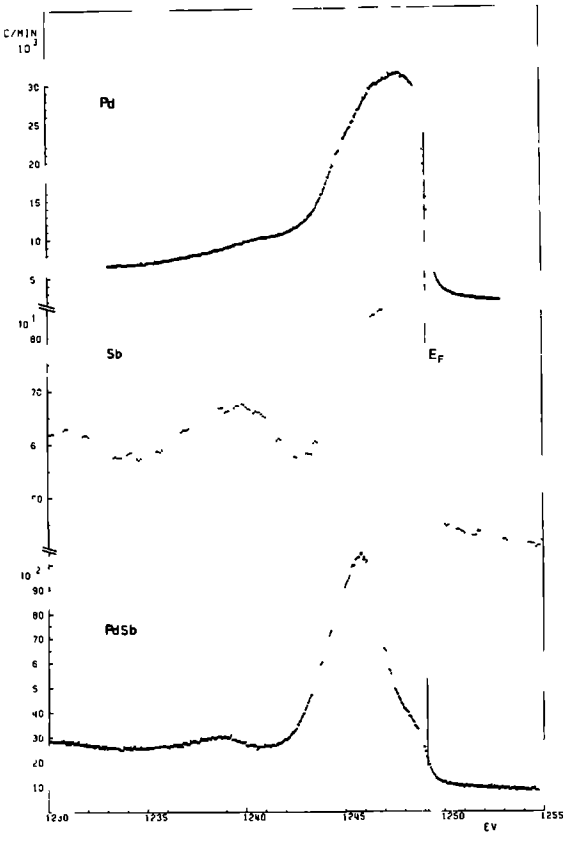

Figure 5.1 Photoemission spectra of the valence bands of Pd, Sb and PdSb. The spectra have been corrected for X-ray satellites. The spectrometer resolution was 0.64 eV. Along the horizontal axis the kinetic energy of the photoelectrons is plotted (E_B = 0 at 1249.15 eV).

The measured valence bands of the pure metals agree with the existing literature. A comparison with theoretical density of states (DOS) has been made for Au (Smith et al, 1974), Pt (Smith et al, 1974), Pd (Smith et al, 1974), Sb (Bullet, 1975) and Bi (Baer and Myers, 1977). The DOS of Sn was calculated by Ament and de Vroomen (1974) and a comparison with the experimental spectrum is given in Figure 5.4. The theoretical DOS was convoluted with the instrumental

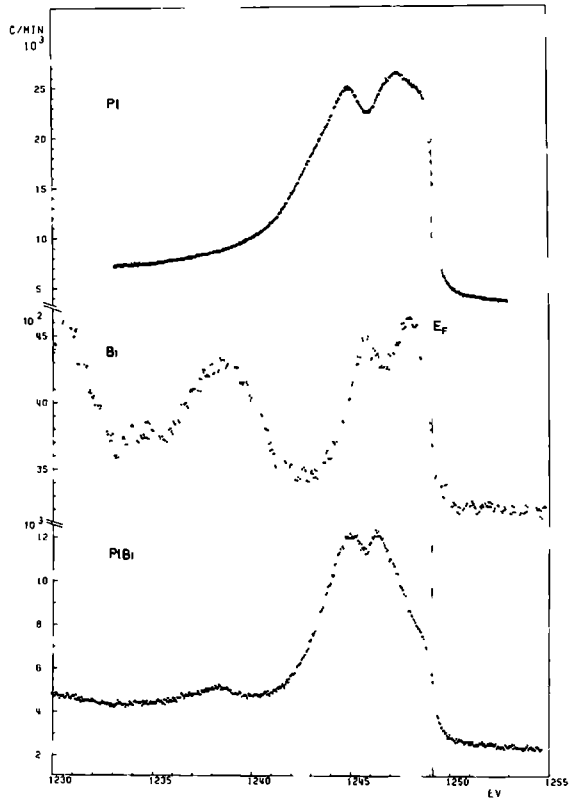

Figure 5.2 Photoemission spectra of the valence bands of Pt, Bi and PtBi. The spectra have been corrected for X-ray satellites. The spectrometer resolution was 0.64 eV. Along the horizontal axis the kinetic energy of the photoelectrons is plotted (E_B = 0 at 1249.15 eV).

resolution function, which to a good approximation is a Lorentzian with a width of 0.64 eV. The agreement between the experimental and "broadened" theoretical spectrum is excellent considering the fact, that no cross section effects have been taken into account: according to Scofield (1976) $\sigma(5s)/\sigma(5p)$ = 1.6.

A common feature of the valence bands of all three alloys studied is a narrowing of the transition metal d-band. This is most clear in AuSn: the valence band resembles closely that observed in Au(I) and Au(III) complexes (van Attekum et al, 1979). The 5d-band splitting is, however, slightly larger

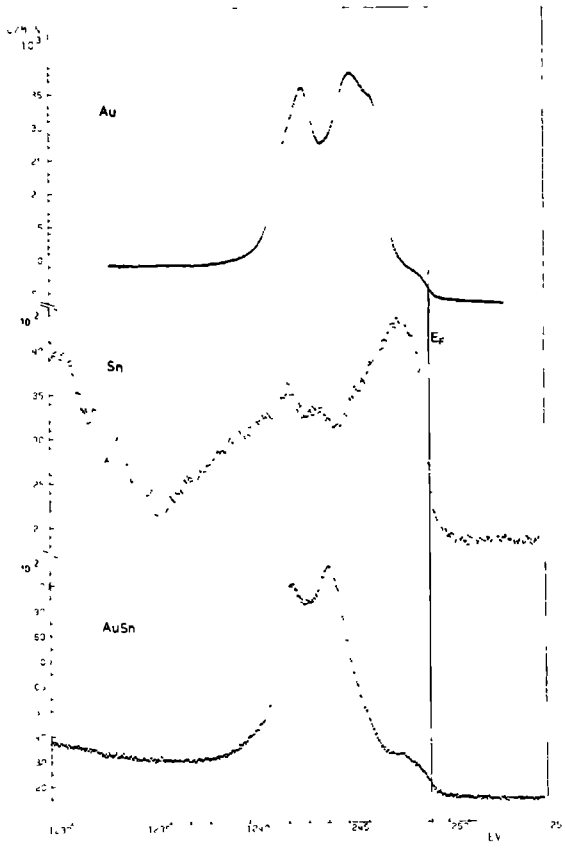

Figure 5.3 Photoemission spectra of the valence bands of Au, Sn and AuSn. The spectra have been corrected for X-ray satellites. The spectrometer resolution was 0.64 eV. Along the horizontal axis the kinetic energy of the photoelectrons is plotted (E_B = 0 at 1249.15 eV).

in the present case: 1.8 eV compared to a free atom spin-orbit splitting of 1.5 eV (Moore, 1958). Shevchik (1975) has found, that the splitting of the Au(5d) band increases with increasing Au-content in Au-Cd alloys and has attributed the increase in splitting to effects of banding. Apparently, the dilution of the gold by the tin in AuSn results in an almost core like Au(5d) level with a weak d-d interaction leading to the slight increase in apparent spin-orbit splitting. The valence band near the Fermi edge then has mainly Au(6s) and Sn(5p) character. The position of the maximum of the 5d peak is

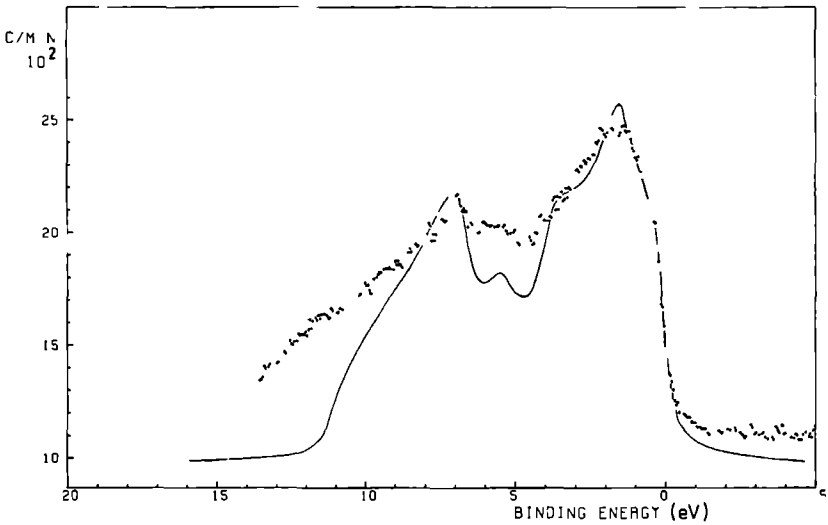

Figure 5.4 Comparison between the "broadened" theoretical density of states (Ament and de Vroomen, 1974) [solid line] and experimental valence band of Sn metal. In the theoretical spectrum no cross section effects and background corrections were incorporated.

about 5 eV below the Fermi edge in agreement with optical data obtained by Casteljns et al (1978).

For PtBi a similar increase of the apparent spin-orbit splitting of Pt (5d) is observed. The free atom spin-orbit splitting is 1.05 eV (Moore, 1958) whereas in PtBi the splitting is 1.3 ± 0.1 eV. The larger relative intensity at the Fermi level, when compared to AuSn or PdSb indicates an important Pt (5d) contribution to the DOS at the Fermi level.

For PdSb a theoretical calculation of the valence band density of states is available (Myron and Mueller, 1978). In Fig. 5.5 the DOS convoluted with the instrumental resolution function is compared with the measured spectrum. The agreement is reasonable in view of the fact, that a proper comparison can only be made if matrix elements for the photoelectric effect are taken into account. In general, sharp peaks in claculated DOS have not shown up in the measured XPS spectra. The peak in the measured spectrum, attributed mainly to the Pd(4d) band lies 3.3 eV below the Fermi edge again in agreement with the conclusion drawn from optical measurements by Casteljns et al (1978). The latter measurements also indicated, that the character of the bands at the

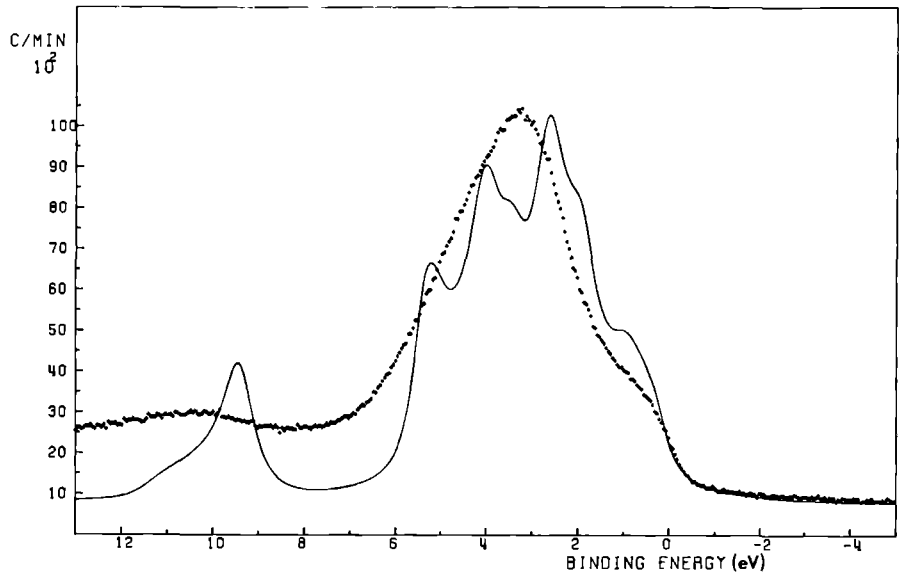

Figure 5.5 Comparison between the "broadened" theoretical density of states (Myron and Mueller, 1978) [solid line] and experimental valence band of PdSb. In the theoretical spectrum no cross section effects and background corrections were incorporated.

Fermi energy is mainly derived from Sb(5p) states.

		metal	alloy
Pd	$\Gamma^L(3d_{5/2})$	0.84	0.54
	$\Gamma^R(3d_{5/2})$	0.56	0.54
	$\Gamma(3d_{5/2})$	1.40	1.08
Pt	$\Gamma^L(4f_{7/2})$	0.90	0.60
	$\Gamma^R(4f_{7/2})$	0.50	0.50
	$\Gamma(4f_{7/2})$	1.40	1.10
Bi	$\Gamma^L(5d_{5/2})$	0.48	0.60
	$\Gamma^R(5d_{5/2})$	0.45	0.52
	$\Gamma(5d_{5/2})$	0.93	1.12

Table 5.4 Lefthand (Γ^L), righthand (Γ^R) and total (Γ) width at half maximum of the $Pd(3d_{5/2})$, $Pt(4f_{7/2})$ and $Bi(5d_{5/2})$ level in the pure metal and the alloys PdSb and PtBi, respectively. The values quoted are in eV and the estimated errors are 0.05 eV.

From the measured valence band spectra it is clear, that the density of states at the Fermi energy in PtBi is larger than in PdSb. This explains the asymmetry due to electron-hole excitations (Doniach and Sunjic, 1970) which is still present in the core lines of Pt in PtBi, whereas the Pd lines in PdSb are symmetric, see Table 5.4. Consequently, as illustrated in Fig. 5.6,

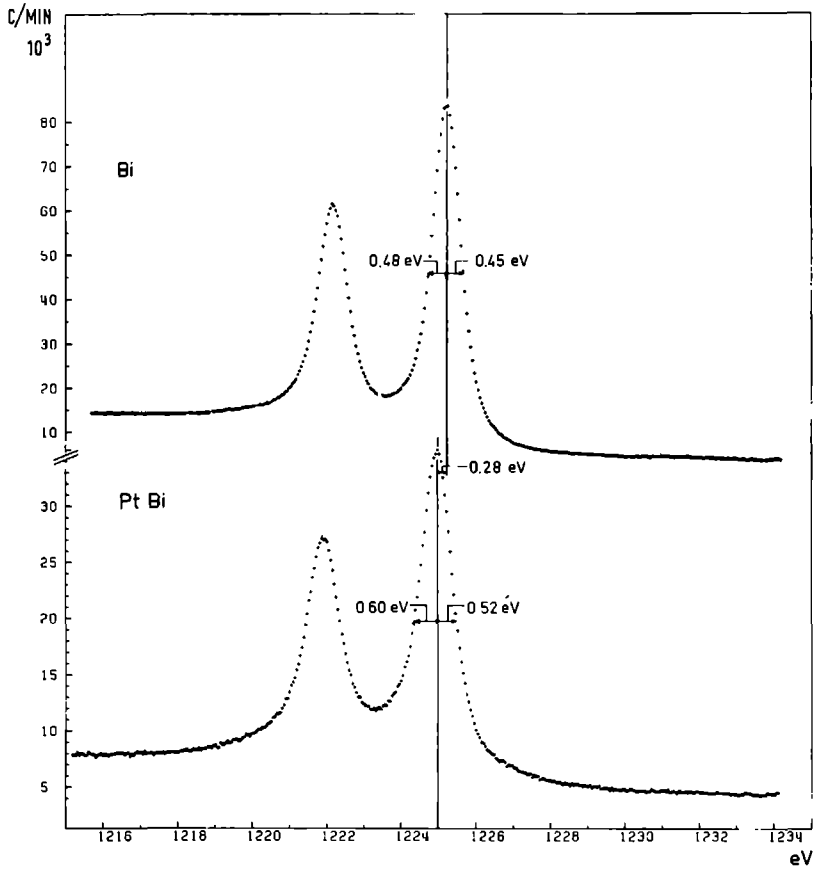

Figure 5.6 The Bi(5d) lines in Bi metal and PtBi. The increased asymmetry of the lines in the alloy is due to the increase in electron density at the Fermi level.

the Bi(5d) lines, which are symmetric in Bi metal (except for a tail due to

interband transitions (Wertheim and Buchanan, 1977)) become clearly asymmetric in the alloy.

The metals Sb and Sn have clear plasmon-loss satellite lines (at ~ 15 eV) accompanying the core lines, valence bands, as well as Auger peaks. In the alloys PdSb and AuSn no indication for plasmon-loss satellites was found, which is probably due to the occurrence of interband transitions (Hummel, 1971).

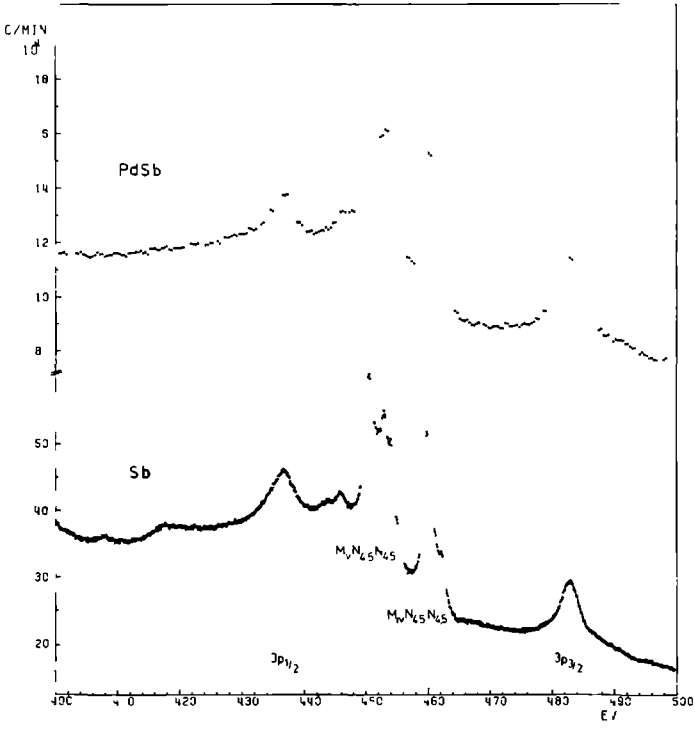

Figure 5.7 The Sb(3p) and Sb($M_{IV,V}N_{4,5}N_{4,5}$) Auger spectrum in Sb metal and PdSb. No change of the lineshape occurs in the Auger spectrum on alloying.

As can be seen from Fig. 5.7, the $M_{IV,V}N_{4,5}N_{4,5}$ Auger peaks of Sb do not change their shape on alloying. The same is true for the other Auger lines studied. The kinetic energy of jkl Auger electrons with final hole configuration X in a conductor can be written (Hoogewijs et al, 1977):

$$E(jkl;X) = E_B(j) - E_B(k) - E_B(l) - F(kl;X) + R(kl;X) \qquad (5a)$$

where $E_B(j)$, $E_B(k)$, $E_B(l)$ are the core level binding energies (from experiment relative to the Fermi level), F(kl;X) describes the Coulomb energy of the holes in the k and l level and R(kl;X) is the additional relaxation energy of the two-hole final state, above the sum of the two one-hole relaxation energies, already included in $E_B(k)$ and $E_B(l)$. Defining U_{eff} (Antonides et al, 1977), the effective Coulomb interaction of the two holes on one site reduced from the free atom value by extra atomic relaxation, Eq.(5a) can be rewritten:

$$E(jkl;X) = E_B(j) - E_B(k) - E_B(l) - U_{eff}(kl;X) \qquad (5b)$$

The resulting values for U_{eff} calculated from Tables 5.1 and 5.3 are: 3.3, 6.7 and 7.3 eV for Pd, Sn and Sb, respectively. As in the case of the first transition metal series (Antonides et al, 1977) U_{eff} increases with atomic number, but the absolute values are importantly smaller. U_{eff} is the same for the pure metal and the alloy, even for Pd where valence bands participate in the $M_{IV,V}N_{4,5}N_{4,5}$ Auger transitions. As F(kl;X) is an intra atomic quantity, it is invariant to the chemical environment of the atom (Citrin et al, 1976) - [for instance $\Delta F(L_3M_{4,5}) \simeq 0.2$ eV for Zn → ZnO (Antonides and Sawatzky, 1976)], and because U_{eff} does not change on alloying it follows, that the additional relaxation, R(kl;X), does not change on alloying).

In Table 5.5 we list the average shift between the core levels and Auger peaks of each element in the metal and the alloy, respectively. The shift of the Auger peaks has the same magnitude, but opposite sign, as the corresponding shifts in the core level binding energy. This can be understood as follows: For all core levels of a given element we find the same shift, ΔE_B, going from the metal to the alloy, therefore according to Eq.(5b) the shift in kinetic energy of Auger electrons going from the metal to the alloy is:

$$\Delta E(jkl;X) = - \Delta E_B - \Delta U_{eff}(kl;X) \qquad (6a)$$

	average shift (eV)
Pd(core levels)	-1.1 (1)
Pd(Augers)	+1.2 (1)
Sb(core levels)	+0.2 (1)
Sb(Augers)	-0.4 (1)
Pt(core levels)	-0.1 (1)
Bi(core levels)	-0.25(10)
Au(core levels)	-0.9 (1)
Sn(core levels)	-0.3 (1)
Sn(Augers)	+0.3 (1)

Table 5.5 Averaged measured shifts (metal minus alloy) in core binding and Auger kinetic energy, respectively. The errors are given in units of the last decimal.

Since we have already found that $U_{eff}(kl;X)$ does not change on alloying, this results in:

$$\Delta E(jkl;X) = - \Delta E_B \tag{6b}$$

As the Fermi level is used as reference for the binding energy of the core levels, the shift, ΔE_B, of the core levels upon alloying is given by (Watson and Perlman, 1975):

$$- \Delta E_B = \Delta \varepsilon_i - \Delta \varepsilon_F \tag{7}$$

$\Delta \varepsilon_i$ is the difference in one electron binding energy in the metal and the alloy with respect to the crystal zero and $\Delta \varepsilon_F$ is the change in position of the Fermi level. Since $\Delta \varepsilon_F$ is unknown, a quantitative estimate of the change in one electron binding energy is impossible. However, Mössbauer experiments on Sb (Montgomery and Ruby, 1970) and Au and Sn (Watson and Perlman, 1975; Chou et al, 1976) have shown, that for PdSb and AuSn only a minor charge transfer (< 0.1) electron), but appreciable modification of the electron configuration around the Pd and Au nucleus (increase in s electron density at the cost of d electron density) occurs. Therefore, it is probable that the shifts in the core level binding energies are mainly due to electron configuration changes and differences in the position of the Fermi level on going from the pure metals to the alloys.

5 5 Conclusions

The alloys PdSb, PtBi and AuSn were investigated with XPS together with their constituent metals. The valence bands of the alloys all have a narrower d-band than the pure metals, but the apparent spin-orbit splitting in case of Au in AuSn and Pt in PtBi is still larger than the free atom value. The changes in the electronic structure on going from the metal to the alloy also leads to shifts of the positions of the core level lines and Auger peaks, a change of the asymmetry of some of the core lines and the disappearance of the plasmon-loss satellite lines in the alloys. The composition of the alloy samples was studied by comparing the experimentally determined relative cross sections with calculated ones. From this it was found, that the PdSb sample had the nominal composition, PtBi was slightly enriched in Bi and AuSn was appreciably enriched in Au.

5 6 Acknowledgement

We gratefully acknowledge the technical assistance of Mr. A.E.M. Swolfs.

5 7 References

Allen J.W. and Mikkelsen J.C., 1977, Phys. Rev. B, 15, 2952.

Ament M.A.E.A. and de Vroomen A.R., 1974, J. Phys. F, 4, 1359.

Antonides E. and Sawatzky G.A., 1976, J. Phys. C, 9, L547.

Antonides E., Janse E.C. and Sawatzky G.A., 1977, Phys. Rev. B, 15, 1669.

van Attekum P.M.Th.M. and Trooster J.M., 1977, J. Electron Spectrosc. Relat. Phenom., 11, 363.

van Attekum P.M.Th.M. and Trooster J.M., submitted to J. Electron Spectrosc. Relat. Phenom.

van Attekum P.M.Th.M., van der Velden J.W.A. and Trooster J.M., to be published.

Baer Y., Heden P.F., Hedman J., Klasson M., Nordling C. and Siegbahn K., 1970, Physica Scripta, 1, 55.

Baer Y. and Myers H.P., 1977, Solid State Commun., 21, 833.

Bongi G., Fischer O. and Jones H., 1974, J. Phys. F, 4, L259.

Bullet D.W., 1975, Solid State Commun., 17, 965.

Castelijns J.P.P. and de Vroomen A.R., 1978, Solid State Commun., 25, 461.

Chou T.S., Perlman M.L. and Watson R.E., 1976, Phys. Rev. B, 14, 3248.
Citrin P.H., Rowe J.E. and Christman S.B., 1976, Phys. Rev. B, 14, 2642.
Doniach S. and Sunjic M., 1970, J. Phys. C, 3, 285.
Fadley C.S., Baird R.J., Siekhaus W., Novakov T. and Bergström S.A.L., 1974, J. Electron Spectrosc. Relat. Phenom., 4, 93.
Franzen H.F. and Sawatzky G.A., 1975, J. Solid State Chem., 15, 229.
Friedman R.M., Hudis J., Perlman M.L. and Watson R.E., 1973, Phys. Rev. B, 8, 2433.
Hoogewijs R., Fiermans L. and Vennik J., 1977, Surf. Sci., 69, 273.
Höchst H., Hüfner S. and Goldmann A., 1976, Solid State Commun., 19, 899.
Höchst H., Hüfner S. and Goldmann A., 1976, Phys. Lett., 57A, 265.
Hummel R.E., 1971, Optische Eigenschaften von Metallen und Legierungen, Springer, Berlin.
Hüfner S., Wertheim G.K. and Buchanan D.N.E., 1974, Chem. Phys. Lett., 24, 527.
Hüfner S., Wertheim G.K., Wernick J.H., 1975, Solid State Commun., 17, 417.
Ley L., Pollak R.A., Kowalczyk S.P. and Shirley D.A., 1973, Phys. Rev. B, 8, 641.
Montgomery H. and Ruby S.L., 1970, Phys. Rev. B, 1, 4529.
Moore C.E., 1958, NBS Circular 467, U.S.G.P.O., WA, D.C.
Myron H.W. and Mueller F.M., 1978, Phys. Rev. B, 17, 1828.
Nöller H.G., Polaschegg H.D. and Schillalies H., 1974, J. Electron Spectrosc. Relat. Phenom., 5, 705.
Penn D.R., 1976, J. Electron Spectrosc. Relat. Phenom., 9, 29.
Pollak R.A., Ley L., McFeely F.R., Kowalczyk S.P. and Shirley D.A., 1974, J. Electron Spectrosc. Relat. Phenom., 3, 381.
Reilman R.F., Msezane A. and Manson S.T., 1976, J. Electron Spectrosc. Relat. Phenom., 8, 389.
Robins J.L., 1962, Proc. Phys. Soc., 79, 119.
Scofield J.H., 1976, J. Electron Spectrosc. Relat. Phenom., 8, 129.
Shevchik N.J., 1975, J. Phys. F, 5, 1860.
Siegbahn K., 1977, Molecular Spectroscopy, Ed. A.R. West, Heyden and Son, London.
Smith N.V., Wertheim G.K., Hüfner S. and Traum M.M., 1974, Phys. Rev. B, 10, 3197.
Sueoka O., 1965, J. Phys. Soc. Japan, 20, 2203.
Watson R.E. and Perlman M.L., 1975, Structure and Bonding, 24, 83.
Wertheim G.K. and Hüfner S., 1975, Phys. Rev. Lett., 35, 53.

Wertheim G.K. and Walker L.R., 1976, J. Phys. F, 6, 2297.

Wertheim G.K. and Buchanan D.N.E., 1977, Phys. Rev. B, 16, 2613.

CHAPTER 6

AN X-RAY PHOTOELECTRON SPECTROSCOPY STUDY OF SOME Au(I) AND Au(III) DITHIOCARBAMATES*

P M Th M van Attekum and J M Trooster

Abstract - *The factors influencing the decomposition rate of two gold(III) complexes in an X-ray photoelectron spectroscopy experiment were studied. It is shown, that the decomposition rate can be slowed down by using graphite as substrate and by lowering the sample temperature. From the Au(4f) spectrum a direct measure of the shift in the binding energy between Au(III) and Au(I) was determined and shown to be dependent on the electronegativity of the ligands. The valence bands of the complexes show a narrow Au(5d) band with a spin-orbit splitting of ~ 1.6 eV.*

6 1 Introduction

X-ray photoelectron spectroscopy (XPS) studies of gold metal and gold alloys are numerous. On the other hand only a few XPS investigations have been reported on solid samples of gold complexes[1-3]. A possible reason for this is, that the study of inorganic or organic complexes is often hampered by decomposition of the compounds during measurement. As part of an extensive XPS study of gold complexes we report here on the stability of two gold(III)-compounds as function of the sample preparation technique, temperature and X-ray intensity. The decomposition enables us to measure directly the difference in Au(4f) kinetic energy between Au(III) and Au(I) without correcting for charging effects and to study changes in the valence band structure with change in formal valence.

*Submitted to J. Chem. Soc., Dalton Transactions.

6.2 Experimental

The X-ray photoelectron spectra were measured with a Leybold-Heraeus LHS-10 spectrometer using Mg Kα radiation. Lines due to X-ray satellites were removed from the experimentally measured spectra using a computer program described earlier[4]. The spectrometer was set for an instrumental resolution of 0.8 eV. The compounds were prepared by Dr. J.G.M. van der Linden[5] using published methods[6]. We have studied dimethylgold(III)dimethyldithiocarbamate - $(CH_3)_2AuSSCN(CH_3)_2$ - and dibromogold(III)di-n-propyldithiocarbamate - Br_2Au $SSCN(n\text{-}C_3H_7)_2$. The samples for the XPS measurements were prepared either by sublimation in a preparation chamber at a pressure of about 10^{-5} Pa or by evaporation of a dilute solution. Sublimation was carried out on silver plated plated stainless steel platelets and has the advantage, that very homogeneous thin layers can be made, which, in general, yield appreciably narrower lines than can be obtained when measuring on powders. Evaporation of solutions was done on graphite, on glassy carbon and on the silver substrate. The porous surface of graphite induces rapid and even distribution of the liquid resulting in thin homogeneous samples. On the other hand evaporation on the silver substrate or the glassy carbon often results in layers of uneven thickness and visible crystallites. The graphite and glassy carbon substrates have the advantage, that the XPS spectrum is simple with a very weak valence band.

Computer fits were carried out on an IBM 370/158 computer. The fitting program is a least squares procedure described elsewhere[7]. Fitting the spectra with calculated lineshapes is difficult because the lines in general do not have a simple analytical lineshape and the background intensity is not a simple polynomial because of inelastically scattered electrons. If, however, a limited energy range is taken, the Au(4f) lines can be reasonably fitted with a sum of Lorentzians superposed on a sloped background.

6.3 Results

6.3.1 Decomposition rate

In Figures 6.1 and 6.2 the Au(4f) spectra of $(CH_3)_2Audtc$ (dtc = dithiocarbamate) and Br_2Audtc measured on samples prepared by sublimation on the silver substrate are shown as function of time. Clearly, both samples decom-

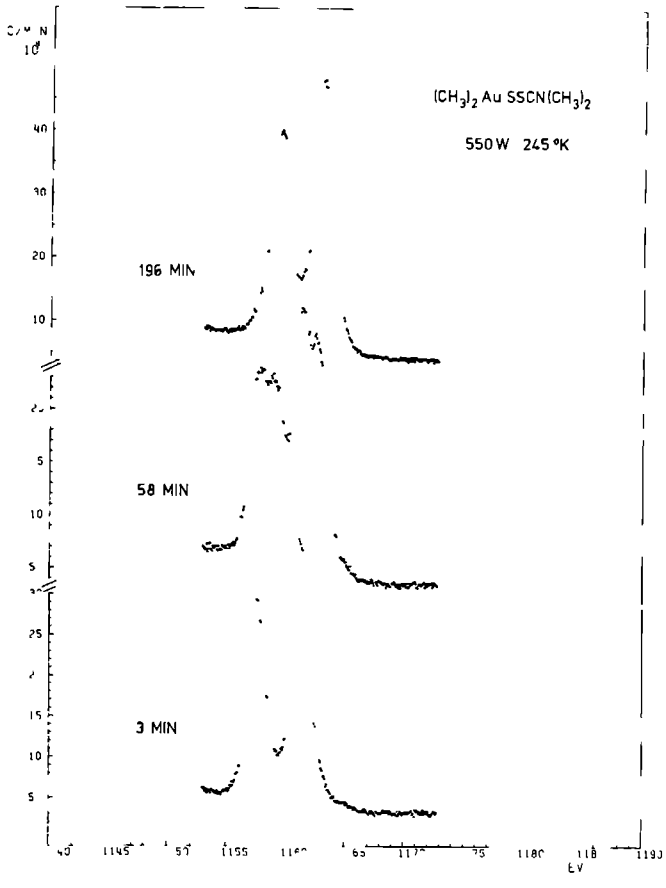

Figure 6.1 Au(4f) core lines of $(CH_3)_2$AuSSCN$(CH_3)_2$ sublimed on the silver substrate as function of the measuring time. The kinetic energy scale is not corrected for charging.

pose in the spectrometer. The decomposition rate for sublimed samples was determined by fitting the experimental 4f-spectra with two pairs of Lorentzians with equal linewidth, a separation of the lines within a pair of 3.70 eV and an intensity ratio equal to 1.25 for the lines within a pair. (The value of 1.25 is the theoretical ratio given by Scofield[8]). In Figure 6.3 the percentage of decomposition product, derived from the intensity ratio of the two pairs in the spectrum, is plotted for $(CH_3)_2$Audtc. It is obvious, that the decomposition rate of $(CH_3)_2$Audtc depends strongly on the X-ray intensity and

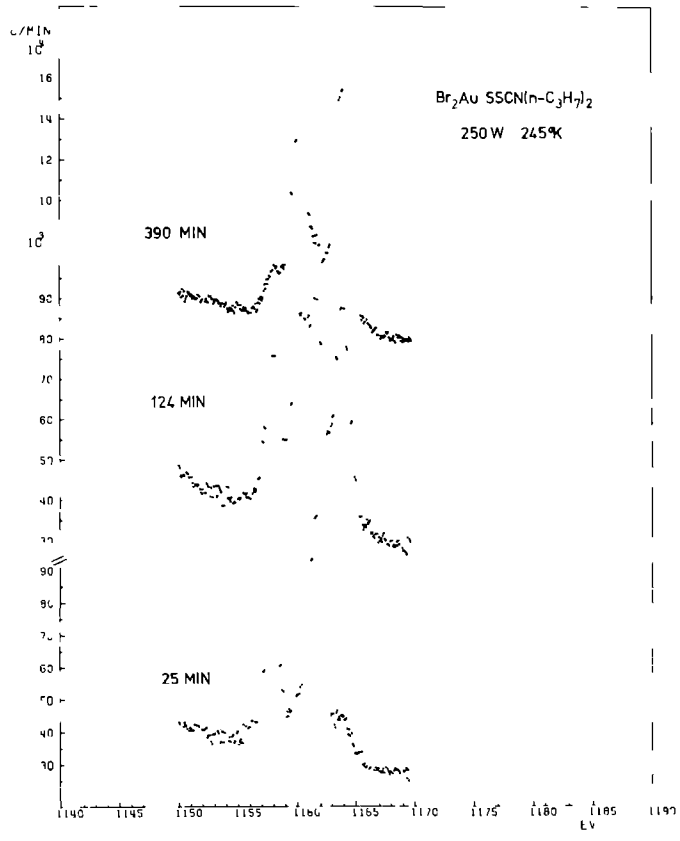

Figure 6.2 Au(4f) core lines of $Br_2Au(SSCN(n\text{-}C_3H_7)_2$ sublimed on the silver substrate as function of the measuring time. The kinetic energy scale is not corrected for charging.

sample temperature. Similar results were found for Br_2AuCl and for samples prepared by evaporation of a dilute solution on the silver substrate. With the X-ray tube switched off no decomposition occurred. The decomposition rate was independent of the thickness of the sample. However, for samples prepared by evaporation of a solution on graphite the decomposition rate is at least an order of magnitude slower. This cannot be due to the presence of carbon, since samples prepared by evaporation on glassy carbon decompose almost as fast as when evaporated on the silver substrate. A possible explanation of the stabilizing effect of graphite could be a binding of the compound with

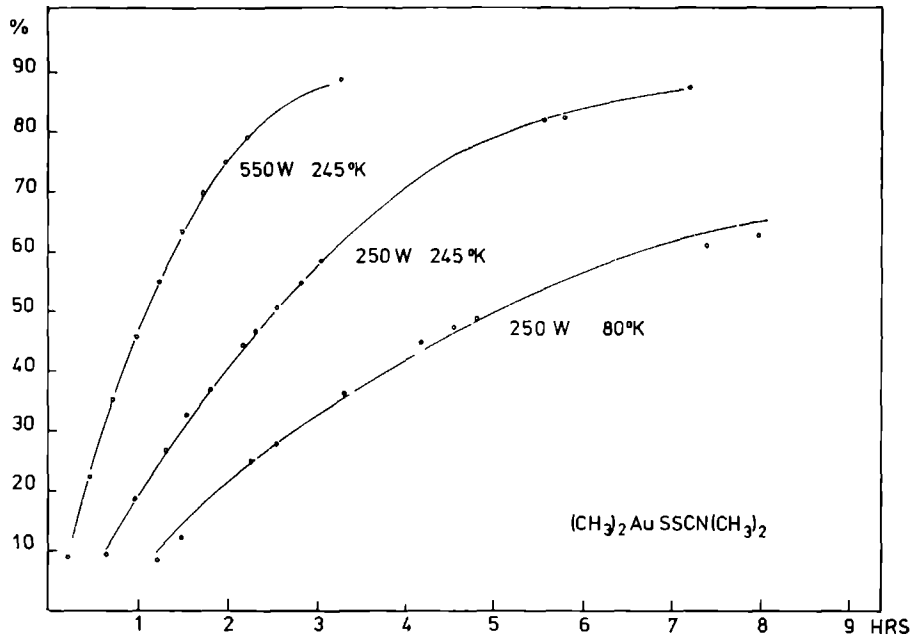

Figure 6.3 Increase of the percentage of the decomposition product of $(CH_3)_2AuSSCN(CH_3)_2$ as function of the sample temperature and X-ray intensity. The points are obtained by fitting the experimental spectra as shown in Figure 6.1 with two pairs of Lorentzians. The estimated error in the percentages is 10%.

the delocalized π-system of graphite (in glassy carbon this delocalization is much smaller). However, ^{197}Au Mossbauer spectra[9] of $(CH_3)_2$Audtc pure and evaporated on graphite show no difference. Thus, the binding has to be weak and does not change the compound under study. Obviously, the substrate plays an important role in the decomposition as well as the X-ray irradiation.

6.3.2 Line positions

In Table 6.1 the experimentally measured kinetic energies of the core lines for the starting and decomposition product of $(CH_3)_2$Audtc and Br_2Audtc are listed. Since the compounds are electrical insulators, charging of the sample can occur, resulting in lower measured kinetic energies. However, charging of samples is smaller the thinner the sample and from a series of

Table 6.1 Kinetic energy, corrected for charging (see text), of the relevant core levels of the compounds studied. The estimated errors are ± 0.2 eV.

	$(CH_3)_2Au(III)SSCN(CH_3)_2$		$Br_2Au(III)SSCN(n\text{-}C_3H_7)_2$			
peak	starting product	decomposition product	starting product	decomposition product	Au(I)SSCN $(n\text{-}C_4H_9)_2$	Au(I)SSCN $(n\text{-}C_3H_7)_2$
C(1s)	964.4	964.4	964.4	964.4	964.4	964.4
$Au(4f_{7/2})$	1163.0[5]	1164.5	1162.2	1164.6	1164.6	1164.8
S(2p)	1085.9	1086.0	1085.7	1086.1	1086.4	1086.6
N(1s)	848.8[5]	848.7	848.8	848.8	849.2	849.3

measurements on very thin samples of $(CH_3)_2$Audtc we derive a maximum value of 1163.0 eV for the kinetic energy of the $Au(4f_{7/2})$ line. This is to be compared with a kinetic energy of 1165.2 eV for $Au(4f_{7/2})$ in Au metal. The C(1s) kinetic energy in this case is 964.4 eV compared to 964.7 eV in graphite. In Table 6.1 we have used this value of C(1s) as an internal standard in all compounds measured to account for the effects of charging.

From the shift in kinetic energy of the $Au(4f_{7/2})$ line during the decomposition it is clear, that the Au is reduced in both cases. The reduced product is probably a Au(I)dtc complex, as the values of the kinetic energies of the core levels of C, Au, S and N in the decomposition product closely resemble those of two Au(I)dtc complexes which were measured separately and did not show any decomposition. The kinetic energy of the Au(4f) lines of starting and decomposition product differs by 2.4 ± 0.1 eV for Br_2Audtc and 1.5 ± 0.1 eV for $(CH_3)_2$Audtc. If we assume, that the endproduct in both cases is Au(I)dtc, the difference in shift of the Au(4f) lines must be attributed to the difference in electronegativity of Br and CH_3. According to Gelius et al.[10] the group-electronegativities of Br and CH_3 as derived from a series of XPS spectra is 3.3 and 2.0, respectively. The larger electronegativity of Br results in a larger positive charge on Au in Br_2Audtc. This is also in agreement with Mossbauer measurements on these compounds[7]. $(CH_3)_2$Audtc has a larger isomer shift and quadrupole splitting than Br_2Audtc indicating a more covalent bonding in the methyl complex. It is unlikely, that the decomposition product is metallic gold as the kinetic energy of the 4f lines of the endproduct is 0.7 eV lower than for Au metal. Van de Vondel et al.[1] found an energy diffe-

rence of 2.0 eV between formal gold(III) and gold(I) compounds. The present results show, however, that the range of Au(4f) binding energies in gold(III) complexes is at least 1.0 eV wide.

6.3.3 Valence bands

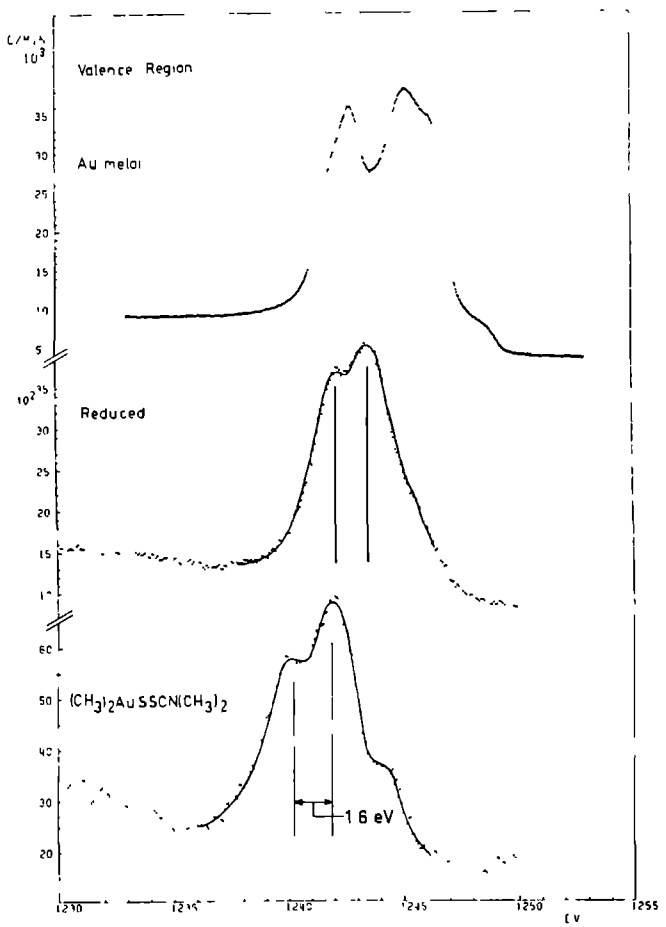

Figure 6.4 Valence bands of $(CH_3)_2AuSSCN(CH_3)_2$, its decomposition product and gold metal. The kinetic energy scale of the gold compounds is adapted such, that the Au(4f) core lines lie at the positions as stated in Table 6.1.

In Figure 6.4 the valence bands of $(CH_3)_2$Audtc and its decomposition product are compared with the valence band of gold metal. To our knowledge, this is the first XPS measurement of the Au(5d) level in a molecular complex. The spectrum of $(CH_3)_2$Audtc is a sum of several measurements of one hour at 80°K and 250 W X-ray power, and the amount of decomposition product formed during this time is less than 5%. The broadening of the $5d_{5/2}$ peak in gold metal due to overlap of Au(5d) bands is reduced in the complexes. In the valence band spectrum of $(CH_3)_2$Audtc the two peaks are attributed to the Au(5d) level with a spin-orbit splitting of 1.6 ± 0.1 eV. The free atom spin-orbit splitting is 1.5 eV[11]. The shoulder on the high kinetic energy side of $(CH_3)_2$ Audtc is ascribed to the bonding MO's. The Au(5d) levels in the decomposition product, Au(I)dtc, are shifted by ~ 1.6 eV with respect to $(CH_3)_2$Audtc in good agreement with the shift of the Au(4f) lines. The shoulder is reduced in intensity presumably reflecting the removal of CH_3.

6.4 Conclusions

The results of this investigation lead to the following conclusions: In XPS measurements of Au(III) complexes and possible of other compounds as well, the decomposition rate can be reduced considerably by using graphite as substrate and by lowering the sample temperature.

The Au(III)dithiocarbamate complexes studied are reduced to a Au(I)dithiocarbamate. The binding energy of the 4f core levels of the Au(III) complexes is strongly dependent on the ligand groupelectronegativity. The shift in binding energy of the 4f core levels on reduction is also found for the Au(5d) level, which shows narrow atomic-like lines with a spin-orbit splitting of 1.6 eV.

6.5 References

1. D.F. van de Vondel, G.P. van der Kelen, H. Schmidbaur, A. Wolleben and F.E. Wagner, Physica Scripta, 16 (1977) 364.
2. C. Battistoni, G. Mattogno, F. Cariati, L. Naldini and A. Sgamelotti, Inorg. Chim. Acta, 24 (1977) 207.
3. J. Knecht, R. Fischer, H. Overhof, F. Hensel, J.C.S., Chem. Commun, 905 (1978).

4. P.M.Th.M. van Attekum and J.M. Trooster, J. Electron Spectrosc. Relat. Phenom., 11 (1977) 363.
5. Dr. J.G.M. van der Linden, Research Institute of Materials, Department of Inorganic Chemistry, University of Nijmegen.
6. H.J.A. Blaauw, R.J.F. Nivard and G.J.M. van der Kerk, J. Organometal. Chem., 2 (1964) 236.
7. M.P.A. Viegers, Thesis, Nijmegen (1976).
8. J.H. Scofield, J. Electron Spectrosc. Relat. Phenom., 8 (1976) 129.
9. G.H.M. Calis, private communication.
10. U. Gelius, P.F. Hedén, J. Hedman, B.J. Lindberg, R. Manne, R. Nordberg, C. Nordling and K. Siegbahn, Physica Scripta, 2 (1970) 70.
11. C.E. Moore, Atomic Energy Levels (U.S. Department of Commerce NBS Circular Nr. 467) (1958).

CHAPTER 7

AN X-RAY PHOTOELECTRON SPECTROSCOPY STUDY OF GOLD CLUSTER AND GOLD(I) PHOSPHINE COMPOUNDS*

P.M.Th.M. van Attekum, J.W.A. van der Velden and J.M. Trooster

Abstract - *X-ray photoelectron spectra have been measured of the gold cluster compounds* $Au_{11}L_7X_3$, $[Au_9L_8]^{3+}[Y]_3$ *and* $[Au_8L_8]^{2+}[Y]_2$ *with L = tri-aryl phosphine, X = Cl, I, SCN or CN and Y =* PF_6, ClO_4 *or* NO_3. *These were compared with XPS spectra of a series of gold(I) compounds with the same ligands. All gold atoms in the gold cluster complexes have the same binding energy for 4f electrons as in the gold(I) compounds. The Au(5d) valence band does not show any broadening attributable to d-electron delocalization. These results support the earlier conclusions drawn from Mössbauer data that there is little interaction between the peripheral gold atoms in the gold cluster compounds. The intensities of XPS lines were also measured and found to be consistent with the composition quoted for the various compounds and with theoretical cross sections.*

7.1 Introduction

In two recent papers Vollenbroek et al.[1,2] have presented results of a Mossbauer study of two types of gold cluster compounds: $Au_{11}L_7X_3$ and $[Au_9L_8]^{3+}[Y]_3$ L = tri-aryl phosphine, X = Cl, I, SCN or CN and Y = PF_6, ClO_4 or NO_3. In both types, one central gold atom has bonds with all other (peripheral) gold atoms of the cluster, which are bonded to the ligands L and X. This is illustrated in Figs. 7.1 and 7.2. From the Mössbauer spectra it was concluded that the electronic structure is best described by considering the peripheral gold atoms to be linearly coordinated to the central gold atom on one side and the tri-aryl phosphine or (pseudo) halide on the other side.

Submitted to: Inorg. Chem.

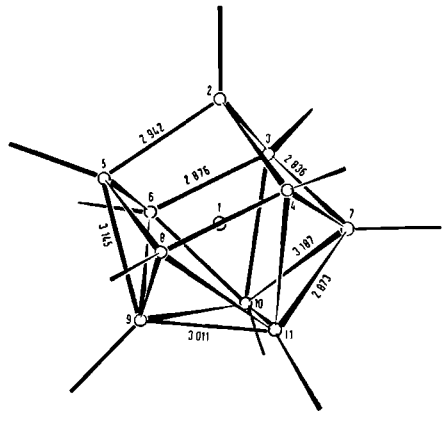

Figure 7.1 Structure of gold cluster in $Au_{11}[P(p\text{-}FC_6H_4)_3]_7I_3$. *Sites 6, 7 and 8 are coordinated to Iodine and the others to* $P(p\text{-}FC_6H_4)_3$.

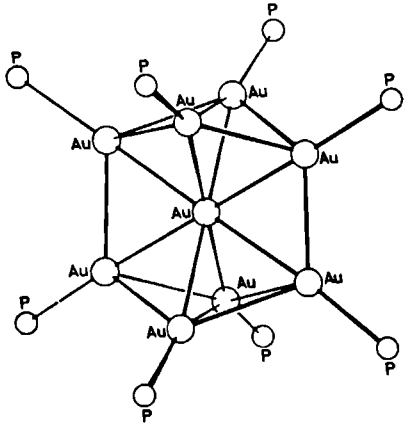

Figure 7.2 Au-P skeleton in $Au_{11}[P(C_6H_5)_3]_8^{3+}$.

This implies that only weak bonding exists between the peripheral gold atoms. Consequently, the main difference in the electronic structure is caused by the attached ligands. This view-point conflicts with Molecular Orbital calculations by Mingos[3] and with an X-ray photoelectron spectroscopy (XPS) study of Battistoni et al.[4]. The M.O. calculations indicated that appreciable dif-

ferences in net charge exist between the various gold atoms in the cluster and the XPS data of Battistoni et al.[4] seemed to corroborate this result as several Au 4f binding energies were found. In this paper we present results of XPS measurements of several Au_9 and Au_{11} clusters, and of a new cluster compound containing eight gold atoms[5]. To aid in the interpretation, we have also measured several Au(I) compounds with the same ligands as present in the cluster compounds.

If there is appreciable bonding between peripheral gold atoms in the cluster, one expects this to have a measurable effect on the width of the gold 5d level. Calculations of the bandstructure of small metallic clusters of Ni and Pt indicate that already for thirteen atoms the d-band width resembles that of the bulk metals[6]. We have therefore measured the 5d bands of both Au(I) and gold cluster compounds rather extensively. The large number of compounds measured has prompted us to measure the intensities of the various XPS lines as well in an attempt to assess the possibilities of XPS for quantitative analysis.

7.2 Experimental

A Leybold-Heraeus LHS-10 spectrometer equipped with a Mg anode was used to measure the X-ray photoelectron spectra. Lines due to X-ray satellites were removed from the measured spectra with a computer program described elsewhere[7]. Although the minimum instrumental resolution of this spectrometer is 0.64 eV, we have used a resolution of 0.8 eV throughout this study to increase the count-rate.

The cluster compounds were prepared by F.A. Vollenbroek[8] and the Au(I) phosphine complexes by J.G.M. van der Linden[8]. Samples for XPS measurements were prepared by evaporation on graphite of a dilute solution of the compound in dichloromethane. It was found recently, that by using graphite as a substrate, the decomposition rate of Au(III) dithiocarbamate complexes can be considerably reduced[9]. In those cases where decomposition was found to be appreciable (cluster compounds), the decomposition was further reduced by decreasing the temperature of the sample to -150 °C. The Au(4f) line was monitored repeatedly and the measuring time limited to prevent build-up of decomposition.

Although graphite has a very weak valence band intensity in XPS spectra [10], the samples were usually so thin that the graphite background interfered

with the valence bands of the compounds. The measured valence band spectra were, therefore, corrected for the graphite background by subtracting the spectrum of pure graphite. The scaling factor was determined from an analysis of the measured C(1s) line.

7.3 Results

A list of the Au(I) compounds, that were measured, is given in Table 7.1,

Table 7.1 Kinetic energies, corrected for differences in charging with P(2p) = 1117.0 eV, of the core levels in the gold(I) phosphine compounds. The estimated uncertainty in the positions is ± 0.2 eV.

compound	Au(4f 7/2)	P(2s)	Cl(2p 3/2) [b]	C(1s) [c]	Br(3d 5/2)	Br(3d)	I 3d 5/2)	I(3d 5/2)	S 2p)	S 2s)	O(1s)
AuL(L 3)	1163.5	1059.7		1050.1							
AuL Cl	1163.3	1059.5	1198.1	1050.5							
Au Br	1163.4	059.5			1066.7	1180.1					
AuL'Br	63.5	1059.5	059.4		1066.7	71.8					
AuLI	1163.7	1059.5					629.1	1138.9			
AuL'I	1163.8	1059.7	1198.7					1138.7			
Au 'CN	1163.2	1059.5	1048.4							850.3	
Au 'SCN	1 63.4	1059.5	1048.6						1486.0	850.7	
Au PMC	1163.4	1059.3		1050.5							
Au PPhCl	1163.5	059.3		1050.6							
Au PPCl	1163.4	1059.5		1050.5							
AuNO$_3$	1163.6	1059.5								849.0	716.5
AuL NO$_3$	1163.9	1059.6									717.1
Au$_2$PM(Ac)$_2$	1163.9	1059.7									716.8
Au D(C H _	1163.6	059.3									

a) L = P(C H) , ' = P(p-(C H) , PM = (C H) PCH = (C H) , PPh = (H) P-C H P(C) PP = ( ) m (( )

b) chlorine substituted in the benzene ring

c) chlorine directly bound to gold

which presents the positions of the main XPS lines of each element present. All these compounds are nearly linearly coordinated with a tri-aryl phosphine ligand on one side and, with a few exceptions, a (pseudo) halide on the other side.

The determination of the binding energy of electrons in non-conducting solids presents a fundamental difficulty. In conducting solids the absolute binding energy can be determined from the photoelectron kinetic energy, only when the workfunction of the compound is known. Where this is mostly not the case, binding energies in conductors are usually referred to the Fermi energy. Such an internal standard is not available in non-conducting solids. This problem is confounded by the fact that due to photoemission an insulating solid can acquire a net positive charge and the resulting potential diffe-

rence with the spectrometer housing sometimes leads to very large shifts (several eV) in the measured kinetic energy of the photoelectrons. In our case all compounds contain phosphorous in a di- or tri-aryl phosphine ligand and we have chosen the P(2p) line of this phosphorous atom as the internal standard. The popular choice of an aryl or alkyl C(1s) as a standard was not used because of overlap with the C(1s) of the graphite substrate. The P(2p) kinetic energy was set at 1117.0 eV. The kinetic energy values can be compared with binding energy values relative to the C(1s) line at a binding energy of 285.0 eV[11] using the relation $E_{kin} = 1249.15 - E_B$, where E_{kin} and E_B are the kinetic energy of the photoelectron and the binding energy, respectively, and the value of 1249.15 is the kinetic energy of an electron ejected from the Fermi level.

Table 7.2 Ratios of the area intensities per atom in the Au(I) compounds. The estimated errors in the ratios are 10%.

Compound	Au(4f)/P(2p)	Cl(2p)/P(2p)	Au(4f)/Cl(2p)
AuCl a)	13.9	0.65	1.70	8.1
AuCl	11.3	0.57	1.96	7.3
AuBr	12.7	0.61		
AuBr	13.7	0.75	1.72	8.0
AuI	9.7	0.0		
AuI	11.7	0.0	1.86	7.5
AuSCN	17.7	0.7	2.3	6.2
Au(PMe3)Cl	15.9	0.73	1.99	8.1
Au(PEt3)Cl	12.1	0.71	1.7	7.6
AuPPh3Cl	14.3	0.9	1.86	8
Average	1.2	0.67	1.8	7.8
Calculated c)	1	0.81	1.95	7.7

a) Au - P(2p) P(2p)-Cl(2p) , Au - Cl(2p) P(2p)-Cl(2p) ,
Au(4f) (Au-P-Cl(2p)) , Au(4f) (Au-Cl-P(2p))

b) Au determined due to overlap of P(2s) and Cl(2s)

c) From ref. [11]

In Table 7.2 we list the experimental ratios of the area intensities per atom of the Au, P and Cl in the Au(I) compounds. The values obtained on the different compounds agree within 10-15%. Theoretically the intensities per atom are given by:

$$\frac{I_1'}{I_2'} = \frac{I_1/N_1}{I_2/N_2} = \frac{\sigma_1(\varepsilon_1)}{\sigma_2(\varepsilon_2)} \frac{[1 + \beta_1(\varepsilon_1)/16]}{[1 + \beta_2(\varepsilon_2)/16]} \frac{T(\varepsilon_1)}{T(\varepsilon_2)} \frac{\lambda(\varepsilon_1)}{\lambda(\varepsilon_2)} \qquad (1)$$

where $\sigma_i(\varepsilon_1)$ is the cross section for photoionization from level i, $\beta_i(\varepsilon_1)$ is the angular anisotropy parameter, $T(\varepsilon_1)$ is the transmission of the spectro-

meter at energy ε_1 and $\lambda(\varepsilon_1)$ is the mean free path in the sample under consideration of an electron with energy ε_i. The theoretical values of the cross section for photoionization with Mg $K\alpha_{1,2}$ radiation have been calculated by Scofield[12]. The anisotropy parameters $\beta_1(\varepsilon_i)$ are given by Reilman et al.[13]. The transmission of the LHS-10 electron spectrometer is inversely proportional to the kinetic energy of the electron[14]. Penn[15] has presented calculations of the mean free path for pure elements and for compounds, but his results deviate strongly from experimental data on KI[16]. We use the approximate expression $\lambda(\varepsilon_i) = \alpha(\varepsilon_i)^{\frac{1}{2}}$ where α is a constant. The theoretical values for I_1'/I_2' calculated with Eq.(1) are also given in Table 7.2. The agreement between calculated and experimental values is good, except for the P(2s)/P(2p) ratio. In view of the general agreement between experimental and theoretical values it is probable that the calculated value of the P(2s) cross section is too large.

Table 7.3 Kinetic energies, corrected for differences in charging with P(2p) of the tri-aryl phosphine group set equal to 1117.0 eV, of the core levels in the gold cluster compounds. The estimated uncertainty in the positions is ± 0.2 eV. The measurements were done at -150 °C.

compound	Au(4f$_{7/2}$)	P(2s) [b]	P(2p) [c]	Cl($2p_{3/2}$) [d]	Cl($2p_{3/2}$) [e]	F(1s)	S(2p)	N(1s)	O(1s)
$Au_8[P(C_6H_5)_3]_8(ClO_4)_2$ [a]	1163	1059.3			1641.2				716.1
$Au_8[P(C_6H_5)_3]_8(PF_6)_2$	1163.4	1059.3	1105.4	1112.3		687.3			
$Au_8[P(C_6H_5)_3]_8(NO_3)_2$ [f]	1163.9	1059.5							716.7
$Au[P(C_6H_5)_3](SCN)_2$	1163.7	1059.4					1082.8	850.6	
$Au[P(C_6H_5)_3](SCN)_3$	63.5	59.5		948.2			1082.8		
$Au_8[P(C_6H_5)_3]_8(PF_6)_2$	1163.5	1059.4	1105.3	1112.4		687.6			

a) $P = P(C_6H_5)_3$, $P' = P(p\text{-}ClC_6H_4)$
b) phosphorous of the tri-aryl phosphine group
c) phosphorous of the PF_6-group
d) chlorine substituted in the benzene ring
e) chlorine of the ClO_4-group
f) measured at room temperature

Table 7.3 lists the positions of the main XPS lines of the cluster compounds that have been investigated. The $Au_8[P(C_6H_5)_3]_8[PF_6]_2$ complex is a new cluster compound reported recently by Vollenbroek et al.[5]. The geometry of the Au_8 skeleton can be described as being derived from that of the Au_{11} cluster given in Figure 7.1 by removal of the three gold atoms in the basal triangle. Only one Au 4f doublet was observed in all cluster compounds. Fig.

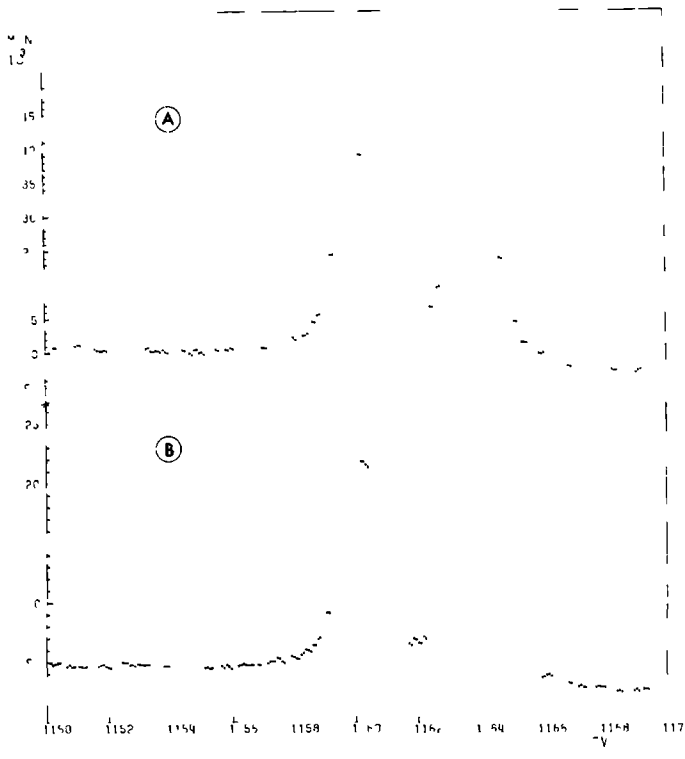

Figure 7.3 X-ray photoelectron spectrum of the Au(4f) levels in $AuI(p\text{-}ClC_6H_4)_3Br$ (A) and $Au_9[P(C_6H_5)_3]_8[ClO_4]_3$ (B). The spectra have been corrected for the X-ray satellites, but no correction for the charging was made.

7.3 illustrates the close similarity between the Au(4f) spectrum of a gold(I) phosphine complex and a cluster compound. The observed linewidth is in both cases 1.5 + 0.1 eV. This is larger than measured on gold metal (1.2 eV) at the same spectrometer resolution and is probably due to small inhomogenities in the charging of the sample. Table 7.4 gives the experimental ratios of the area intensity per atom of the Au, P and Cl in the gold cluster compounds. There is excellent agreement with the values found for the gold(I) phosphine complexes.

In Fig. 7.4 are shown the valence bands of AuLSCN, AuL'SCN, $Au_{11}I_7(SCN)_3$ and $Au_1L'_7(SCN)_3$ where $L = P(C_6H_5)_3$ and $L' = P(p\text{-}ClC_6H_4)_3$. As in the case of the binding energies a close similarity is found for the gold(I) phosphine

compounds and the gold cluster complexes.

Table 7.1 Ratios of the area intensities per atom in the gold cluster compounds. The estimated errors in the ratios are 10%.

Compound	Au 4f/P(2p)	P(C6H5)3(2p)	C(1s)/P	Au(4f)/C(2p)	Pt4/P(2p)[a] [b]
Au[P(C6H5)3]3Cl	1.3	0.74	1.5	1.3	
Au4[PP3]	1.0	0.66			0.37 [0.38]
Au6[P(SO3)3]6	6.8	0.72			
Au[P(SC6H5)]	1.5	0.67			
Au[P(SC6H5)]	1.4	0.65	2.1	6.7	
Au4[PP3]	1.3	0.74			0.25 [0.25]

a) P = P(C6H5)3 or P(C6H5)2(CH2)2P(C6H5)2

b) Experimental ratio of the two isotopic lines of the PP3 group and the P(C6H5)3 group. The values between brackets are the theoretical values.

7.4 Discussion

$AuP(C_6H_5)_3Cl$ and $Au_2(C_6H_5)_2P(CH_2)P(C_6H_5)_2Cl_2$ have been measured by van de Vondel et al.[11] and there is excellent agreement with the present results. Battistoni et al.[4] studied a series of mononuclear gold compounds. After correction for the different internal standards, there is good agreement between their values and those reported here. For the gold(I) compounds studied by us there is surprisingly little variation in the kinetic energy of the Au(4f) lines, but there is significant difference with the kinetic energy of the Au(4f) lines reported elsewhere[9] for gold(I) dithiocarbamates (Audtc), where gold is coordinated to two sulphur atoms. The kinetic energy of the Au(4f) lines of the Au(I)dtc complexes is 1.0 eV larger. A similar difference was found by van de Vondel et al.[11] between $AuP(C_6H_5)_3Cl$ and $Au_2(S_2P(C_2H_5)_2)_2$, which also contains two sulphur atoms directly connected with Au(I).

The present results support the description of peripheral gold atoms in the cluster compounds as being linearly coordinated: the binding energies of the Au(4f) electrons are identical to those of the gold(I) phosphine compounds and most importantly, the valence bands do not show any broadening which would point to a significant d-electron delocalization in the gold clusters. It is surprising, though, that in the 4f spectra no trace is found of the central gold atom, for which one expects an electronic structure different from the peripheral gold atoms. Apparently, the Au(4f) binding energy of the central gold atom is very close to that of the peripheral gold atoms.

Figure 7.4 X-ray photoelectron spectra -after correction for the substrate valence band- of the valence bands in AuLSCN (A), AuL'SCN (B), $Au_{11}L_7(SCN)_3$ (C) and $Au_{11}L'_7(SCN)_3$ (D) where L = $P(C_6H_5)_3$ and L' = $P(p\text{-}ClC_6H_4)_3$. The spectra are normalized on the $Au(4f_{7/2})$ line.

In view of the widths of the 4f lines and the small relative intensity of the line due to the central gold atom, we estimate the maximum binding energy difference to be less than 0.5 eV. Battistoni et al.[4] observed the appearance of extra 4f lines in the XPS spectra of the cluster compounds. These extra lines, however, must be ascribed to decomposition products, since we observe

these extra lines only after prolongated measuring times.

The valence band of both the gold(I) phosphine compounds and gold cluster complexes consists, generally, of a doublet due to the spin orbit split Au(5d) bands and a shoulder the intensity of which depends on the ligands. The spin orbit splitting is 1.6 ± 0.2 eV. When P(p-ClC_6H_4) is present the splitting of the 5d lines is no longer resolved: the Cl(3p) line of this ligand is situated between the two 5d bands. Subtracting the normalized valence band spectrum of $Au_pL_qX_r$ from that of $Au_pL'_qX_r$ - L = $P(C_6H_5)_3$ and L' = $P(p\text{-}ClC_6H_4)_3$ - we found a single line at 1242.3 ± 0.3 eV. The energy difference with the corresponding $Cl(2p_{3/2})$ line is 193.9 + 0.4 eV in good agreement with the separation of 193.2 eV found in KCl[17].

A number of other results are noteworthy: The kinetic energy of the $Cl(2p_{3/2})$ line of the chlorine directly bound to gold is 2.1 ± 0.2 eV higher than of the chlorine in the benzene rings. For the phosphorous atoms in PF_6 and $P(C_6H_5)_3$ a difference of 4.5 ± 0.2 eV is found, in good agreement with literature[18]. The cross section ratios per atom for the gold(I) phosphine complexes agree with each other within 10-15%. The corresponding ratios for the gold cluster compounds lie within the same range, i.e. they are in agreement with the quoted nominal composition of the gold cluster compounds. However, the determination of the composition of a sample with XPS is only possible within 10-15%.

7 5 References

1. F.A. Vollenbroek, P.C.P. Bouten, J.M. Trooster, J.P. van den Berg and J.J. Bour, Inorg. Chem., 17, 1345 (1978).
2. F.A. Vollenbroek, J.J. Bour, J.M. Trooster and J.W.A. van der Velden, J. Chem. Soc., Chem. Commun., 907 (1978).
3. D.M.P. Mingos, J. Chem. Soc., Dalton Trans., 1163 (1976).
4. C. Battistoni, G. Mattogno, F. Cariati, L. Naldini and A. Sgamelotti, Inorg. Chim. Acta, 24, 207 (1977).
5. F.A. Vollenbroek, W.P. Bosman, J.J. Bour and P.T. Beurskens, to be published.
6. R.P. Messmer and S.K. Knudson, K.H. Johnson, J.B. Diamond and C.Y. Yang, Phys. Rev. B, 13, 1396 (1976).
7. P.M.Th.M. van Attekum and J.M. Trooster, J. Electron Spectrosc. Relat. Phenom., 11, 363 (1977).

8. Research Institute of Materials, Department of Inorganic Chemistry, University of Nijmegen.
9. P.M.Th.M. van Attekum and J.M. Trooster, to be published.
10. F.R. McFeely, S.P. Kowalczyk, L. Ley, R.G. Cavell, R.A. Pollak and D.A. Shirley, Phys. Rev. B, 9, 5268 (1974).
11. D.F. van de Vondel, G.P. van der Kelen, H. Schmidbaur, A. Wolleben and F.E. Wagner, Physica Scripta, 16, 364 (1977).
12. J.H. Scofield, J. Electron Spectrosc. Relat. Phenom., 8, 129 (1976).
13. R.F. Reilman, A. Msezane, S.T. Manson, J. Electron Spectrosc. Relat. Phenom., 8, 389 (1976).
14. H.G. Noller, H.D. Polaschegg and H. Schillalies, J. Electron Spectrosc. Relat. Phenom., 5, 705 (1974).
15. D.R. Penn, J. Electron Spectrosc. Relat. Phenom., 9, 29 (1976).
16. J. Szajman, J. Liesegang, R.C.G. Leckey and J.G. Jenkin, Phys. Rev. B, 18, 4010 (1978).
17. Unpublished results.
18. E.Fluck and D. Weber, Z. Naturforsch., 29b, 603 (1974).

SAMENVATTING

Fotoelektron spektroskopie is een relatief nieuwe experimentele methode om de bindingsenergie van de elektronen in een atoom of molekuul te bepalen. Het te onderzoeken preparaat wordt in vakuum bestraald met licht, waardoor elektronen uit het preparaat kunnen worden vrijgemaakt. De aldus gekreeerde fotoelektronen bezitten een kinetische energie gelijk aan het verschil tussen de energie van het lichtkwant en de bindingsenergie van het vrijgemaakte elektron. In de experimenten, die hier besproken worden, werd steeds magnesium rontgenstraling als lichtbron gebruikt. Aangezien de energie van de rontgenkwanten bekend is, kan door meting van de kinetische energie van het fotoelektron de bindingsenergie van het vrijgemaakte elektron bepaald worden. De elektronen van een atoom -al dan niet opgenomen in een groter geheel- kunnen sterk verschillende bindingsenergieen bezitten. In het algemeen maakt men een onderverdeling in core elektronen -die elektronen, die zich dicht bij de kern van het atoom bevinden en in molekulen niet aan de binding deelnemen- en valentie-elektronen. Naast de verschillen in bindingsenergie binnen een element, bestaan er ook grote verschillen tussen de elementen. Dientengevolge kan rontgen fotoelektron spektroskopie als een analyse-techniek gebruikt worden. De mogelijkheden zijn echter uitgebreider. De bindingsenergie van een core elektron is afhankelijk van de chemische en/of elektronische omgeving van het atoom en de bindingsenergie van de valentie-elektronen wordt in sterke mate bepaald door de binding. In principe kunnen gassen, vloeistoffen en vaste stoffen met rontgen fotoelektron spektroskopie bestudeerd worden. In dit proefschrift worden echter alleen experimenten aan vaste stoffen besproken.

Alvorens in te kunnen gaan op de toepassingen van rontgen fotoelektron spektroskopie moet een experimentele moeilijkheid opgelost worden. De gebruikte rontgenstraling is niet monochromatisch. Door de rontgen-satellieten ontstaan duplikaten van de aanwezige spektraallijnen, die het experimentele spektrum extra gekompliceerd maken. In hoofdstuk 2 wordt een numerieke methode beschreven om deze duplikaten uit het experimentele spektrum te verwijderen. De resolutie, die met deze kwasi-monochromatische lichtbron bereikt kan worden, bedraagt 0.64 eV (zie hoofdstuk 3).

In dit proefschrift worden drie soorten van toepassingen van rontgen fotoelektron spektroskopie besproken nl. de excitatie van plasmonen, de veranderingen in de elektronische struktuur bij het vormen van legeringen uit twee metalen en een studie van goudverbindingen.

Plasmonen zijn oscillaties in de elektronendichtheid. Een fotoelektron kan interaktie vertonen met de plasmonen zowel tijdens zijn kreatie (intrinsiek) als tijdens het transport van het fotoelektron door het preparaat (extrinsiek). Als gevolg hiervan neemt de kinetische energie van het fotoelektron met een diskrete hoeveelheid af in vergelijking met een fotoelektron, dat geen interaktie met de plasmonen heeft ondergaan. In het experimentele spektrum resulteert dit in een serie (ook meerdere plasmonen kunnen geexciteerd worden) van satellieten met een lagere kinetische energie dan de piek van de ongestoorde fotoelektronen. In het geval van vrije elektron metalen (bijv. Mg, Al) zijn de plasmon-verlies pieken scherp en intens. Door een analyse van de oppervlakte-intensiteiten van de plasmon-verlies pieken kan een schatting gemaakt worden van de bijdragen van extrinsieke en intrinsieke processen in de excitatie van plasmonen. Voor Mg en Al metaal blijkt de bijdrage van de intrinsieke plasmon excitaties ongeveer 25% te zijn. In overeenstemming hiermee werd een plasmon-gain piek gevonden in het KLL Auger spektrum van zowel Mg als Al. De lijnvorm van de plasmon-verlies pieken kan, met name voor de hogere orde pieken, niet met bestaande theorieen beschreven worden, ook als met de dispersie rekening wordt gehouden.

De elektronische struktuur van een atoom in een legering kan sterk verschillen met die van het pure metaal. Voor de legeringen PdSb, PtBi en AuSn hebben we de veranderingen in de elektronische struktuur onderzocht met behulp van rontgen fotoelektron spektroskopie. De relatieve intensiteiten van de verschillende core lijnen werden vergeleken met theoretische waarden. Ofschoon de nauwkeurigheid van de intensiteitsmetingen niet erg groot is, kunnen grote afwijkingen van de bulk-samenstelling op deze manier aan het licht komen. Aldus werd gevonden, dat in AuSn een zeer aanzienlijke verrijking van het oppervlak met Au optreedt. Het verschil in elektronische struktuur van een atoom in het pure metaal en in een legering wordt onderneer weerspiegeld in een versmalling van de valentie d-banden in de legeringen. De spin-baan opsplitsing is evenwel groter dan in het vrije atoom. Voorts verandert de lijnvorm van verschillende core lijnen. Bij een vergelijking van de posities van zowel core lijnen als Auger pieken treden belangrijke verschuivingen op tussen het pure metaal en de legering. Deze verschuivingen zijn terug te voeren tot verschillen in werkfunktie en konfiguratieveranderingen op de respektievelijke atomen. Tenslotte blijkt de duidelijke plasmon struktuur in Sn en Sb metaal geheel verdwenen in de legeringen AuSn en PdSb.

Het is een bekend fenomeen in rontgen fotoelektron spektroskopie dat

preparaten kunnen ontleden onder invloed van de rontgenstraling. Bij goud(III) dithiocarbamaat komplexen en goud kluster verbindingen treedt deze ontleding op. Door een systematische studie van de faktoren, die de ontledingssnelheid beïnvloeden, bleek dat voor bovengenoemde goudverbindingen de ontledingssnelheid zover gereduceerd kan worden, dat bestudering met rontgen fotoelektron spektroskopie mogelijk is. De aanzienlijke reduktie in ontledingssnelheid kan bereikt worden door de temperatuur van het preparaat te verlagen en het preparaat op een grafiet substraat aan te brengen.

Voor goud(III)dithiocarbamaat komplexen blijkt de bindingsenergie van de Au(4f) nivo's sterk afhankelijk van de (groeps)elektronegativiteit van de liganden. Bij een serie goud(I)fosfine verbindingen en goud kluster komplexen werd vrijwel geen afhankelijkheid gevonden. De bindingsenergie van de Au(4f) elektronen is echter in de goud(I)fosfine verbindingen en goud kluster komplexen ongeveer 1 eV groter dan in Au(I)dithiocarbamaat verbindingen. De lijnbreedte van de Au(4f) lijnen is in alle gevallen ongeveer hetzelfde. In het Au(4f) spektrum van de goud kluster verbindingen wordt niet meer dan één gouddoublet gevonden. De valentiebanden van de goud kluster verbindingen lijken zeer sterk op die van de goud(I)fosfine komplexen en zijn samengesteld uit de Au(5d) banden -opgesplitst door de spin-baan koppeling- en pieken die toe te kennen zijn aan de liganden. Uit bovenstaande volgt, dat de netto lading op de perifere goud atomen, en wellicht ook op het centrale goud atoom, vrijwel gelijk is aan die in goud(I)fosfine verbindingen en dat er geen d-elektron delokalisatie plaatsvindt. Dit is in overeenstemming met een eerder gepubliceerde beschrijving van de goud klusters als een verzameling lineaire goud verbindingen met een gemeenschappelijk goud atoom, zodanig dat alleen goud-goud interaktie optreedt tussen het centrale goud atoom en ieder van de perifere goud atomen. Met behulp van de metingen aan de goud(I)fosfine verbindingen werd een ruwe kwantitatieve analyse van de samenstelling van de goud kluster verbindingen gemaakt: Binnen de experimentele nauwkeurigheid van 10% werden geen afwijkingen van de nominale samenstelling gevonden.

CURRICULUM VITAE

Paul van Attekum werd geboren op 27 mei 1952 te Wateringen. Het gymnasium β werd eerst gevolgd op het Aloysius College te Den Haag en daarna voortgezet op het Henric van Veldeke College te Maastricht. In 1970 begon hij zijn scheikunde studie aan de K.U. te Nijmegen. Het kandidaatsexamen (S3) werd afgelegd op 28 mei 1973, het doktoraalexamen op 21 april 1975 met als hoofdvak molekuulspektroskopie en bijvakken computer science en capita uit de natuurkunde. Sindsdien heeft hij als wetenschappelijk medewerker van de K.U. een promotie onderzoek verricht in de werkgroep molekuulspektroskopie. Gedurende die periode werd geassisteerd op het fysisch chemisch praktikum en bij het werkkollege algemene chemie.

ERRATA

Page 37 : Fig. 3.2A horizontal axis should be 384 till 364

Page 38 : Fig. 3.3A horizontal axis should be 372 till 364

Page 116: Table 7.1 DPP = $(C_6H_5)_2P$ n-C_3H_6 $P(C_6H_5)_2$

Page 117: Table 7.2 DPP = $(C_6H_5)_2P$ n-C_3H_6 $P(C_6H_5)_2$

STELLINGEN

I

De konklusies, die Petitt en Meder trekken uit ^{57}Fe Mössbauer metingen van $FeSb_2O_4$, zijn ten onrechte gebaseerd op de door hen bepaalde parameters van het kernenergieniveauschema.

G.A. Petitt and M.R. Meder, Hyp. Int., 5 (1978) 323; J. van Dongen Torman, R. Jagannathan and J.M. Trooster, Hyp. Int., 1 (1975) 135.

II

Ten onrechte stellen Rigler en Ehrenberg, dat een onveranderde amino-acyleringsreaktie na chemische modifikaties van gist $tRNA^{Phe}$ impliceert, dat deze tRNA's biologisch aktief zijn.

R. Rigler and M. Ehrenberg, Quart. Rev. Biophys., 9 (1976) 1.

III

Uit de karakteristieke struktuur boven de aluminium K absorptiekant in elektron energieverlies spektra kunnen geen struktuurparameters bepaald worden op de manier, die Leapman en Cosslett aangeven.

R.D. Leapman and V.E. Cosslett, J. Phys. D, 9 (1976) L29.

IV

Schaefer et al. bepalen uit het hoge resolutie NMR spektrum van vaste polymeren de spin-rooster relaxatietijd in het roterend assenstelsel, $T_{1\rho}$, door de beginhelling te bepalen van de magnetisatie als funktie van de spin-lock tijd. Dit is een twijfelachtige methode.

J. Schaefer, E.O. Stejskal and R. Buchdal, Macromolecules, 10 (1977) 384; W.S. Veeman, E.M. Menger, W.M. Ritchey and E. de Boer, to appear in Macromolecules.

De bewering, dat een kleine interatomaire afstand tussen goud atomen betekent, dat er een binding bestaat tussen die goud atomen, is in strijd met experimentele gegevens.

W.S. Crane and H. Beall, Inorg. Chim. Acta, 31 (1978) L469;
M.P.A. Viegers, Thesis, Nijmegen (1976).

VI

Ten gevolge van een tekenfout is de door Batley en Bramley bepaalde triplet nulveldsplitsingstensor van 4,4'-dimethoxybenzofenon X-traps niet spoorloos. Daardoor zijn de D en E waarden, die hieruit berekend zijn door Chakrabarti en Hirota niet in overeenstemming met hun experimenten.

M. Batley and R. Bramley, Chem. Phys. Lett., 15 (1972) 337;
Asok Chakrabarti and Noboru Hirota, J. Phys. Chem., 80 (1976) 2966.

VII

De methode, die Banna en Shirley hebben gebruikt om de lijnbreedte op halve hoogte van de $K_{\alpha_{1,2}}$ röntgenlijn te bepalen, leidt tot onjuiste resultaten.

M.S. Banna and D.A. Shirley, J. Electron Spectrosc. Relat. Phenom., 8 (1976) 23.

VIII

Laboratoriumratten en -muizen draaien nachtdienst als ze overdag leertaken moeten vervullen.

P.M.Th.M. van Attekum Nijmegen, 18 mei 1979